TKK Dissertations 167
Espoo 2009

PERFORMANCE LIMITING FACTORS IN FLEXIBLE DYE SOLAR CELLS

Doctoral Dissertation

Janne Halme

Helsinki University of Technology
Faculty of Information and Natural Sciences
Department of Applied Physics

TKK Dissertations 167
Espoo 2009

PERFORMANCE LIMITING FACTORS IN FLEXIBLE DYE SOLAR CELLS

Doctoral Dissertation

Janne Halme

Dissertation for the degree of Doctor of Science in Technology to be presented with due permission of the Faculty of Information and Natural Sciences for public examination and debate in Auditorium K216 at Helsinki University of Technology (Espoo, Finland) on the 1st of June, 2009, at 12 noon.

Helsinki University of Technology
Faculty of Information and Natural Sciences
Department of Applied Physics

Teknillinen korkeakoulu
Informaatio- ja luonnontieteiden tiedekunta
Teknillisen fysiikan laitos

Distribution:
Helsinki University of Technology
Faculty of Information and Natural Sciences
Department of Applied Physics
P.O. Box 4100
FI - 02015 TKK
FINLAND
URL: http://tfy.tkk.fi/
Tel. +358-9-451 3198
Fax +358-9-451 3195
E-mail: eila.jylkas@tkk.fi

ISBN 978-951-22-9900-3
ISBN 978-951-22-9901-0 (PDF)
ISSN 1795-2239
ISSN 1795-4584 (PDF)
URL: http://lib.tkk.fi/Diss/2009/isbn9789512299010/

TKK-DISS-2607

Picaset Oy
Helsinki 2009

ABSTRACT OF DOCTORAL DISSERTATION	HELSINKI UNIVERSITY OF TECHNOLOGY P.O. BOX 1000, FI-02015 TKK http://www.tkk.fi

Author Janne Halme

Name of the dissertation
Performance limiting factors in flexible dye solar cells

Manuscript submitted 10.3.2009	Manuscript revised 11.5.2009
Date of the defence 1.6.2009	
☐ Monograph	☒ Article dissertation (summary + original articles)

Faculty	Faculty of Information and Natural Sciences
Department	Department of Applied Physics
Field of research	Solar cells
Opponent(s)	Professor Laurence Peter
Supervisor	Professor Peter Lund
Instructor	Professor Peter Lund

Abstract

Photovoltaic cells convert the electromagnetic energy of sunlight to electrical energy. An example of this is the electrochemical dye solar cell (DSC). In this work, preparation of DSCs on flexible plastic and metal substrates was studied concentrating on the factors that limit their energy conversion efficiency. Flexible substrates enable manufacturing of solar cells with cost-effective roll-to-roll techniques, but set restrictions to their materials and fabrication processes.

An improved method for the preparation of nanoparticle films on plastic was developed using spray deposition and mechanical pressing at room-temperature. With the method, deposition of nanostructured TiO_2 photoelectrodes was fast but their photocurrent output was low. To investigate this, an improved experimental method was introduced that allows determining the quantum efficiencies of photocurrent generation in DSC by conventional optical spectroscopy and spectral response measurements. The reason was low electron collection efficiency due to too short electron diffusion length in the pressed TiO_2 films.

Stainless steel 304 was found to possess excellent electrochemical properties for its use as the photoelectrode substrate. 4.4 % cell efficiency was reached with a steel based DSC. When the effects of different cell components on the current-voltage curve of the cell were studied using electrochemical impedance spectroscopy (EIS), it was found that the stainless steel decreased the electron recombination resistance of the TiO_2 photoelectrode film. The performance of the plastic substrate based cells at low light intensities was significantly limited by electron recombination *via* the substrate. Preparing a 4 nm thick compact TiO_2 layer on the substrate by atomic layer deposition (ALD) suppressed the recombination, but introduced an additional contact resistance that decreased the fill factor and cell efficiency.

The dynamic photocurrent and photovoltage response of DSC is significantly affected by non-uniform generation profile and inefficient collection of electrons. This complicates the interpretation of the dynamic data and can lead to erroneous conclusions when a common approximate way of analysis is used. As a solution to this, a new dynamic performance characteristic was introduced, that allows also determining the effective electron diffusion coefficient and lifetime at the short circuit condition consistently with the steady state cell performance.

Keywords	Solar cell, nanoparticle, dye, spray deposition, electron diffusion		
ISBN (printed)	978-951-22-9900-3	ISSN (printed)	1795-2239
ISBN (pdf)	978-951-22-9901-0	ISSN (pdf)	1795-4584
Language	English	Number of pages	72 p. + app. 102 p.
Publisher	Helsinki University of Technology		
Print distribution	Department of Applied Physics		
☒ The dissertation can be read at http://lib.tkk.fi/Diss/2009/isbn9789512299010/			

VÄITÖSKIRJAN TIIVISTELMÄ	TEKNILLINEN KORKEAKOULU PL 1000, 02015 TKK http://www.tkk.fi

Tekijä Janne Halme

Väitöskirjan nimi

Performance limiting factors in flexible dye solar cells

Käsikirjoituksen päivämäärä 10.3.2009	Korjatun käsikirjoituksen päivämäärä 11.5.2009
Väitöstilaisuuden ajankohta 1.6.2009	
☐ Monografia	☒ Yhdistelmäväitöskirja (yhteenveto + erillisartikkelit)

Tiedekunta	Informaatio- ja luonnontieteiden tiedekunta
Laitos	Teknillisen fysiikan laitos
Tutkimusala	Aurinkokennot
Vastaväittäjä(t)	Professori Laurence Peter
Työn valvoja	Professori Peter Lund
Työn ohjaaja	Professoti Peter Lund

Tiivistelmä

Aurinkokennot muuntavat auringonvalon sähkönmagneettista säteilyenergiaa sähköenergiaksi. Esimerkkinä tästä on sähkökemiallinen väriaineaurinkokenno. Tässä työssä tutkittiin väriaineaurinkokennon valmistusta taipuisille muovi- ja metallialustoille keskittyen niiden energian konversion hyötysuhdetta rajoittaviin tekijöihin. Taipuisat alustat mahdollistavat aurinkokennojen valmistamisen kustannustehokkailla rullalta rullalle -tekniikoilla, mutta asettavat rajoituksia niiden materiaaleille ja valmistusprosesseille.

Työssä kehitettiin parannettu menetelmä nanopartikkelikalvojen pinnoittamiseen muoville ruiskupinnoituksen ja huoneen lämpötilassa tapahtuvan mekaanisen painamisen avulla. Menetelmän avulla nanorakenteisten TiO_2-valoelektrodien valmistus oli nopeaa, mutta niiden valovirran tuotto oli heikko. Tämän tutkimiseksi kehitettiin parannettu kokeellinen menetelmä, jonka avulla väriainekennon valonvirran tuoton kvanttihyötysuhteet voidaan määrittää tavanomaisen optisen spektroskopian ja spektrivastemittausten avulla. Syynä oli huono elektronien keräyshyötysuhde johtuen painettujen TiO_2-kalvojen liian lyhyestä elektronien diffuusiopituudesta.

Ruostumattoman teräksen (304) havaittiin soveltuvan sähkökemiallisilta ominaisuuksiltaan erinomaisesti valoelektrodin alustaksi. Teräspohjaisella kennolla saatiin 4.4 % hyötysuhde. Tutkittaessa kennon eri osien vaikutusta virta-jännite-käyrään sähkökemiallisella impedanssispektroskopialla havaittiin, että teräs pienensi TiO_2-valoelektrodikalvon elektronien rekombinaatiovastusta. Muovialustaisten kennojen suorituskykyä matalilla valon intensiteeteillä rajoitti merkittävästi alustan kautta tapahtuva elektronien rekombinaatio. Atomikerroskasvatuksella (ALD) alustalle valmistettu 4 nm paksu tiivis TiO_2-kerros pienensi rekombinaatiota, mutta sai aikaan ylimääräisen kontaktivastuksen, mikä pienensi täyttökerrointa ja hyötysuhdetta.

Elektronien epätasaisesti jakautunut tuottoprofiili ja niiden matala keräyshyötysuhde vaikuttavat huomattavasti väriainekennon dynaamiseen valovirta- ja valojännitevasteeseen. Tämä vaikeuttaa dynaamisten tulosten tulkintaa ja voi johtaa vääriin johtopäätöksiin käytettäessä yleistä approksimatiivista analyysitapaa. Ratkaisuna tähän esiteltiin uusi kennon dynaamista suorituskykyä kuvaava suure, jonka avulla voidaan lisäksi määrittää elektronien diffuusiokerroin ja elinaika oikosulkutilassa yhdenmukaisesti kennon vakiotilan suorituskyvyn kanssa.

Asiasanat	Aurinkokenno, nanopartikkeli, väriaine, ruiskupinnoitus, elektronien diffuusio		
ISBN (painettu)	978-951-22-9900-3	ISSN (painettu)	1795-2239
ISBN (pdf)	978-951-22-9901-0	ISSN (pdf)	1795-4584
Kieli	Englanti	Sivumäärä	72 s. + liit. 102 s.
Julkaisija	Teknillinen korkeakoulu		
Painetun väitöskirjan jakelu	Teknillisen fysiikan laitos		
☒ Luettavissa verkossa osoitteessa http://lib.tkk.fi/Diss/2009/isbn9789512299010/			

Preface

This work was carried out during 2002-2009 at the New and Renewable Energy Systems group (NRES), Department of Applied Physics at the Helsinki University of Technology (TKK), Espoo, Finland. The work was financially supported by the Finnish Funding Agency for Technology and Innovation (Tekes), the Nordic Energy Research (Norden), and the Graduate School of Energy Technology. I thank the Fortum Foundation, the Finnish Academy of Science and Letters, and the Graduate School of Energy Technology for the travel scholarships to scientific conferences and meetings.

I thank my supervisor Prof. Peter Lund for giving me the opportunity and challenge to work on dye solar cells in my thesis, for the excellent research environment, and for his endless support and trust in me during the years. It has been a pleasure working at TKK. I thank all the present and former members of the NRES group, as well as the former Laboratory of Advanced Energy Systems for the friendly and inspiring atmosphere.

Foundations for this work were laid already when I joined the group as a third year student in the summer 1999. My first task was to measure the internal voltage losses in a polymer electrolyte membrane fuel cell, which in the end turned out to be practically impossible. Obviously, I had to pick up the gauntlet again with the solar cells. I thank the former and present fuel cell team members, especially Matti Noponen, Olli Himanen and Mikko Mikkola for the inspiring discussions and encouragement.

Carrying out this work required setting up new lab facilities for the fabrication and characterization of solar cells at TKK. I express my gratitude to all the many people who took part in that process. I am grateful to Minna Toivola, Antti Tolvanen, Jaakko Saarinen, Paula Vahermaa, Tapio Saukkonen and others for their high quality contributions to the experimental work reported here. Teamwork with Kati Miettunen was both fruitful and pleasant. Thanks Kati for your determined and critical researcher's attitude that made a big difference to the outcome of this work. I enjoyed also the discussions late in the afternoons with Timo Peltola sparked by his unprejudiced ideas. It was a great time working with you all and the others in the NRES group.

My sincere thanks to Prof. Anders Hagfeldt, Gerrit Boschloo, Thomas Edvinsson, Jarl Nissfolk, Tannia Marinado, Maria Quintana and others in the Center of Molecular Devices at the Royal Institute of Technology (KTH) for their kind hospitality and help during my visit at April 2005 - Nov 2005 and in June 2006.

I thank my friends and fishing buddies for the memorable and invigorating time together in the nature and on the waters.

Vanhempani Marja ja Kari, kiitos siitä tuesta ja rohkaisusta jonka olette antaneet minulle kaikissa valinnoissani. Tämä väitöskirja on omistettu teille.

Thank you Noora.

Janne Halme Helsinki, May 13th 2009

Table of contents

List of Publications

This thesis is an introduction to the following original publications:

I **Halme, J**.; Saarinen, J.; Lund, P.; Spray deposition and compression of TiO_2 nanoparticle films for dye-sensitized solar cells on plastic substrates; *Solar Energy Materials and Solar Cells*, 2006, 90, 887-899

II **Halme, J**.; Toivola, M.; Tolvanen, A.; Lund, P.; Charge transfer resistance of spray deposited and compressed counter electrodes for dye-sensitized nanoparticle solar cells on plastic substrates, *Solar Energy Materials and Solar Cells*, 2006, 90, 872-886

III Miettunen, K.; **Halme, J.**; Toivola, M.; Lund, P.; Initial performance of dye solar cells on stainless steel substrates; *J. Phys. Chem. C*, 2008, 112(10), 4011-4017

IV Miettunen, K.; **Halme, J.**; Vahermaa, P.; Saukkonen, T.; Toivola, M.; Lund, P.; Dye solar cells on ITO-PET substrates with TiO_2 recombination blocking layers, *Accepted for publication in the Journal of The Electrochemical Society*

V **Halme, J.**; Boschloo, G.; Hagfeldt, A.; Lund, P.; Spectral characteristics of light harvesting, electron injection and steady state charge collection in pressed TiO_2 dye solar cells; *J. Phys. Chem. C*, 2008, 112(14), 5623-5637

VI **Halme, J.**; Miettunen, K.; Lund, P.; Effect of non-uniform generation and inefficient collection of electrons on the dynamic photocurrent and photovoltage response of nanostructured photoelectrodes, *J. Phys. Chem. C*, 2008, 112(51), 20491-20504

Author's contribution:

I: The author planned the research, developed the spray method, analyzed the principle of film formation, did additional confirming optical microscopy, and wrote the paper.

II: The author planned the research, interpreted the EIS data, and was mainly responsible for writing the paper.

III: The author contributed to planning the experiments, analyzing the results, and shared the responsibility for writing the paper with Kati Miettunen.

IV: The author contributed in planning the experiments, analyzing the results, and writing the paper.

V: The author is mainly responsible for all parts of this work and writing the paper.

VI: The author is mainly responsible for all parts of this work and writing the paper.

Abbreviations and symbols

Abbreviations

AC	alternating current
APCE	absorbed-photon-to-collected-electron efficiency
CB	conduction band
CE	counter electrode
CELL	solar cell
CO	contact
COL	(electron) collection
CT	charge transfer
D	diffusion; dye
DC	direct current
DIF	differential
DSC	dye solar cell
EIS	electrochemical impedance spectroscopy
EL	electrolyte
F	Fermi
FTO	fluorine doped tin oxide
GEN	(electron) generation
HOMO	highest occupied molecular orbital
IMPS	intensity-modulated photocurrent spectroscopy
IMVS	intensity-modulated photovoltage spectroscopy
IN	incident
INJ	(electron) injection
IPCE	incident-photon-to-collected-electron efficiency
ITO	indium-tin-oxide
IV	current-voltage
KTH	Kungliga tekniska högskolan (Swedish); Royal Institute of Technology
LH	light harvesting
LUMO	lowest unoccupied molecular orbital
MPP	maximum power point
OC	open circuit
PE	photoelectrode
PET	polyethlyeneterephtalate
PV	photovoltaic; photovoltaics
redox	reduction-oxidation
S	series
SC	short circuit
StS	stainless steel
SU	substrate
TCO	transparent conductive oxide
TKK	teknillinen korkeakoulu (Finnish); Helsinki University of Technology
W_p	peak watt

Symbols

C	capacitance per unit area, (C/m^2)
D	diffusion coefficient (of electrons), (m^2/s)
d	thickness; photoelectrode film thickness, (m)
e^-	electron
E	energy, (J)
f	frequency, (Hz)
f	spatial (e.g. light harvesting) efficiency, (m^{-1})
F	transfer function, (the units depend on the type)
FF	fill factor, (no units)
$h\nu$	photon
i	current density, (A/m)
I^-	iodide ion
I_3^-	tri-iodide ion
k	index of resistance component
L	electron diffusion length, (m)
n	electron concentration (number density), (m^{-3})
P	power density, (W/m^2)
q	electron concentration, (C/m^3)
q_e	elementary charge, (C)
R	reflectance, (%)
R	resistance (per unit area), (Ωm^2)
S	sensitizer
S^*	excited sensitizer
S^+	oxidized sensitizer
t	time, (s)
T	transmittance, (%)
V	voltage, (V)
x	spatial coordinate, (m)
Z	impedance (per unit area), (Ωm^2)
Φ	photon flux ($m^{-2}s^{-1}$); spectral photon flux, ($m^{-2}s^{-1}nm^{-1}$)
α	light absorption coefficient (of the PE film), (m^{-1})
δ	delta function; spatial
η	efficiency, (%)
λ	light wavelength, (m)
τ	time constant, (s)
ω	angular frequency, (s^{-1})
ξ	spatial coordinate, (m)

Note: The symbols and abbreviations used in the Appendix and those that were explained at the point of use are not listed here. Definitions of the equivalent circuit impedance parameters are listed in Chapter 4.3.

1. Introduction

1.1. Background and motivation

The global energy consumption is expected to be 530 EJ in 2010 and to grow to 880 EJ by 2050 [1] and 1360 EJ by 2100 [2]. This means that more than 20 TW of new power generation capacity needs to be installed worldwide within the next 90 years. Doing this without compromising the climate and environment, and the security, safety and well-being of people is a major challenge and calls for large scale utilization of carbon-neutral renewable energy sources. One of the most promising options in this regard is solar energy [2-4].

The solar energy resource can be utilized by photovoltaic (PV) solar cells that convert the electromagnetic energy of the sunlight directly to electricity. 70 000 km^2 of solar cells with 10 % conversion efficiency installed in the so-called "solar belt" between 20º and 30º latitude that receive 2000-2500 kWh/m^2 yearly solar irradiation on a horizontal surface would satisfy all the present global energy consumption. The land area requirement for massive solar energy generation is huge, but not overly large when compared to the land already devoted to man-made constructions. For example, covering all the 70 million detached homes in the United States with solar panels would give already 0.25 TW [3].

Photovoltaics is proven, reliable, sustainable, and environmentally friendly energy technology. It is thus more than natural that it is generally embraced by people. The possibility to generate electricity directly from the sunlight anywhere in the world with a device that has no moving parts and needs hardly any maintenance is almost too good to be true. Concern about the detrimental effects of our present fossil fuel based energy economy on the environment and climate has generated a great motivation to increase the PV's share of the global energy production significantly from the current 0.1 % [5]. As a solid evidence of this, more than 2.8 GW_p [6] of PV systems are sold and installed globally with an annual market growth rate of 35-40 % [3,5].

These advantages must be contrasted with the reality that the cost of PV electricity is presently higher compared to the market price of grid electricity. The cost of grid-connected PV depends on the investment and maintenance costs of the PV system, operational lifetime of the system components, and naturally, on the yearly available solar irradiation ($kWh/m^2/a$) at the installation site. As an optimistic comparison, the price of solar electricity generated by a 500 kW grid-connected PV system in the solar belt conditions is about 0.17 €/kWh [7], i.e. about twice the grid electricity price in Europe for industrial customers [8].

To reduce the cost of PV, cheaper and more efficient solar cells are needed. The present (3/2009) market price of crystalline silicon based solar modules is about 4.6 €/W_p [9] while the commonly acknowledged goal is 1 €/W_p or less. There are mainly two ways to aim for cheaper PV modules: to reduce their manufacturing costs (€/m^2) or to increase their efficiency (W_p/m^2). According to Green [10], new PV technologies that aim primarily to cheaper manufacturing compared to the present crystalline silicon wafer based "1st generation" PV technology are called 2nd generation solar cells and include thin film PV like CdTe, $CuInGa(Se)_2$, and amorphous silicon, whereas solar cells characterized by higher theoretical efficiency, such as multi-junction (tandem) solar cells, hot-carrier solar cells, etc. belong to the 3rd generation of solar cells.

Except for the tandem cells that are used in space applications and concentrated PV, most of the 3rd generation concepts have remained so far as subjects of fundamental research. In fact, it is the 2nd generation solar cells that still stimulate most of the practical PV research activities and commercialization efforts at the present. In particular, during the last 20 years or so we have witnessed a growing interest to use nanotechnology for devising low-cost solar cells based on molecular materials and semiconductor nanoparticles and nanostructures. The organic solar cells [11] and electrochemical dye solar cells [12-14] are the most well known examples in this category.

Low-cost manufacturing of PV modules requires not only cheap materials but also cost-effective production processes. Large scale automated volume production is necessary to benefit from the economies of scale and to satisfy the increasing demand of PV. With this regard, roll-to-roll processing of thin film solar cells on flexible low-cost substrates such as plastic or metal foils is considered a promising, perhaps inevitable, direction of development. Indeed, work towards roll-to-roll processing and flexible substrates is common to practically all thin film PV technologies [15].

Flexible substrates are attractive not only from the economic but also from the application point of view. Flexible solar cells may be competitive alternatives in many applications with varied requirements for efficiency, price, stability, and functionality. In the low-cost and large scale end, flexibility is beneficial as it allows installation of solar panels on curved surfaces and existing building structures making it easier to engage large surface areas for solar power generation. In applications where functionality is more important than price, bendable, unbreakable, and extremely light-weight solar cell foils that can be rolled or folded up for storage and transportation may find or create new markets for portable backup power sources for mobile electronics like personal communication or emergency and rescue applications. Moderately efficient but extremely low-cost printed solar cells may be suitable for powering the emerging applications of printed electronics.

This thesis deals with a solar cell type that is considered to be particularly promising for realizing low-cost flexible PV: the dye-sensitized solar cell, or simply dye solar cell (DSC) [12-14]. Dye solar cells built on glass substrates are efficient and stable. Small lab size cells reach over 10 % efficiencies, e.g. [16-20], and withstand more than 1000 hours of accelerated aging at 80 °C in the dark and visible light soaking at 60 °C with negligible or minor performance degradation, e.g. [19,20].

The DSC has many characteristics ideal for low-cost roll-to-roll processing. Its active materials are nanoparticles, dye molecules, and organic materials that can be deposited on various substrates in ambient temperature and pressure at non-clean-room conditions using solution processing like printing and spraying. Currently companies such as G24i are establishing production lines for flexible plastic DSCs, and Corus is working in collaboration with Dyesol to integrate DSCs on flexible stainless steel roofing products. However, transfer of the DSC technology from glass to flexible substrates while maintaining the high cell performance and stability proven on glass is challenging and not fully accomplished yet. This forms the underlying research problem of this thesis.

1.2. Objectives and scope

The purpose of this study was to contribute to the transfer of the DSC technology from rigid glass substrates to alternative flexible substrates such as plastic foils and metal sheets. The

basic criteria for evaluating the success of this transfer are the same as for evaluating the competitiveness of any PV technology: cell performance, long-term stability, and manufacturing costs. Each of these criteria is equally important in reaching the ultimate goal: low-cost generation of solar electricity. Nevertheless, this thesis focuses only on of one these criteria: *the solar cell performance*.

Issues related to the manufacturing costs and stability played a role in the selection of the research topics, but were not the subjects of research as such. For instance, cheaper manufacturing is the main motivation for aiming at the flexible substrates in the first place, but is not elaborated in this thesis. Cost analyses carried out by others have estimated that with the present-day materials and manufacturing technology, the glass based DSCs can reach module cost of 2-3 €/W_p at 1-4 MW_p/year manufacturing and 7-8 % active area cell efficiency, and less than 1.5 €/W_p through large volume production and material optimization [19]. The goal of large scale roll-to-roll production of flexible DSCs on low-cost substrates should thus be considerably below 1 €/W_p.

Stability for its part is a major challenge for flexible solar cells, as well as for organic electronics in general, and the DSCs are no exception in this respect. Electronic materials are usually sensitive to water in the long run, and there is hardly a better moisture barrier than a thick sheet of glass. Nevertheless, before systematic investigations of the long-term stability and performance degradation of flexible dye solar cells can be sensibly carried out, the factors that determine the cell performance need to be well understood and characterized.

This brings us to the *main objectives* of this thesis. They were to:

1. Demonstrate and evaluate the technical feasibility of manufacturing dye solar cells on flexible substrates and develop better methods for the cell preparation

2. Generate fundamental understanding of the factors that limit the photovoltaic performance of these solar cells, and

3. Develop experimental methods that allow better resolution and accuracy for identifying and quantifying the performance limitations by measurements carried out with complete solar cells under realistic operating conditions

In the transfer from glass to flexible substrates the main problems regarding solar cell performance are related to the properties of the substrates, their interaction with the other cell components, and the restrictions that they set to the cell fabrication. Consequently, the *specific research questions* in this study were:

1. How to prepare over 10 μm thick colloidal TiO_2 photoelectrode films with good electron transport properties on flexible ITO-PET plastic substrates below 150 ºC?

2. How to prepare catalytic counter electrodes with charge transfer resistance below 1 Ωcm^2 on ITO-PET plastic?

3. Is the ITO-PET as good photoelectrode substrate as the conventional FTO-glass? Or is there a need for a blocking layer to suppress back-reaction of electrons at the ITO-electrolyte interface? How could such a layer be deposited below 150 ºC?

4. Can the DSC be integrated directly on a stainless steel sheet in such a way that the metal functions as the current collector and back contact of the cell, without compromising the cell efficiency?

5. The photocurrent of a solar cell is a result of at least three consecutive processes: light absorption, charge separation, and charge collection. What determines the quantum efficiency of these photoconversion steps in the DSC, and how can they be measured?

6. DSCs with nanostructured TiO_2 photoelectrodes prepared by room-temperature compression technique suffer from lower photocurrent output compared to equivalent cells that use high-temperature treated photoelectrodes. Why?

7. Electrochemical impedance spectroscopy (EIS) and intensity-modulated photocurrent (IMPS) and photovoltage (IMVS) spectroscopy are widely used dynamic measurement techniques that give information on the electrical and opto-electrical function of the DSC. What is the correct interpretation of this information and how is it related to the steady state IV curve of the cell?

Not coincidentally, these questions are answered in the Publications I-VI and Chapters 3-5 of this thesis.

1.3. Outline of the thesis

The thesis is organized as follows.

First, the background and motivation for the study are presented and the objectives and scope of the thesis are defined in Chapter 1.

In Chapter 2.1 the general principle of a generalized photovoltaic converter is reviewed following a modern description that is suitable for understanding the function of all kinds of solar cells, in particular the "excitonic" solar cells, like the organic and dye solar cells. This is followed by a short introduction to the operating principle of the DSC and its advantageousness compared to the function of inorganic p/n-junction solar cells in Chapter 2.2.

A theoretical description of the factors that affect the conversion efficiency of DSCs is given in Chapter 3. Here, a main focus is given to the factors that determine the short circuit current density of DSC, since this was a central topic of the thesis.

Chapter 4 gives an overview of the main experimental techniques used in this work. In particular, a concise introduction to EIS, IMPS and IMVS is presented pointing out their relation to each other and to the steady state IV curve of the solar cell.

In Chapter 5 the main results of the thesis, reported originally in the Publications I-VI, are summarized and discussed. The results are complemented with previously unpublished data when available and fruitful to the discussion.

The results and the main conclusions of the thesis are summarized in Chapter 6.

The Appendix outlines the time-dependent standard diffusion model and presents its general solution for small amplitude harmonic light modulation. This simple model played a major role in this thesis.

The original Publications I-VI are reproduced at the end of the thesis with kind permission from the copyright holders.

2. The dye solar cell

2.1. Principle of photovoltaic energy conversion

A common feature for all types of solar cells is their ability to convert the electromagnetic energy of light to electrical potential energy that can be supplied to an external electric circuit connected to the cell. This photoconversion process can be divided generally into two principal steps [21,22]:

1. Creation of an excited electronic state by photon absorption in the absorber material. The excited state may be considered as a pair of positive and negative electronic charges.

2. Separation of the photogenerated electronic charges to the different terminals (contacts) of the device.

Depending on the type of solar cell the excited state can be an electron-hole pair in a crystalline semiconductor (e.g. silicon solar cells), a bound exciton in an organic polymer (organic solar cells), or an electronic excitation in a dye molecule (dye solar cells). Thermodynamically, in the light absorption process the electromagnetic energy of the photon is converted to chemical energy in the absorber, corresponding to change in the population of the electronic states available in the material.

To produce electrical energy, the chemical energy of the photoinduced excited state must be transformed to electrical potential difference (electrostatic potential energy) between the contacts of the solar cell (Figure 1). In this charge separation process the positive and negative electronic charges that correspond respectively to the occupation and vacancy in the higher and lower energy states of the electronic excitation, are dissociated (spatially separated) and transported to the opposite contacts. This process requires certain asymmetry in the solar cell so that one of the contacts collects predominantly the negative charge carriers while the other contact receives predominantly the positive charges. In other words, the contacts of the solar cell display different selectivity to the type of the charge carriers.

The existence of at least one selective contact to the absorber can be taken as a minimum prerequisite for a photovoltaic device (Figure 1). The physical location and the mechanism behind the contact selectivity can be quite different in different types of solar cells, but can nevertheless be always identified [21,22]. For example, in the standard p/n-junction silicon solar cells the selectivity arises from the drift of electrons and holes into the opposite direction in the electric field of the space charge region in the p/n-junction, whereas in the organic bulk-heterojunction solar cells the selectivity arises from difference in the interfacial properties of the electron and hole conducting organic materials and their metal contacts.

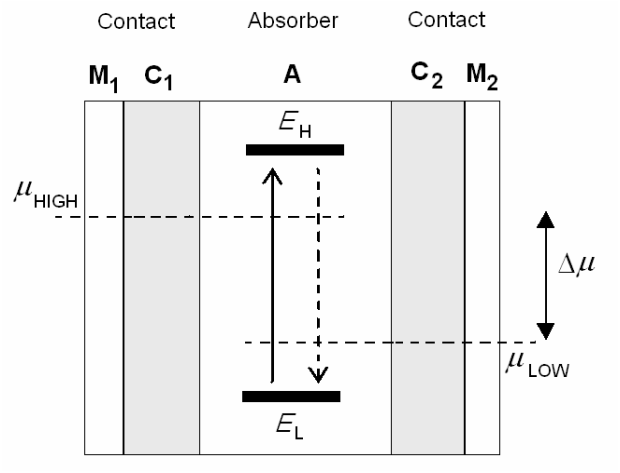

Figure 1. General principle of an idealized photovoltaic converter consisting of an absorber (A) and two selective contacts (C_1 and C_2) [21]. Upon light absorption the photon energy is converted to chemical potential ($\Delta\mu = \mu_{HIGH} - \mu_{LOW}$) of the exited electronic states in the absorber by lifting electrons from a low-energy level (E_L) to a high-energy level (E_H). At the steady state the rates of generation (solid arrow) and relaxation (a.k.a. recombination, dashed arrow) of the exited states balance each other, leading to a shift in the chemical potential $\Delta\mu$ of electrons in the absorber. The chemical potential difference corresponds to the maximum available free energy of electrons. When the contact C_1 is selective to the electrons in the high-energy level (or above it) and the contact C_2 to the electrons (holes) in the low-energy level (or below it), the chemical potential of the absorber can be addressed as an electrostatic potential difference between the metal contacts (M_1 and M_2), and used to do electrical work in the external circuit connected to the solar cell.

2.2. Operating principle of the dye solar cell

The dye solar cell (DSC), also known as the Grätzel cell, is a photoelectrochemical device that combines light-absorbing dye molecules with semiconductor nanoparticles and a redox electrolyte to generate electricity from the sunlight.

Figure 2 shows the structure of a typical DSC. The photoelectrode consists of visible light absorbing dye molecules (photosensitizers) that are chemisorbed as a monolayer on the surface of TiO_2 nanoparticles having ca. 20 nm diameter. The TiO_2 nanoparticles are in contact with each other forming a ca. 10 μm thick nanoporous electrode film deposited on a transparent conductive oxide (TCO) coated glass substrate. The nanoporous structure of the TiO_2 film provides high internal surface area to accommodate the large amount of dye required for efficient light absorption while ensuring that each dye molecule is in direct contact with both the TiO_2 and the electrolyte. A few hundred nanometers thick TCO layer forms an electronic contact to the TiO_2 film. The counter electrode of the cell consists of a similar TCO glass substrate coated with platinum catalyst particles.

A thermoplastic polymer film is used as an edge sealant and spacer to attach the photoelectrode and counter electrode together to form a sandwich-like thin layer electrochemical cell. A liquid electrolyte fills the few tens of micrometers thick gap between the electrodes and penetrates to the pores of the TiO_2 film making contact with the dye molecules. Ideally, the only light absorbing material in the cell is the dye molecules while other parts of the cell are transparent. This includes the nanostructured large band-gap semiconductor particles (TiO_2) that absorbs light only in the UV region.

Figure 3 shows the operating principle of the DSC. Upon light absorption an electron is excited from a low-energy state (highest occupied molecular orbital, HOMO) to a high-energy state (lowest unoccupied molecular orbital, LUMO) of the dye (1). The excited state of the dye is relaxed by electron injection to the TiO_2 conduction band (2). The oxidized dye is regenerated by electron capture from the redox electrolyte (3). The electron moves by diffusion in the TiO_2 film until it is collected at the TCO contact of the photoelectrode (4), and is returned to the redox electrolyte in an electrochemical reaction at the counter electrode (5). The electrical circuit is closed by ionic transport between the photoelectrode and counter electrode (6).

The regenerative operating cycle of the cell can be summarized as follows:

Photoelectrode (photoanode) reactions:

$S + h\nu \rightarrow S^*$	*light absorption by the dye*	(1)
$S^* \rightarrow S^+ + e^-(\mathrm{TiO_2})$	*electron injection*	(2)
$2S^+ + 3I^- \rightarrow 2S + I_3^-$	*dye regeneration*	(3)
$3I^- + 2h\nu \rightarrow I_3^- + 2e^-(\mathrm{TiO_2})$	*overall photoelectrode reaction*	(4)

Counter electrode (cathode) reactions:

$I_3^- + 2e^-(\mathrm{CE}) \rightarrow 3I^-$	*overall charge transfer reaction*	(5)

Overall cell reaction:

$e^-(\mathrm{CE}) + h\nu \rightarrow e^-(\mathrm{TiO_2})$	(6)

Investigation of the role of each of these (and other) processes in determining the energy conversion efficiency of the DSC, and limitations thereof, is a central topic in this thesis.

The DSC is a particularly interesting realization of the generalized photovoltaic converter (cf. Figure 1). In the DSC the absorber material is the dye molecules at the TiO_2-electrolyte interface. The selective contact to the high-energy state of the dye (LUMO) is provided by the TiO_2 conduction band whereas the redox electrolyte forms a selective contact to the ground state (HOMO) of the dye.

The molecular TiO_2-dye-electrolyte interface carries therefore the role of both light absorption and charge separation, whereas the transport of negative (electron) and positive (effectively I_3^-) charge carriers takes place in the TiO_2 nanoparticles and the electrolyte respectively. This is in fact a significant advantage of the DSC compared to the way how conventional PV cells work. In the silicon solar cells as well as in the inorganic thin film solar cells, the semiconductor material is responsible for both light absorption and carrier transport, and recombination of the electrons and holes occurs in the bulk of the material (in addition to surface recombination). To suppress bulk recombination the semiconductor material needs to be of high purity which tends to make it expensive. In DSC however, the tasks of light absorption, and carrier transport are separated to different materials. This gives more freedom and possibilities to design and optimize the cell materials with respect to performance, cost and stability.

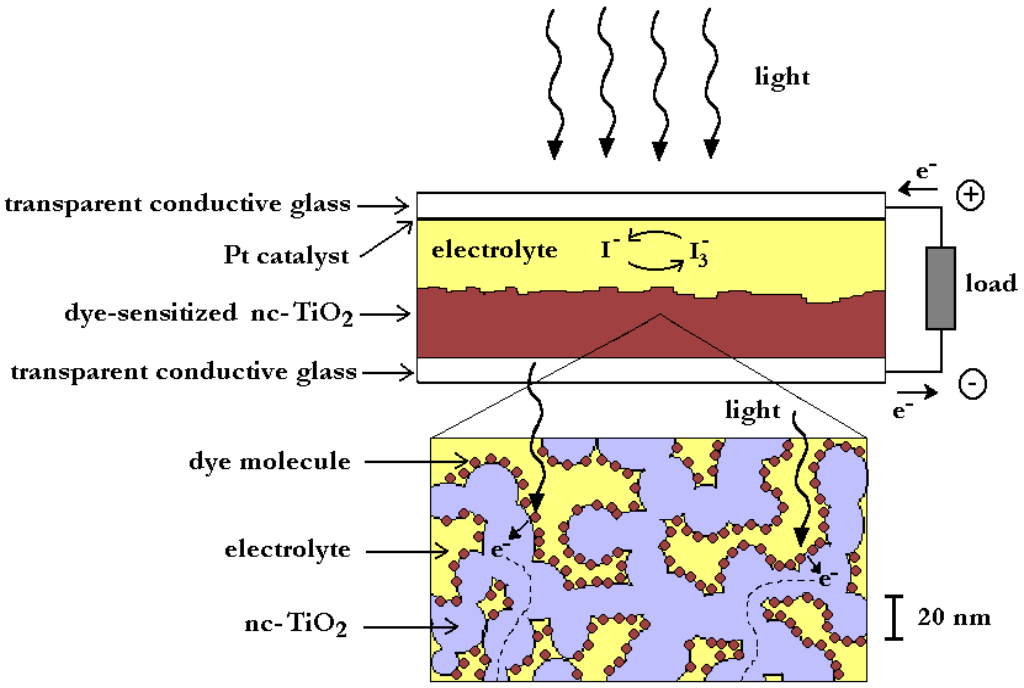

Figure 2. Structure and components of the dye solar cell. When transparent substrates and weakly absorbing counter electrode catalyst is used, the DSC can operate also with backside illumination, as indicated in the figure.

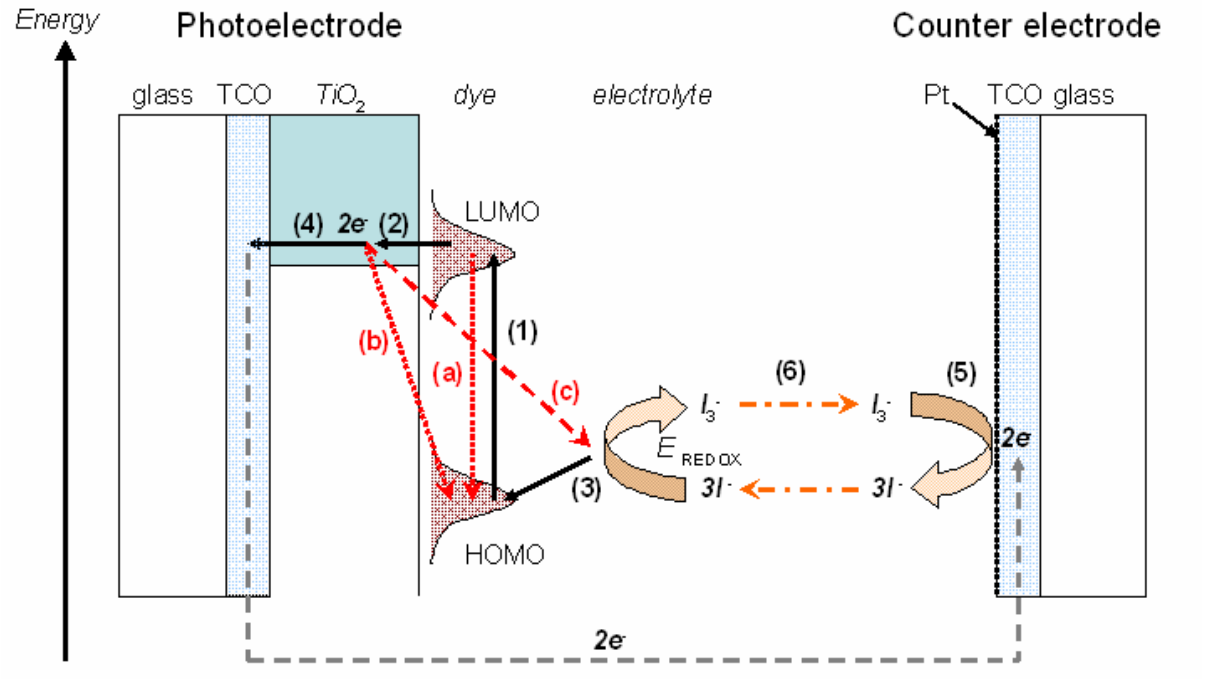

Figure 3. Operating principle of the dye solar cell. The numbers indicate the forward reactions of the operating cycle of DSC as described in the text. Unwanted back-reactions are indicated with red arrows including: (a) radiationless relaxation of the exited state of the dye, (b) recombination of the injected electrons with the oxidized dye, (c) recombination of the electrons by interfacial electron transfer to the electrolyte.

3. Photovoltaic function of dye solar cells

The photovoltaic performance of a solar cell is described by its current-voltage (IV) curve and reported in terms the IV characteristics: short circuit current density i_{SC}, open circuit voltage V_{OC}, and fill factor FF (Figure 4).

The fill factor is defined as

$$FF = \frac{V_{MPP} i_{MPP}}{V_{OC} i_{SC}} \tag{7}$$

where i_{MPP} and V_{MPP} are respectively the current density and voltage at the maximum power point (MPP). Using the fill factor, the maximum power per unit area delivered by the solar cell can be written as

$$P_{MAX} = V_{OC} i_{SC} FF \tag{8}$$

The light-to-electricity energy conversion efficiency of the solar cell is defined as the ratio of the maximum power produced by the cell (W/m^2) to the incident light intensity P_{IN} (W/m^2)

$$\eta = \frac{P_{MAX}}{P_{IN}} \tag{9}$$

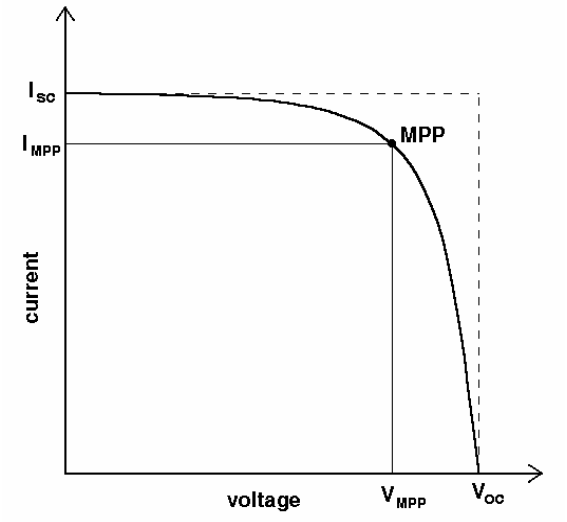

Figure 4. Typical solar cell IV curve and its characteristic parameters.

In general, the IV characteristics and efficiency of a solar cell depend on the intensity and spectral distribution of the incident light, and on the cell temperature. For this reason, standard measurement conditions have been defined to facilitate comparison of solar cell data between different laboratories. The standard conditions relevant for terrestrial applications are: light intensity 1000 W/m^2, spectral distribution according to AM1.5 global standard solar spectrum, and cell temperature 25°C. The power output of the solar cell at these conditions is called the nominal power of the cell and is indicated by reporting the data in units of W_P, called *peak watt*.

3.1. Short circuit current density

An essential quantity describing the effectiveness of the solar cell in generating steady state photocurrent is the spectral *incident-photon-to-collected-electron efficiency* (IPCE) $\eta_{\mathrm{IPCE}}(\lambda)$, also known as the external quantum efficiency EQE. When reported in units A/W it is also known as the spectral response of the solar cell. The IPCE is defined as the number of electrons delivered to an external electric circuit per number of photons with wavelength λ incident on the cell. The η_{IPCE} is normally measured at the short circuit conditions, corresponding to the situation where the cell delivers its maximum photocurrent at a given monochromatic light intensity

$$\eta_{\mathrm{IPCE}}(\lambda) = \frac{i_{\mathrm{SC}}(\lambda)}{q_{\mathrm{e}}\Phi_{\mathrm{DC}}(\lambda)} \tag{10}$$

where i_{SC} is the steady state short circuit current density, Φ_{DC} the steady state photon flux, λ the light wavelength, and q_{e} the elementary charge. A simple IPCE measurement involves measurement of the steady state i_{SC} and the photon flux incident on the cell while scanning the light wavelength with a monochromator.

Alternatively, we may define the differential IPCE as the ratio of a small (differential) change in i_{SC} due to small change in the incident photon flux relative to some steady state background intensity

$$\eta_{\mathrm{IPCE,DIF}}(\lambda) = \frac{1}{q_{\mathrm{e}}}\frac{\partial i_{\mathrm{SC}}(\lambda)}{\partial \Phi_{\mathrm{DC}}(\lambda)} \tag{11}$$

The differential IPCE can be measured by comparing the amplitude of the short circuit photocurrent response generated by small modulation of the incident light intensity, using e.g. chopped monochromatic light and a lock-in amplifier. Note that the differential IPCE equals with the total IPCE only when i_{SC} is exactly linear with photon flux. In practice, DSCs typically show light-intensity dependent η_{IPCE} meaning that the differential $\eta_{\mathrm{IPCE,DIF}}$ is not equal to the total η_{IPCE} [23-25].

The η_{IPCE} of the DSC can be expressed as a product of the partial efficiencies (probabilities) of the light harvesting η_{LH}, electron injection η_{INJ}, and electron collection η_{COL} processes (Figure 5).

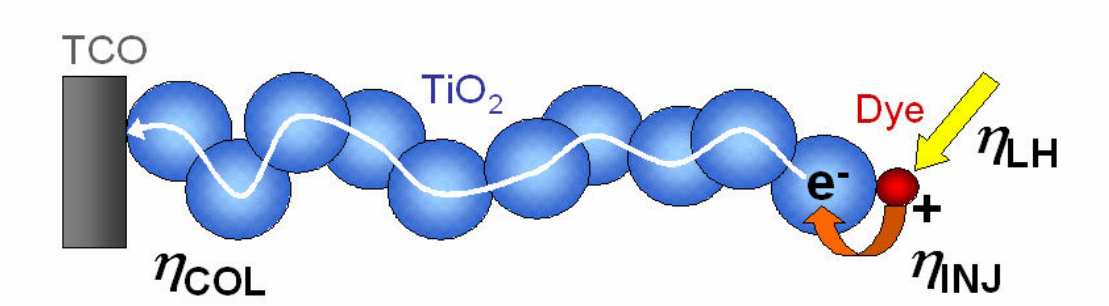

Figure 5. The photocurrent of the dye solar cell depends on the quantum efficiencies of light harvesting (η_{LH}), electron injection (η_{INJ}), and electron collection (η_{COL}).

$$\eta_{\mathrm{IPCE}} = \eta_{\mathrm{LH}}\eta_{\mathrm{INJ}}\eta_{\mathrm{COL}} \tag{12}$$

The ratio $\eta_{\mathrm{IPCE}}/\eta_{\mathrm{LH}}$ defines further the *absorbed-photon-to-collected-electron efficiency* η_{APCE}, also known as the internal quantum efficiency IQE

$$\eta_{\mathrm{APCE}} = \eta_{\mathrm{INJ}}\eta_{\mathrm{COL}} \tag{13}$$

The η_{IPCE} has thereby an optical part, η_{LH}, and an electrical part, η_{APCE}. Additionally, the quantum efficiency of electron generation

$$\eta_{\mathrm{GEN}} = \eta_{\mathrm{LH}}\eta_{\mathrm{INJ}} \tag{14}$$

tells us the probability at which a photon incident on the cell generates an electron in the TiO_2 via excitation and electron injection by the dye. The η_{IPCE} is a spectral quantity, i.e. it is defined for a monochromatic light wavelength only. The short circuit current of the solar cell under white light illumination with *spectral* photon flux $\Phi_{\mathrm{DC}}(\lambda)$ (units $m^{-2}s^{-1}nm^{-1}$) is

$$i_{\mathrm{SC}} = q_{\mathrm{e}}\int_{\lambda_{\min}}^{\lambda_{\max}}\Phi_{\mathrm{DC}}(\lambda)\eta_{\mathrm{IPCE}}(\lambda)d\lambda = q_{\mathrm{e}}\int_{\lambda_{\min}}^{\lambda_{\max}}\Phi_{\mathrm{DC}}(\lambda)\eta_{\mathrm{LH}}(\lambda)\eta_{\mathrm{INJ}}(\lambda)\eta_{\mathrm{COL}}(\lambda)d\lambda \tag{15}$$

where $\lambda_{\min}$ … $\lambda_{\max}$ defines a wavelength range where both η_{IPCE} and $\Phi_{\mathrm{DC}}(\lambda)$ are non-zero. Note that in eq. 15 each of the three factors, η_{LH}, η_{INJ}, and η_{COL} are generally wavelength-dependent.

3.1.1. Light harvesting efficiency

Of the three factors of η_{IPCE} the light harvesting efficiency η_{LH} is perhaps the best understood. It is defined as the probability that a photon with wavelength λ incident on the cell is absorbed by a dye molecule somewhere in the cell and its energy is converted to the chemical energy of the exited state of the dye. Accordingly, the η_{LH} depends on the molar light absorption coefficient of the dye, its concentration in the photoelectrode and the thickness of the photoelectrode film, and is affected by optical losses due to light reflection and absorption in the other cell components.

Due to light attenuation the local absorption rate varies over the thickness of the photoelectrode film. It is therefore useful to define a *spatial light harvesting efficiency* $f_{\mathrm{LH}}(x,\lambda)$, in units m^{-1}, as the probability per unit length that a photon incident on the cell is absorbed at the position x within the photoelectrode film. f_{LH} gives the light absorption profile in the film and is related to the total light harvesting efficiency η_{LH} as

$$\eta_{\mathrm{LH}}(\lambda) = \int_0^d f_{\mathrm{LH}}(x,\lambda)dx \tag{16}$$

where d is the photoelectrode film thickness. Note that in f_{LH} we incorporate *all* optical effects and losses that determine the local photon flux in the photoelectrode film.

In the simplest (ideal) case η_{LH} is given by the Beer-Lambert law. This assumes that the light absorption profile f_{LH} is exponential and light scattering is insignificant, and neglects all optical losses other than the transmittance of the photoelectrode itself. In this case

$$f_{LH}(x) = \alpha_D e^{-\alpha_D x} \tag{17}$$

where α_D is the light absorption coefficient of the dye. The light harvesting efficiency becomes then (eq 16)

$$\eta_{LH} = 1 - e^{-\alpha_D d} \tag{18}$$

If the dye molecules are not the only light absorbing component in the photoelectrode film, we have

$$f_{LH}(x) = \alpha_D e^{-\alpha x} \tag{19}$$

and

$$\eta_{LH} = \frac{\alpha_D}{\alpha}\left(1 - e^{-\alpha d}\right) \tag{20}$$

where α is the total absorption coefficient of the photoelectrode film. In practice, α includes a contribution from the light absorption by the I_3^- in the electrolyte in the pores of the film.

A slightly more realistic optical model was used in Publications V and VI taking into account transmittance of the substrates and reflectance of the moderately light scattering photoelectrode film. Assuming that the reflectance of the film is interfacial despite the fact that it originates mainly from the light scattering in the bulk of the film, f_{LH} and η_{LH} become for the PE illumination

$$f_{LH,PE}(x) = T_{TCO}\left[1 - R_{PE}\right]\alpha_D e^{-\alpha x} \tag{21}$$

$$\eta_{LH,PE} = T_{TCO}\left[1 - R_{PE}\right]\frac{\alpha_D}{\alpha}\left(1 - e^{-\alpha d}\right) \tag{22}$$

and for the CE illumination

$$f_{LH,CE}(x) = T_{CE}T_{EL}\left[1 - R_{PE}\right]\alpha_D e^{\alpha(x-d)} \tag{23}$$

$$\eta_{LH,CE} = T_{CE}T_{EL}\left[1 - R_{PE}\right]\frac{\alpha_D}{\alpha}\left(1 - e^{-\alpha d}\right) \tag{24}$$

where T_{TCO}, T_{CE} and T_{EL} are respectively the transmittance of the TCO-coated glass substrate of the photoelectrode, the counter electrode and the free electrolyte layer, and R_{PE} is the reflectance of the photoelectrode film (Figure 6). Note that in Publication V, it was necessary to take additionally into account the dependence of the parameters α, T_{EL}, and R_{PE} on the photoelectrode thickness d.

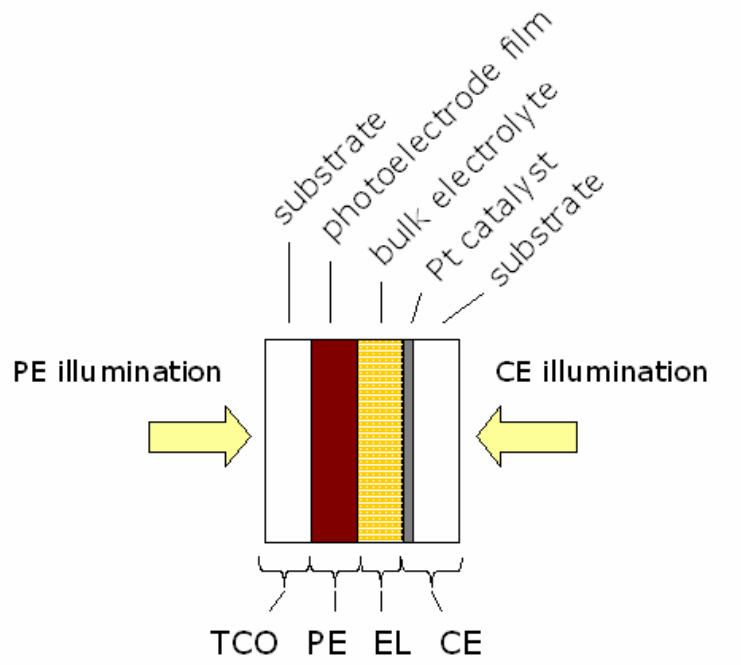

Figure 6. Schematic representation of the optical components in the dye solar cell and the corresponding nomenclature used in eqs. 21-24.

The simple optical model described above (eqs 22 and 24) could be improved for example by including back reflection of light from the counter electrode, or more generally, multiple reflection of light in the multi-layered structure of the cell. Light scattering in the photolectrode film can be modeled by four-flux radiative transfer calculations [26] applied to single [27] or multilayer films [28]. Interference effects may need to be accounted for when the thickness of an optical layer is comparable to the light wavelength, such as in the case of the TCO layers [29].

Nevertheless, whatever the optical model might be like, it needs to be coupled with the electrical model of the cell. As shown in Publication VI, this is particularly straightforward and simple in the case of the standard electron diffusion model discussed in Chapter 3.1.3 and the Appendix, and used throughout this thesis.

3.1.2. Electron injection efficiency

The electron injection efficiency η_{INJ} is defined as the average probability that the generation of an excited state of the dye (somewhere in the photoelectrode) by a photon of wavelength λ leads to a successful transfer of an electron from the dye to the electronic transport states in the TiO_2. The injection is taken successful and completed when the electron becomes a statistically indistinguishable member of the excess electron population in the TiO_2. This marks the initial photoinduced charge separation at the TiO_2-dye-electrolyte interface.

The η_{INJ} depends on the density and mutual energetic overlap of the excited state energy levels of the dye (donor states) and the electronic states (acceptor states) in the semiconductor oxide. This energetic matching can be tuned by suitable co-adsorbent molecules or electrolyte species [30-37] that upon adsorption to the semiconductor surface influence the magnitude and distribution of the electrostatic potential difference across the electrochemical Helmholtz layer at the semiconductor-dye-electrolyte interface [38,39](Figure 7).

While η_{INJ} is sensitive to the selection of the semiconductor oxide, the dye, and the electrolyte composition, it is normally considered to independent of the position in the photoelectrode film.

3.1.3. Electron collection efficiency

The electron collection efficiency η_{COL} is the probability that the electron injected from the dye to the TiO_2 is successfully collected from the solar cell, i.e. it contributes to the measured electric current in the external electric circuit. In other words, it is the probability that the electron avoids recombination with the oxidized dye or the electrolyte species. The η_{COL} depends on the characteristic rate constants of the electron transport and recombination processes in the photoelectrode. In Publication V η_{COL} was determined based on steady state η_{APCE} data, whereas Publication VI presents a general description of the dynamic electron generation-collection problem in terms of the IMPS and IMVS response discussed later in Chapter 4.5.

Considering the collection events of individual electrons, it is useful to define a *spatial electron collection efficiency* $\eta_{COL,\delta}$ as the probability that an electron injected at the position x into the photoelectrode film becomes collected at the contact. According to the standard diffusion model (Appendix) $\eta_{COL,\delta}$ depends on the distance from the point of electron generation (x) to the collecting contact (at $x = 0$), and on the electron diffusion length L and film thickness d as

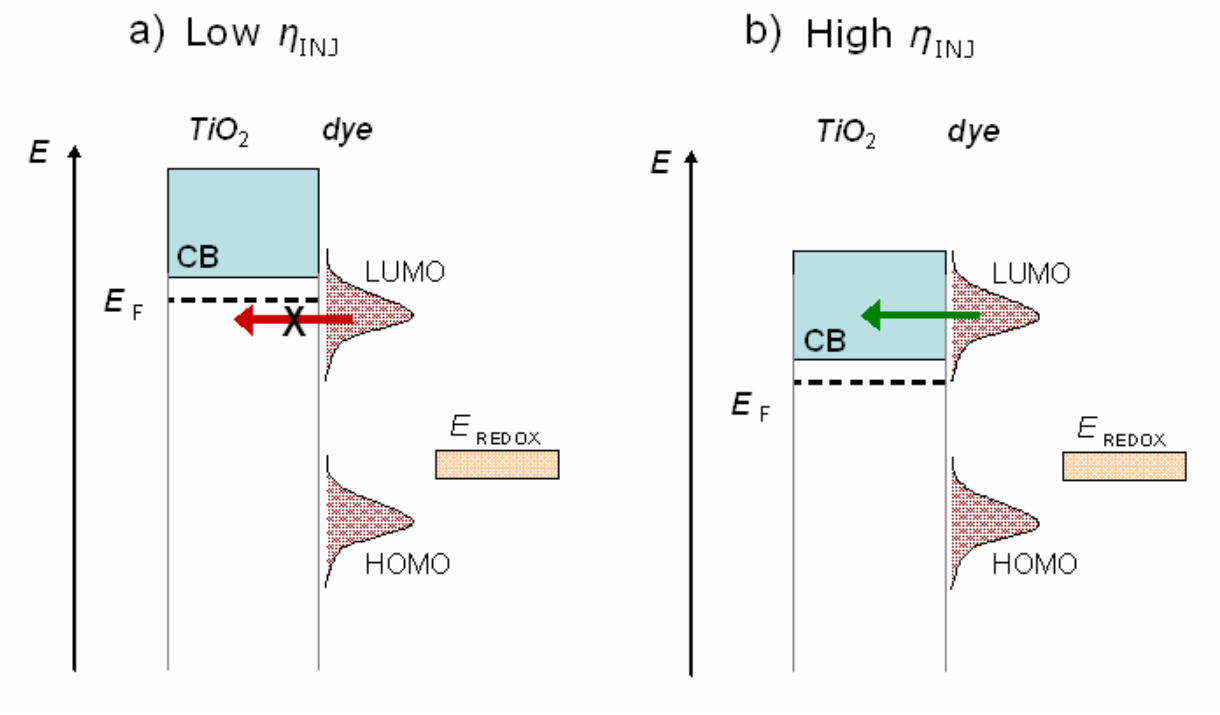

Figure 7. Effect of conduction band position on the electron injection efficiency. a) If the TiO_2 conduction band energy E_{CB} is significantly higher than the excited state E_{LUMO} of the dye, electron injection is restricted. b) The conduction band energy may be lowered electrostatically by adsorbing small positive ions (e.g. H^+ or Li^+) on the TiO_2 surface. This enables efficient injection, but with the expense that the open circuit voltage of the cell may be lower due to smaller E_{CB}-E_{redox} energy difference (see Chapter 3.2).

$$\eta_{\mathrm{COL},\delta}(x) = \frac{\cosh\left(\frac{d-x}{L}\right)}{\cosh\left(\frac{d}{L}\right)} \tag{25}$$

Eq 25 tells us essentially that the probability of the photogenerated electrons to reach the collecting contact prior to their recombination is the higher the closer to the contact they are generated (Figure 8a).

The overall collection efficiency is simply the weighted average of the (spatial) collection efficiencies of electrons generated in the photoelectrode film according to a profile $f_{\mathrm{LH}}(x)$, $0 < x < d$

$$\eta_{\mathrm{COL}} = \frac{\int_0^d f_{\mathrm{LH}}(x)\eta_{\mathrm{COL},\delta}(x)dx}{\int_0^d f_{\mathrm{LH}}(x)dx} \tag{26}$$

Figure 8b shows the effect of film thickness on η_{COL} in different cases. According to the Beer-Lambert law, the generation profile is determined by the absorption coefficient of the film (α) and the direction of illumination. The case of uniform generation corresponds to weakly absorbed light, whereas localized generation at the far edge of the film ($x = \xi = d$) corresponds to strongly absorbed light incident from the CE side.

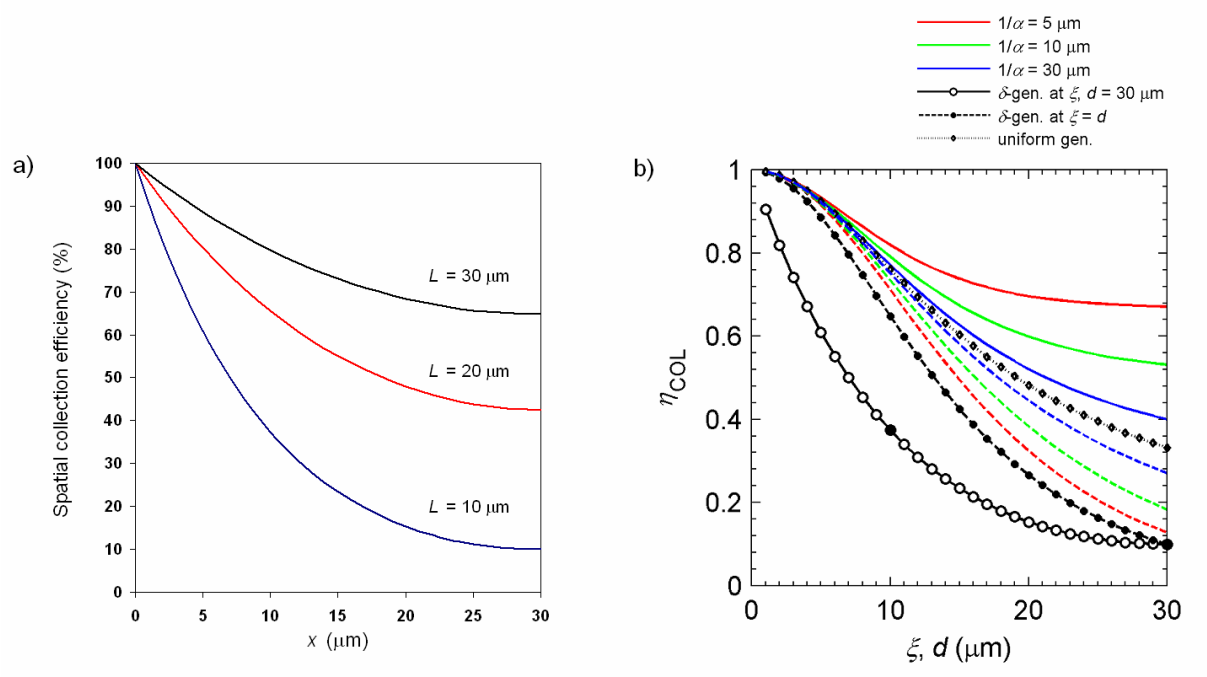

Figure 8. a) Effect of electron diffusion length (L) on the spatial electron collection efficiency in a 30 μm thick photoelectrode film. b) Effect of film thickness (d), light absorption coefficient (α), and illumination direction on η_{COL} when L = 10 μm. Continuous lines: PE illumination; dashed lines: CE illumination. Shown is also the purely theoretical case of localized generation at $x = \xi$ when d = 30 μm. [118]

The general feature is that, the shorter L is compared to d, the more sensitive is η_{COL} to the generation profile that determines the average distance the electrons have to travel to reach the collecting contact. When $L >> d$, $\eta_{COL} \approx 100$ % irrespective of the generation profile and the fill thickness.

Similar spatial quantities can be defined for the quantum efficiencies of IPCE and electron generation as well. Note that the denominator in eq. 26 is the total light harvesting efficiency (eq 16). Eq. 26 can thus be written as

$$\eta_{COL}\eta_{LH} = \int_0^d f_{LH}(x)\eta_{COL,\delta}(x)dx \tag{27}$$

and hence η_{IPCE} (eq 12) as

$$\eta_{IPCE} = \eta_{INJ}\int_0^d f_{LH}(x)\eta_{COL,\delta}(x)dx \tag{28}$$

If also η_{INJ} needs to be considered position-dependent, we have

$$\eta_{IPCE} = \int_0^d f_{LH}(x)\eta_{INJ}(x)\eta_{COL,\delta}(x)dx \tag{29}$$

This implies the definition of the *spatial IPCE*, f_{IPCE}:

$$\eta_{IPCE} = \int_0^d f_{IPCE}(x)dx \tag{30}$$

$$f_{IPCE}(x) = f_{LH}(x)\eta_{INJ}(x)\eta_{COL,\delta}(x) \tag{31}$$

Similarly, the *spatial electron generation efficiency* f_{GEN} becomes

$$\eta_{GEN} = \int_0^d f_{LH}(x)\eta_{INJ}(x)dx \tag{32}$$

$$f_{GEN}(x) = f_{LH}(x)\eta_{INJ}(x) \tag{33}$$

3.2. Open circuit voltage

A theoretical upper limit for the open circuit voltage (V_{OC}) of the dye solar cell is given by the free energy of the electronic excitation of the dye, i.e. E_{LUMO}-E_{HOMO} energy difference (cf. Figure 1 and Figure 3). This energy corresponds to the edge of the absorption spectrum of the dye, and is ca. 1.8 eV for the common Ru based dyes. However, in practice the selective contacts to the HOMO and LUMO levels by the TiO_2 and the redox electrolyte respectively,

are less than ideal, which leads to losses in the free energy, and hence V_{OC} available at the external metallic contacts of the cell. These losses can be summarized as follows:

1. **Thermalization of injected electrons to the TiO_2 conduction band edge.** For efficient electron injection from the dye to TiO_2 the LUMO level of the dye needs to be at somewhat higher energy than the electron acceptor levels in the TiO_2 conduction band. While electrons can be injected to the TiO_2 from high energy (vibrationally) excited states [40-43], these hot electrons are rapidly thermalized to the bottom of the TiO_2 conduction band after injection. The loss of V_{OC} due to this energetically downhill process is approximately $(E_{LUMO}\text{-}E_{CB})/q_e$, and depends on the dye and the semiconductor in question.

2. **Dye regeneration.** To facilitate rapid regeneration of the oxidized dye, i.e. reduction of the dye to its ground state after electron injection, the redox energy level of the electrolyte needs to be somewhat above the HOMO level of the dye in order to provide sufficient driving force for the electron transfer. This energy difference leads to a V_{OC} loss of ca. $(E_{redox}\text{-}E_{HOMO})/q_e$, and depends on the dye and redox pair in question.

3. **Electron recombination.** At the steady state open circuit conditions the overall rates of electron injection and recombination are equal. As a result of this balance, a light intensity dependent electron concentration and corresponding electron Fermi level is established in the TiO_2. The electron Fermi level is measurable as electric potential at the photoelectrode contact and depends, besides light intensity, on the quantum efficiency of electron generation, the kinetic rate constant of the electron recombination, and the density of states in the semiconductor. Nevertheless, due to large density of states in the TiO_2 conduction band, the Fermi level is always somewhat below the conduction band edge, bringing rise to a V_{OC} loss of ca. $(E_{CB}\text{-}E_F)/q_e$.

As a result of these primary loss factors, the V_{OC} of the DSC corresponds to the difference between the electron Fermi-level in the TiO_2 and the redox level in the electrolyte

$$-q_e V_{OC} = E_F - E_{redox} \tag{34}$$

Other, normally minor factors affecting the photovoltage include:

1. Upward shift in the TiO_2 conduction band edge energy due to light induced electrostatic charging of the Helmholtz layer at the TiO_2-dye-electrolyte interface. This effect may be significant at very high light intensities where the electron concentration is high [21]. More importantly, the electrostatic charging can be used to purposely tune the $E_{LUMO}\text{-}E_{CB}$ difference by adsorbing ions and molecules at the surface of the TiO_2 thus modifying the electric field within the Helmholtz double layer [38,39].

2. Downward shift in the redox level of the electrolyte due to light induced charge separation (electron injection to TiO_2) and corresponding change in the relative concentrations of the redox pair in the electrolyte, as described by the Nernst's equation of equilibrium electrode potential [44]. Typically, this effect is expected to be negligible due to high concentration of the redox pair and the diluting effect of the bulk electrolyte in the cell.

3. Decrease of V_{OC} due to additional electron recombination *via* the substrate-electrolyte interface. This loss mechanism can be significant at low light intensities unless the photoelectrode substrate is particularly inactive to the electrolyte reduction reaction, and can be minimized by applying a recombination blocking layer on the substrate [45-48].

Substrate mediated recombination is a central topic of Publications III and IV that investigate the electrochemical function of stainless steel metal and ITO-PET plastic substrates, and their effect on the DSC performance.

3.3. Fill factor

In addition to the photocurrent and photovoltage limitations, the energy conversion efficiency of the dye solar cell is affected by its internal electrical resistance. This arises from the resistivity of the cell materials and the resistance of charge transfer at their interfaces that give rise to *voltage losses* V_k due to electric current flowing in the cell. These voltage losses, called "over-potentials" or "over-voltages" in the field of electrochemistry, act as to decrease the cell voltage from its open circuit value, and decrease the fill factor (FF) of the solar cell IV curve (see Chapter 4.4).

In other words, the solar cell IV curve can be written as

$$V_{\mathrm{CELL}}\left(i_{\mathrm{CELL}}\right) = V_{\mathrm{OC}} + \sum_k V_k\left(i_{\mathrm{CELL}}\right) \tag{35}$$

At the open circuit, the internal voltage losses are zero, since no current is flowing, and the cell produces its maximum photovoltage, V_{OC}, that corresponds to the maximum available free-energy of the photogenerated electrons ($-q_{\mathrm{e}}V_{\mathrm{OC}}$). Yet, no current is taken from the cell at the open circuit, and hence, all this free energy is constantly consumed in electron recombination reactions, generating heat. Also at the short circuit, all the free energy is consumed in the cell, but in this case mainly *via* electron thermalization to the Fermi level and generation of heat by current flow through the internal cell resistances. Between the open and short circuit extremes, when an external load with a finite resistance is connected to the cell, a fraction of the free energy (per unit time) is extracted from the cell and used in the external load, this fraction being highest in the maximum power point, while the rest is still lost due to generation of heat in the cell. Minimization of the internal cell resistance is therefore essential to the performance optimization of any solar cell. The origin and nature of the internal resistances in the DSC is discussed in relation to impedance spectroscopy in Chapter 4.3.

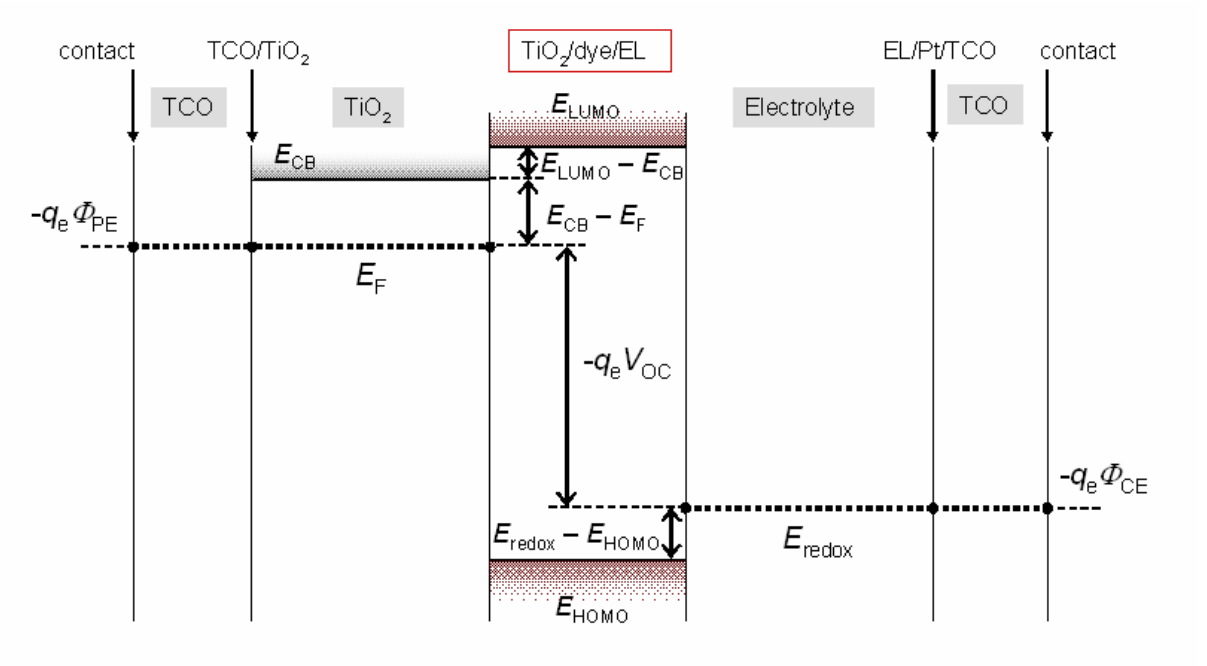

Figure 9. Origin of photovoltage in the dye solar cell. The open circuit voltage corresponds to the difference between electron Fermi energy in the TiO_2 and the redox level in the electrolyte. This is lower than the HOMO-LUMO energy of the dye due to loss of free energy of electors in the electron thermalization, dye regeneration, and electron recombination as discussed in the text.

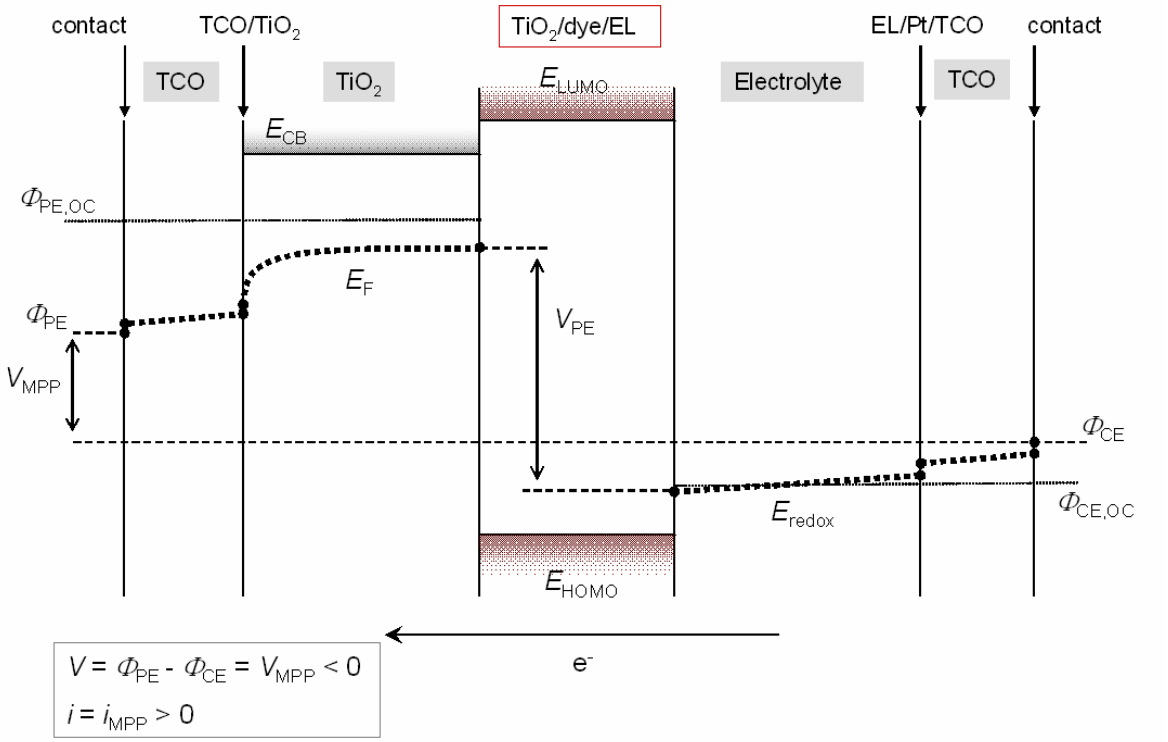

Figure 10. Spatial variation of the free energy of electrons in the dye solar cell at the maximum power point. Gradients and steps in the free energy are induced by the current flow in the resistive components and interfaces in the cell and decrease the cell voltage from its open circuit value $V_{OC} = \Phi_{PE,OC} - \Phi_{CE,OC}$ to $V_{MPP} = \Phi_{PE} - \Phi_{CE}$.

4. Performance characterization of dye solar cells

The goal of experimental solar cell performance characterization is to determine the light-to-electricity conversion efficiency and the factors that limit it in the cell under study. The key physical quantities that describe the cell performance are current, voltage, and the incident photon flux. The main performance characterization techniques used in this thesis quantify the relation between two of these three quantities by measuring the response of one quantity to the variation of the other. Depending on the technique this relation is measured either at the steady state or in dynamic (time or frequency dependent) condition (Figure 11).

The photovoltaic performance of the cell is measured by standard current-voltage (IV) characterization at fixed light intensity. The dynamic equivalent of this is electrochemical impedance spectroscopy (EIS). The ability of the cell to generate steady state photocurrent at fixed cell voltage (typically at short circuit) is determined by incident-photon-to-collected-electron spectroscopy (IPCE), and the dynamic equivalent of this technique is the intensity-modulated photocurrent spectroscopy (IMPS). The dynamic photovoltage response of the cell at fixed current is measured by intensity-modulated photovoltage spectroscopy (IMVS). Finally, optical characterization is used to determine how many of the incident photons at given light wavelength are actually absorbed by the dye molecules, i.e. to quantify the purely optical performance of the cell.

The following Chapters give first a brief description of the standard photovoltaic and optical characterization of the dye solar cells (the IPCE was discussed already in Chapter 3.1). More detailed introduction is given thereafter to the advanced dynamic techniques EIS, IMPS, and IMVS, and their relation with each other.

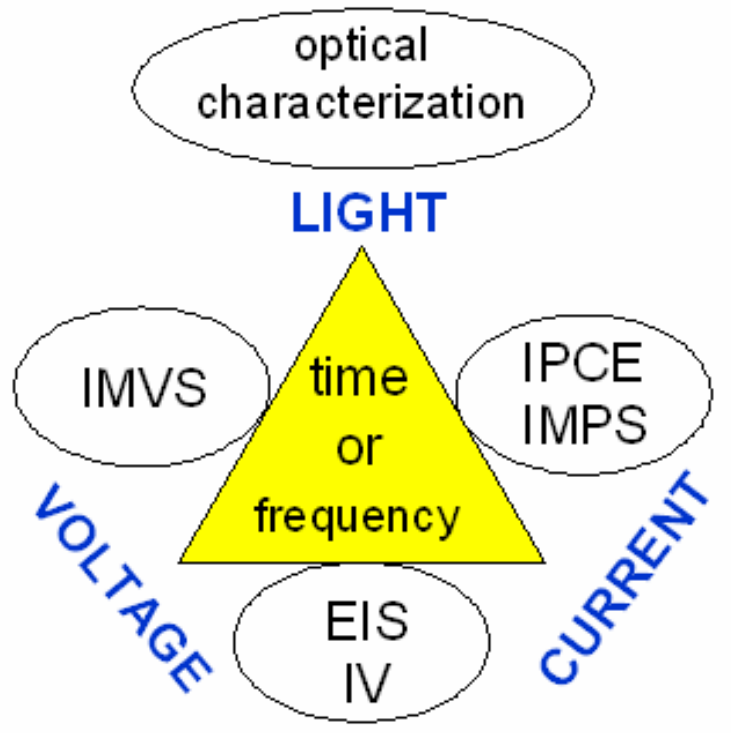

Figure 11. Relation between different dynamic and steady state optical and electrical characterization techniques of the dye solar cells.

4.1. Photovoltaic characterization

The basic photovoltaic characterization involves measuring the steady state IV curve of the cell at (or close to) the Standard Reporting Conditions (SRC): 1000 W/m^2 light intensity with spectral distribution according to the AM1.5G standard solar spectrum, and cell temperature 25 ºC. While this is quite straightforward, certain additional practical issues should be kept in mind to obtain reliable IV characterization of DSCs.

The high capacitance of the nanostructured photoelectrode and slow mass transport in the electrolyte make the response time of the DSC long. To guarantee that the measured IV data corresponds to steady state cell operation the IV curve needs to be recorded with sufficiently slow voltage sweep rate. The suitable sweep rate needs to be determined in practice as it depends on the type of cell and the used light intensity. A practical way to avoid errors is to measure several back-and-forth voltage sweeps in a cycle. If the data displays significant hysteresis, the sweep rate needs to be reduced. Cyclic IV data showing minor hysterisis may also be averaged to estimate the steady state data [49]. The cyclic measurement is also effective in revealing possible drift during the experiment, due for example to warming up of the cell or light-induced changes in the cell chemistry. A stabilization period in the beginning of the measurement may be needed to reach stable and repeatable steady state IV data (Figure 12).

Routine solar cell measurements are performed with artificial light sources called solar simulators. The spectral irradiance of the light source is preferentially close to the AM1.5G standard spectrum. In practice, the light spectrum differs to a certain extent from the standard solar spectrum and introduces a systematic error in the solar cell performance evaluation. This

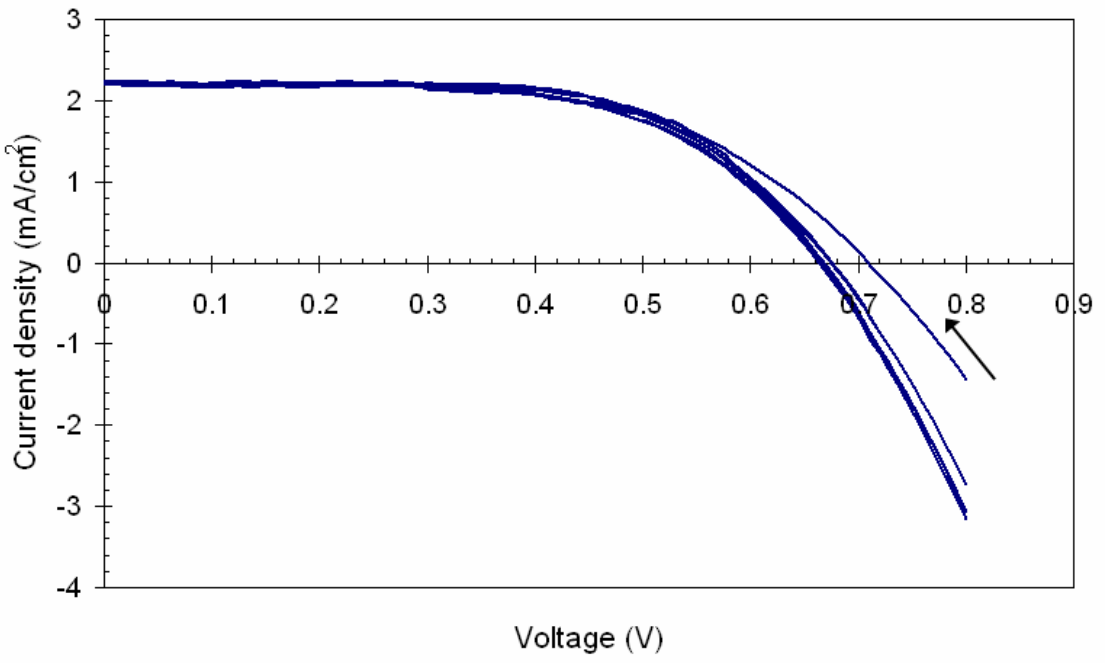

Figure 12. Demonstration of the importance of cyclic measurement for detecting drift in IV characterization of a dye solar cell. This measurement was started soon after placing the cell under 1000 W/m^2 illumination in a solar simulator. The first IV sweep starting at 0.8 V yielded considerably higher open circuit voltage than the subsequent sweeps. The likely reason for this was gradual warming-up of the cell under the high light intensity due to absence of cooling. Only after a few cycles was repeatable data with no hysteresis obtained.

error, called *spectral miss-match error* [50], can be accounted for by correcting the solar cell current densities measured with simulated light ($i_{TEST,SIM}$) to correspond to the standard solar spectrum ($i_{TEST,STD}$) by dividing measured current densities with the correction factor called *spectral miss-match factor*, *M*.

$$i_{TEST,STD} = \frac{i_{TEST,SIM}}{M} \tag{36}$$

The spectral miss-match factor is defined as [50]

$$M = \frac{\int E_{SIM}(\lambda) S_{TEST}(\lambda) d\lambda \int E_{STD}(\lambda) S_{REF}(\lambda) d\lambda}{\int E_{STD}(\lambda) S_{TEST}(\lambda) d\lambda \int E_{SIM}(\lambda) S_{REF}(\lambda) d\lambda} \tag{37}$$

where E_{SIM} is the spectral irradiance ($Wm^{-2}\mu m^{-1}$) of the solar simulator light source, E_{STD} the standard solar spectral irradiance (AM1.5G), S_{REF} the spectral response (A/W) of the reference solar cell used for setting the solar simulator light intensity, and S_{TEST} the spectral response of the solar cell under test. Eq. 37 implies that whenever the solar simulator spectrum differs significantly from the standard spectrum, the spectral miss-match factor *M* depends on the spectral response of the studied solar cell. Hence, for most accurate results the miss-match correction should be done separately for each solar cell sample. In principle, also the cell voltage is subject to similar spectral error but to a much smaller extent and is therefore normally not corrected for.

In this work, the solar cell measurements at TKK were performed using an in-house built solar simulator based on projector halogen light bulbs, the spectral irradiance of which was measured by a spectroradiometer. The solar simulator light intensities were measured and set using a reference silicon solar cell (PV Measurements, Inc.) that had an optical filter to mimic the spectral response of a typical dye solar cell. The spectral response of the reference cell was calibrated by NREL. For simplicity, and due to unavailability of a spectral response measurement system, a constant miss-match factor (1.06) calculated based on typical DSC spectral response data, was used for all measured cells. The solar simulator used in the work done at KTH was calibrated by determining *M* by outdoor measurements of a typical DSC, and using a pyranometer as a reference device that transferred the calibration between the outdoor and simulator measurements.

4.2. Optical characterization

Optical characterization of the dye solar cell is complicated by the relatively thick multilayered structure of the cell and scattering of light by the nanostructured photoelectrode film. To reach reliable quantitative results, all scattered light should be detected in the optical reflectance and transmittance measurements. This requires using a spectrophotometer equipped with an integrating sphere and minimizing the loss of scattered light by preparing the optical samples on thin glass substrates [51,52]. For example in Publication V, optical samples of pressed TiO_2 films were prepared onto microscope cover glass slides.

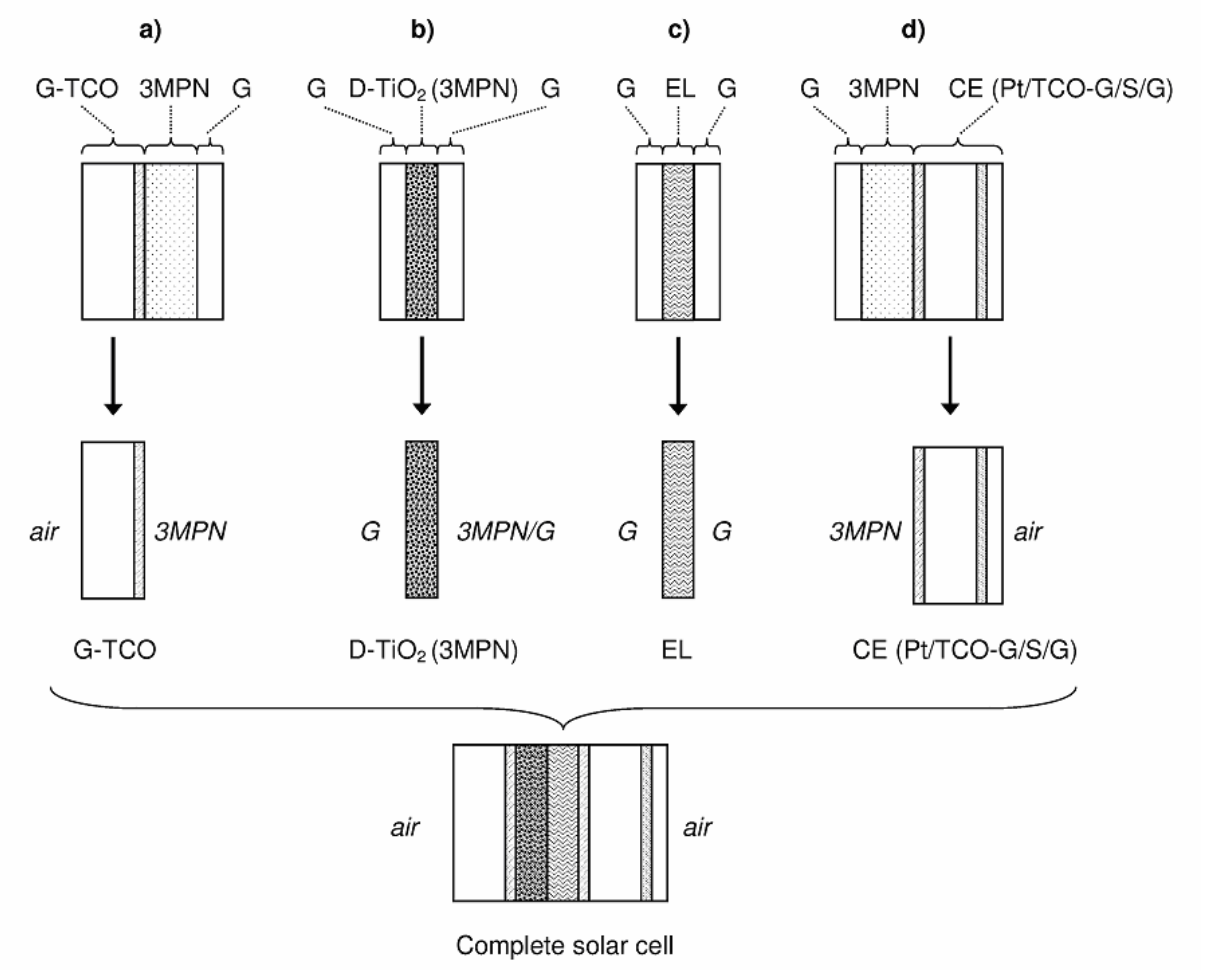

Figure 13. Quantitative estimation of η_{LH}: 1. optical measurement of cell components, 2. extraction of individual component data, 3. calculation of η_{LH}.

Another complication arises from the solvatochromic properties of the dye: its molar absorption spectrum depends on the solvent surrounding it, e.g. [53]. This can be accounted for by preparing optical sample cells where the dyed TiO_2 film is surrounded by the same solvent as used in the actual solar cells [52]. In practice, the sample film deposited on the thin glass substrate is faced with another thin glass substrate and the space in between is filled with the solvent. To allow later measurements the optical cell can be sealed permanently using a frame of thermoplastic foil. Reflectance and transmittance spectra of the other cell components, namely the photoelectrode substrate, the free electrolyte layer and the counter electrode can be measured in the same way (Figure 13).

To extract accurate data that corresponds to the sample film only, the measured reflectance and transmittance spectra of the optical cell needs to be interpreted using an optical model that accounts for the multiple reflection of light in the multilayered cell structure. However, correcting the data only for (one) reflection of light at the front air-glass interface of the optical cell may be sufficient for most purposes.

The absorptance of the dye-sensitized TiO_2 photoelectrode film depends essentially on the total amount of dye adsorbed in the film. The relative amount of dye in different films can be determined by a dye desorption experiment using some extra photoelectrode samples reserved for this purpose.

After washing off excess (non-adsorbed) dye from the dyed TiO_2 films by ethanol and drying briefly with a tissue paper the dye is desorbed from the film by soaking it for a few minutes in a 10 mM aqueous NaOH solution of known volume. The absorbance spectrum of this solution is then measured with standard UV-VIS spectrometry, and the peak absorbance (near 500 nm) is used as measure of the relative amount of dye in the solution.

The absorbance $A(\lambda)$ of the desorption solution measured in a cuvette with optical length l depends on the molar absorption coefficient $\varepsilon(\lambda)$ and concentration c_{sol} of the dye in the solution. The concentration depends further on the volume of the desorption solution V_{sol}, the volume of the TiO_2 film V_{film} and the average dye concentration c_{film} in the TiO_2 film as

$$A(\lambda) = \frac{\varepsilon(\lambda) l}{\ln 10} c_{sol} = \frac{\varepsilon(\lambda) l}{\ln 10} \frac{V_{film}}{V_{sol}} c_{film} \tag{38}$$

The total absolute concentration of the dye in the film can thus be determined based on the measured absorbance if $\varepsilon(\lambda)$, V_{film}, and V_{sol} are known. However, in most cases one is interested only in the relative dye concentration in different samples, in which case knowledge on the absolute value of $\varepsilon(\lambda)$ is not necessary.

4.3. Electrochemical impedance spectroscopy

Our understanding of the photovoltaic function of the dye solar cell may be considered sufficient if we are able to formulate a mathematical model that with a fixed set of parameter values correctly describes the steady state IV curve of the cell at different operating conditions of practical relevance. A good model is detailed enough so that it can explain the effects of measurable material properties and structure of the cell on the cell performance. Yet the model has best practical value if it is simple enough to provide an intuitive picture of the electrical function of the cell and allows straightforward calculations and fitting to experimental data using analytical expressions. A particularly useful approach with this respect is *equivalent circuit modeling* that is closely related to the *electrochemical impedance spectroscopy* (EIS).

In EIS the solar cell is set to desired steady state operating condition (light intensity, temperature, etc.) and polarized to a certain point (V_{CELL}, i_{CELL}) along its IV curve (Figure 14). A small amplitude harmonic AC voltage modulation $V_{\mathrm{AC}}(\omega,t)$ is superimposed on the DC cell voltage and the resulting harmonic AC current $i_{\mathrm{AC}}(\omega,t)$ response is recorded, while varying the modulation frequency over a certain frequency range. This yields information on the solar cell impedance Z_{CELL}

$$Z_{\mathrm{CELL}}(\omega) = \frac{V_{\mathrm{AC}}(\omega,t)}{i_{\mathrm{AC}}(\omega,t)} \tag{38}$$

that is a function of the (angular) frequency ω of the AC modulation. Hence the notions *impedance spectroscopy* and *impedance spectrum*.

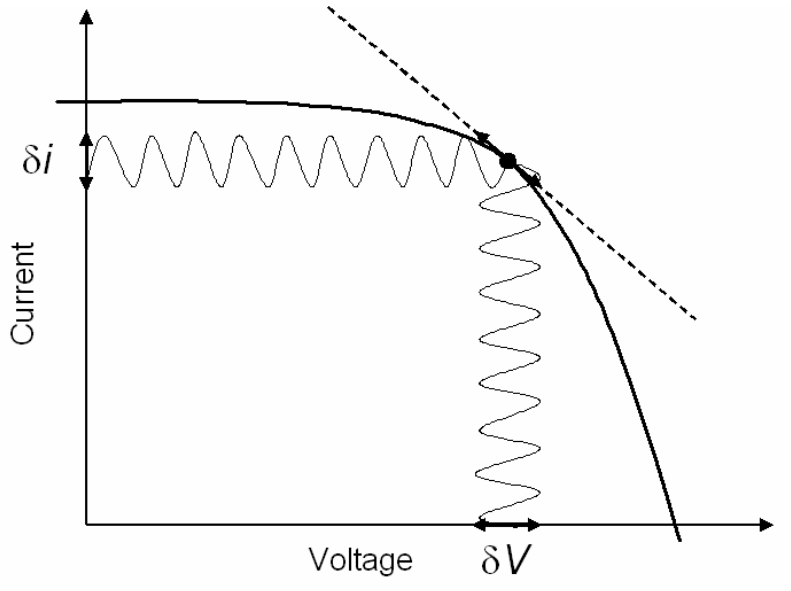

Figure 14. In impedance spectroscopy, the differential resistance of the solar cell at certain point along its IV curve is measured as a function of frequency.

Due to the small amplitude of the AC voltage modulation, typically 10 mV, the solar cell impedance can be regarded as the frequency dependent differential resistance of the IV curve (Figure 14). In the limit of zero frequency the total cell impedance corresponds to the slope of the IV curve at the point (V_{CELL}, i_{CELL})

$$Z_{CELL}(\omega = 0) = R_{CELL} = \frac{\partial V_{CELL}}{\partial i_{CELL}} \tag{39}$$

Since the IV curve of the cell is non-linear, as well as temperature and light intensity dependent, the impedance of the solar cell is a function of the operating point (V_{CELL}, i_{CELL}) and the operating conditions of the cell.

The impedance characteristics of the DSC can be described in a convenient and informative way with an equivalent circuit [54-59]. In equivalent circuit modeling individual cell components and their interfaces are assigned with resistances that correspond to hindrance of charge transport in the material phases and charge transfer across their interfaces, whereas charge accumulation is accounted for by capacitive elements.

Figure 15a shows the general equivalent circuit impedance model of a typical dye solar cell [56,59,60]. The impedance components in the model are:

- r_T (Ωm) : Resistivity of electron transport in the nanostructured TiO_2 photoelectrode film. The total transport resistace of the film is $R_T = r_T d$ (Ωcm^2), where d is the film thickness.
- r_{CT} (Ωm^3) : Charge transfer (recombination) resistance at the TiO_2-dye-electrolyte interface per unit volume of the porous photoelectrode. The total recombination resistance of the film is $R_{CT} = r_{CT}/d$ (Ωcm^2).
- c_μ (Ωm^{-3}) : (Chemical) capacitance per unit volume of the photoelectrode.
- R_{CO} (Ωm^2) and C_{CO} (Fm^{-2}) : Contact resistance and capacitance at the interface between the conducting substrate and the TiO_2 photoelectrode film.

- R_{SU} (Ωm^2) and C_{SU} (Fm^{-2}) : Charge transfer resistance and double layer capacitance at the substrate-electrolyte interface.
- R_{CE} (Ωm^2) and C_{CE} (Fm^{-2}) : Charge transfer resistance and double layer capacitance at the counter electrode-electrolyte interface.
- Z_D (Ωm^2) : Mass transport impedance at the counter electrode due to ionic diffusion in the electrolyte.
- R_S (Ωm^2) : Ohmic series resistance of the cell including contributions from the sheet resistance of the conducting substrates, electrolyte resistivity and external electric contacts and wiring of the cell.

Note that the photocurrent generation enters the model *via* current source elements i_{ph} (Am^{-3}) distributed along the photoelectrode film (Figure 15a-b), and that the model neglects resistivity of the electrolyte in the pores of the film. When defined in the units of Ωcm^2, the values of the model parameters are independent of the active area of the solar cell. Correspondingly, the values of r_T, r_{CT}, and c_μ are independent of the photoelectrode thickness. An exception is the series resistance R_S that naturally depends on the cell geometry, but is nevertheless reported in Ωcm^2 by scaling with the active area of the cell.

Fitting the equivalent circuit model to measured impedance spectrum gives estimates for the individual resistances, capacitances, and other model parameters. This is most conveniently done using impedance analysis software specifically designed for this purpose, e.g. Zview2 by Scribner Associates, Inc. A typical equivalent circuit fitting program has a handy user interface for constructing the equivalent circuit by connecting together different impedance elements, and a non-linear least squares routine for fitting the model to the experimental data. Alternatively, an analytical expression for the impedance can be derived using the basic methods of AC electric circuit analysis and used directly with any mathematical software.

In addition to the simple resistors and capacitors, the equivalent circuit model of DSC (Figure 15) contains two special impedance components: the so-called transmission line impedance Z_{TiO2} of the nanostructured TiO_2 photoelectrode film consisting of the network of the elements r_T, r_{CT}, and c_μ, and the mass transport impedance Z_D at the counter electrode [56,59,60]. The ideal capacitors are also typically replaced with so-called constant phase elements (CPE) that may be regarded as non-ideal capacitors.

The power of EIS can be appreciated by comparing the steady state (DC) and dynamic (AC) response of the equivalent circuits in Figure 15. Remember that a capacitive element conducts only AC current and its impedance decreases with increasing frequency. Hence, in the limit of zero frequency (steady state) the equivalent circuits of Figure 15a and Figure 15c reduce to those in Figure 15b and Figure 15d respectively. I.e. the parallel capacitances can be removed since their impedances are infinite at the steady state. The overall steady state (DC) resistance of the cell is therefore that of the resistor network in Figure 15d

$$R_{CELL} = R_{PE} + R_S + R_D + R_{CE} \tag{40}$$

where

$$R_{PE} = \frac{R_{SU}\left(R_{CO} + R_{TiO2}\right)}{R_{SU} + R_{CO} + R_{TiO2}} \tag{41}$$

a) Under illumination

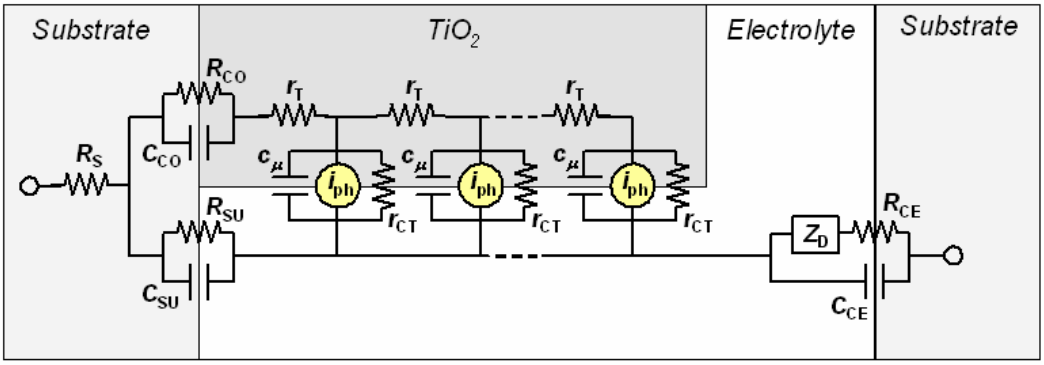

b) Under illumination, steady state

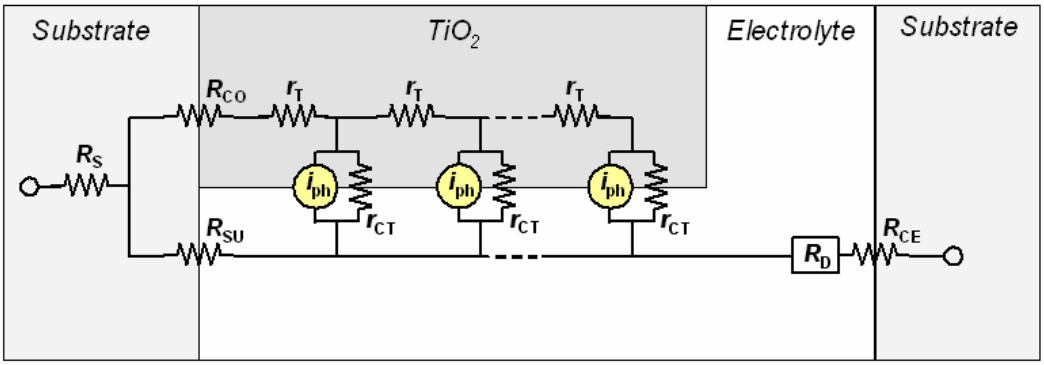

c) In the dark

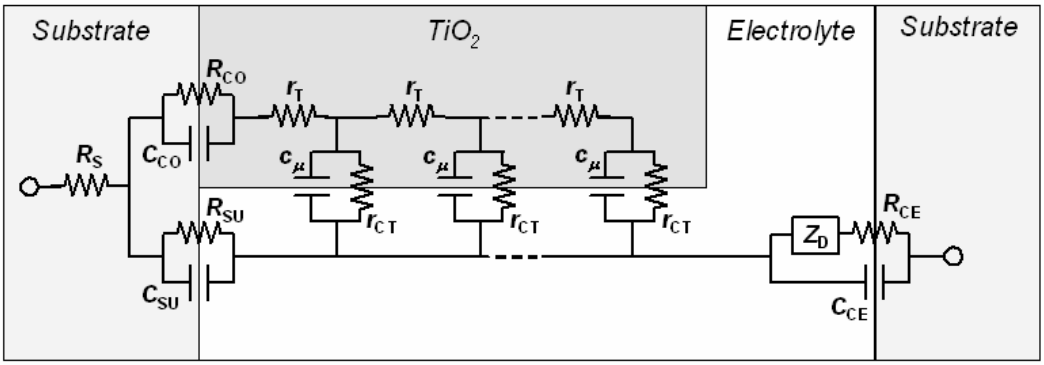

d) In the dark, steady state

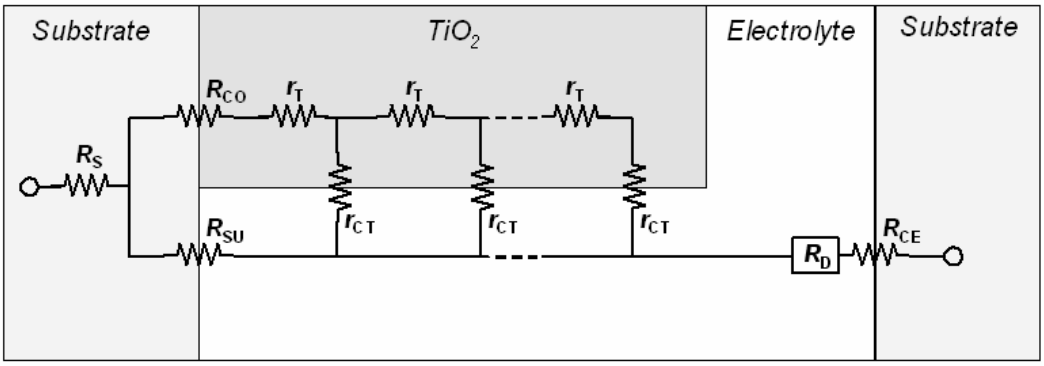

Figure 15. Equivalent circuit models of the dye solar cell at different conditions.

is the combined resistance of the photoelectrode film and its substrate and R_{TiO2} is the DC resistance of the photoelectrode film according to the transmission line model [56,59,60]. On the other hand, at sufficiently high frequencies all the capacitive elements in the cell are effectively short circuited and the impedance of the cell reduces to R_S, the Ohmic series resistance of the cell.

The beauty of EIS is that between these high and low frequency extremes, the impedance spectrum of the cell may contain frequency resolved information that allows determining, by model fitting to data, not only the limiting values R_S and R_{CELL}, but also all the individual (partial) cell resistances that contribute to R_{CELL} according to the equivalent circuit model (eq 40). The reason for this is that whenever a resistance component R is coupled to a parallel capacitance C, it gives rise to an *impedance arc* in the complex plane plot centered at the *characteristic frequency* $f^* = (2\pi\tau)^{-1}$, where τ is the corresponding *characteristic (RC) time-constant* $\tau = RC$. At much lower frequencies than f^* the impedance of the RC parallel connection equals R, whereas at frequencies much higher than f^* the resistance becomes short-circuited by its parallel capacitance and the RC-impedance approaches zero.

Coincidently, due to the materials and structure of the standard DSC, all of its important impedance components exhibit largely different time constants and can thus be separated in the impedance spectrum. This enables fractioning the total internal cell resistance of the DSC into the partial contributions from the different cell components and interfaces by EIS.

As an example, Figure 16 shows typical impedance spectra of DSCs with TiO_2 photoelectrode films prepared with the compression technique either with ("Sintered", "S") or without ("Pressed-only", "P") additional heat treatment at 450 ºC for 1 hour. In both cases the resistance components R_S, R_{CE}, R_{TiO2}, and R_D can be distinguished in the complex plane impedance plot. In the case of the sintered film, the impedance arc corresponding to R_{TiO2} is close to a symmetric semicircle. This is an indication of the condition that the electron diffusion length L is longer than the TiO_2 film thickness d, and occurs when the electron transport resistance $R_T = r_T d$ is negligible compared to the electron recombination resistance $R_{CT} = r_{CT}/d$ [60]. In contrast to this, in the pressed-only cell the R_{TiO2} impedance arc is strongly distorted taking the shape of the so-called Gerischer impedance. This is obtained when $L < d$, corresponding to $R_T > R_{CT}$ [60]. A long electron diffusion length ($L >> d$) is a prerequisite to a high performance solar cell, and in this case, the pressed-only cell fails to meet this criterion. Indeed, the cells of this type were found to suffer from severe photocurrent limitations due to too short L and correspondingly low electron collection efficiency (Publication V).

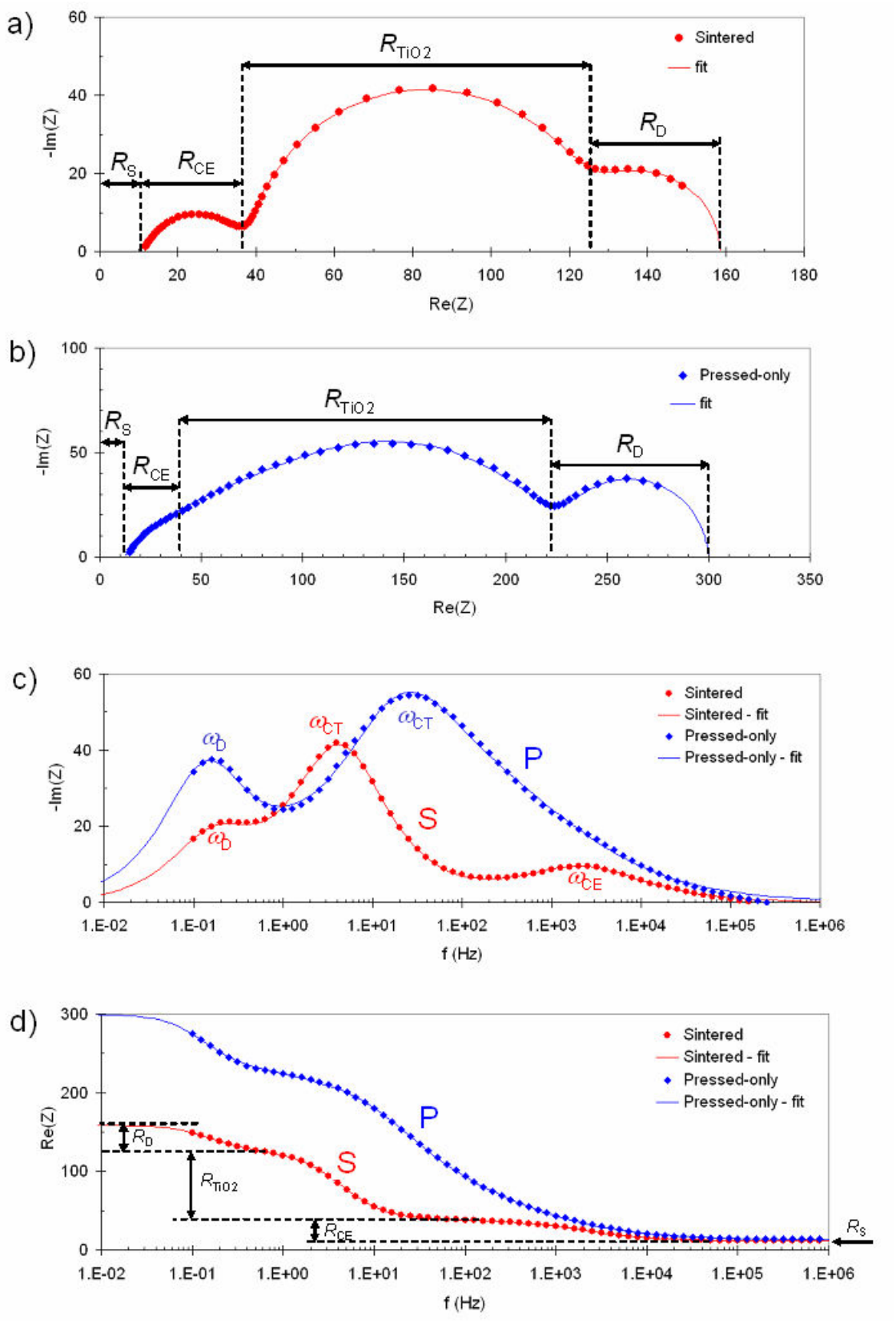

Figure 16. Examples of impedance spectra of dye solar cells measured at the open circuit conditions under illumination. a) Sintered TiO_2 film, b) pressed-only TiO_2 film, c) the imaginary part of the impedance, d) the real part of the impedance. Film thickness d = 22 μm. The open circuit voltage was 0.791 V for the sintered cells and 0.743 V for the pressed-only cells.

4.4. Analysis of the IV curve based on impedance

In addition to EIS data analysis, the equivalent circuit can be used as a basis for analytical modeling of the solar IV curve. Its relation to the differential cell resistance R_{CELL}, measurable with EIS as a function of current density ($i = i_{\mathrm{CELL}}$) is

$$V_{\mathrm{CELL}}(i_{\mathrm{CELL}}) = V_{\mathrm{OC}} + \int_0^{i_{\mathrm{CELL}}} R_{\mathrm{CELL}}(i)di \tag{42}$$

According to eq. 40, R_{CELL} is the sum of the internal cell resistances including the photoelectrode

$$R_{\mathrm{CELL}}(i) = \sum_{k=\mathrm{S,D,CE,PE}} R_{\mathrm{k}}(i) \tag{44}$$

These resistances give rise to *voltage losses* V_{k} over the components due to electric current flowing in the cell as discussed in Chapter 3.3. The solar cell IV curve can thus be written as

$$V_{\mathrm{CELL}}(i_{\mathrm{CELL}}) = V_{\mathrm{PE}}(i_{\mathrm{CELL}}) + \sum_{k=\mathrm{S,D,CE}} V_k(i_{\mathrm{CELL}}) \tag{45}$$

where

$$V_{\mathrm{PE}}(i_{\mathrm{CELL}}) = V_{\mathrm{OC}} + \int_0^{i_{\mathrm{CELL}}} R_{\mathrm{PE}}(i)di \tag{46}$$

$$V_{\mathrm{k}}(i_{\mathrm{CELL}}) = \int_0^{i_{\mathrm{CELL}}} R_{\mathrm{k}}(i)di \tag{47}$$

Note that in eqs. 42 we have chosen the open circuit state ($i_{\mathrm{CELL}} = 0$, $V_{\mathrm{CELL}} = V_{\mathrm{OC}}$) as a known reference point. This is a practical choice since at the open circuit all other parts of the cell except the photoelectrode are in equilibrium, i.e. non-polarized ($V_{\mathrm{k}} = 0$). Figure 17 clarifies the definitions of the internal voltage losses and currents in the DSC.

Eqs 45 and 47 describe the factors that determine the IV characteristics of the dye solar cell. Light absorption at the photoelectrode generates an open circuit voltage V_{OC}. Connecting a load resistance in the cell allows extracting current from the cell with the expense that the cell voltage decreases. This voltage drop arises firstly from the IV characteristics of the photoelectrode and secondly from the voltage losses due to the additional internal resistances. Hence, in the performance optimization of the DSC it is necessary both to optimize the photoelectrode function and to minimize the internal cell resistances.

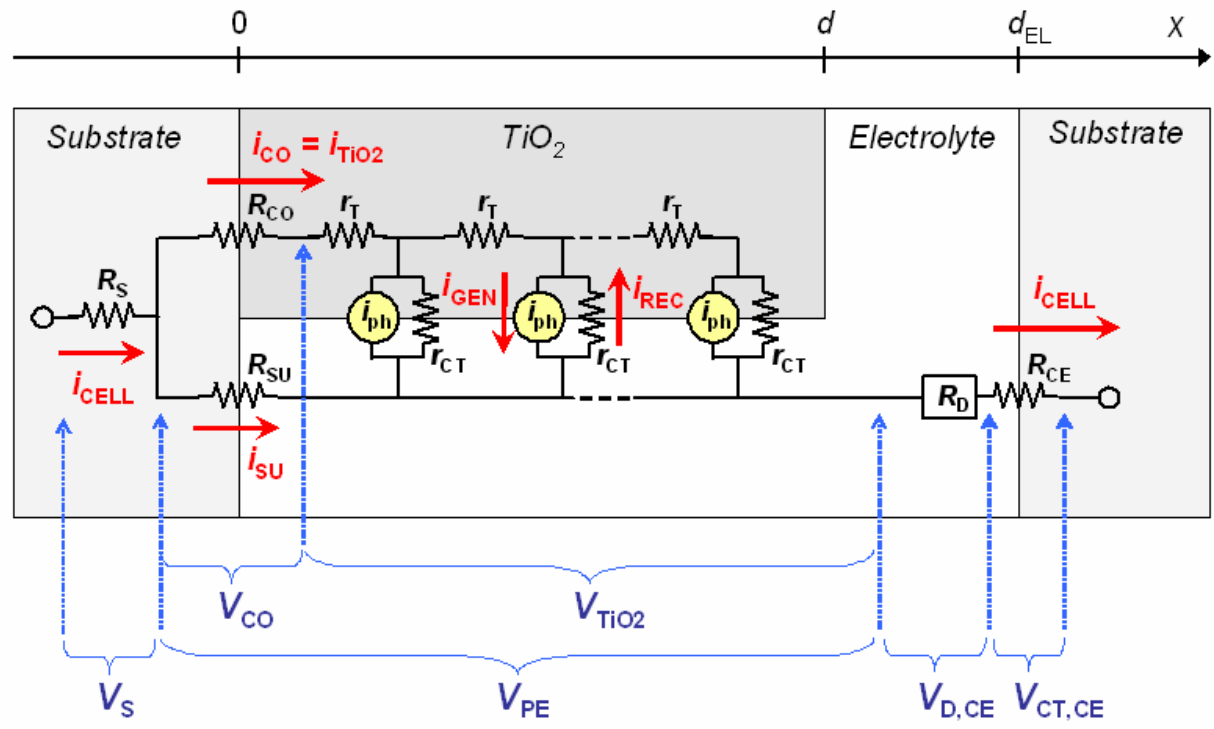

Figure 17. Overview of the internal voltages and currents in the dye solar cell.

4.5. Intensity modulated photocurrent and photovoltage spectroscopy

In addition to EIS important dynamic information of the dye solar cell operation can be obtained by measuring the response of the cell to small amplitude light intensity modulation. The two closely related experimental techniques based on this principle are called *intensity modulated photocurrent spectroscopy* (IMPS) and *intensity modulated photovoltage spectroscopy* (IMVS).

Like in EIS, in IMPS and IMVS the solar cell is first stabilized to desired steady state working conditions defined by the incident light intensity and cell temperature. In the IMPS experiment (Figure 18) the solar cell is held at fixed voltage (potentiostatic control) and the AC current response $i_{\mathrm{CELL,AC}}(\omega,t)$ of the cell is recorded and compared with the simultaneous AC light intensity signal $\Phi_{\mathrm{AC}}(\omega,t)$ giving the IMPS transfer function of the cell

$$F^{*}_{\mathrm{IMPS,CELL}}(\omega) = \frac{i_{\mathrm{CELL,AC}}(\omega,t)}{q_{\mathrm{e}}\Phi_{\mathrm{AC}}(\omega,t)} \qquad \text{(at potentiostatic control)} \qquad (48)$$

In the IMVS experiment (Figure 18) the solar cell is held at fixed current (galvanostatic control) and the AC voltage signal $V_{\mathrm{CELL,AC}}(\omega,t)$ is recorded against the intensity modulation yielding the IMVS transfer function defined as

$$F^{*}_{\mathrm{IMVS,CELL}}(\omega) = \frac{V_{\mathrm{CELL,AC}}(\omega,t)}{q_{\mathrm{e}}\Phi_{\mathrm{AC}}(\omega,t)} \qquad \text{(at galvanostatic control)} \qquad (49)$$

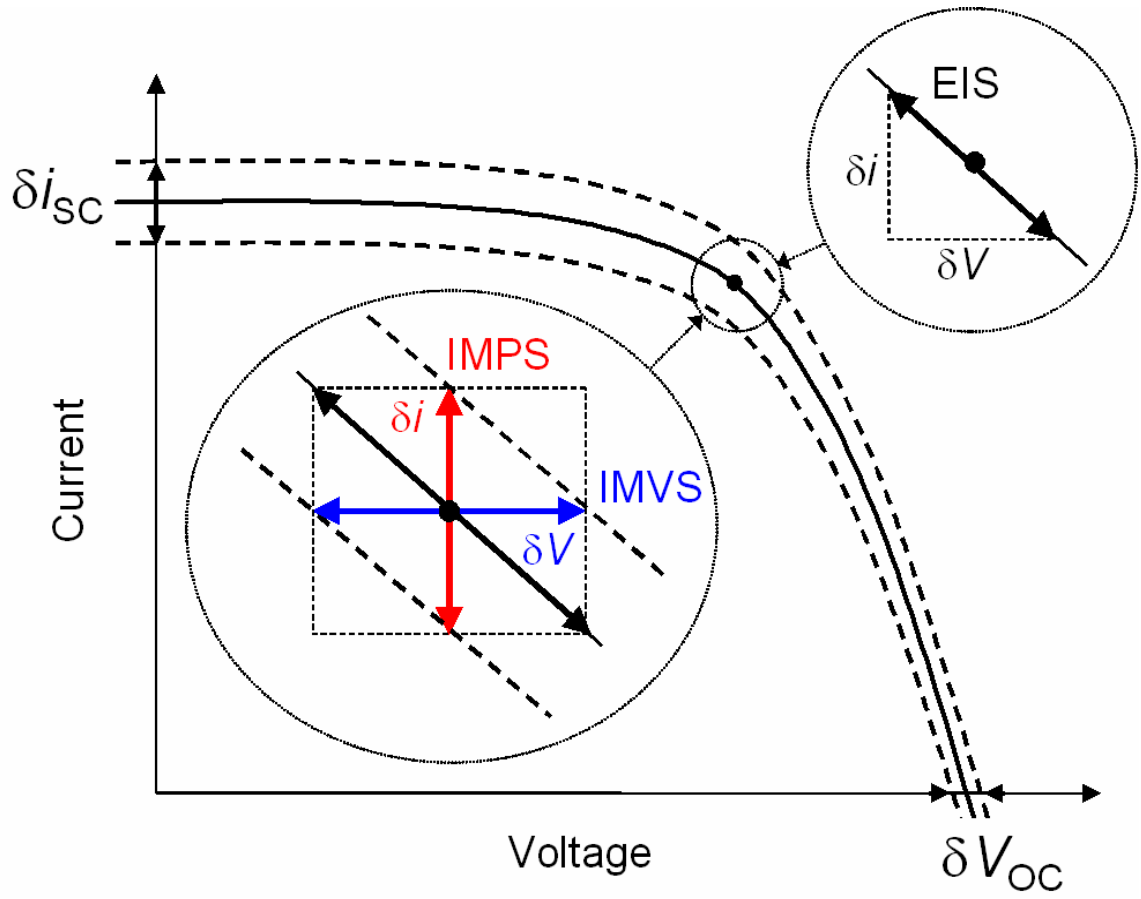

Figure 18. Relation between IMPS, IMVS, EIS and the steady state solar cell IV curve.

The source for the DC illumination may be a solar simulator, some other "white light" source, or a monochromatic light source such as a high power LED. The intensity modulation is most conveniently implemented using an LED with desired wavelength. In the simplest case a single LED provides both the background intensity and its small amplitude modulation. The IMPS and IMVS transfer functions are measured by feeding the measured incident light intensity and the cell current (IMPS) or voltage (IMVS) signals as inputs to a lock-in amplifier or a frequency response analyzer (FRA).

Both the IMPS and IMVS spectra display (usually) only one characteristic frequency ω_{IMPS} and ω_{IMVS} corresponding to time constants $\tau_{IMPS} = \omega_{IMPS}^{-1}$ and $\tau_{IMVS} = \omega_{IMVS}^{-1}$ (Figure 19). Interpretation of these time constants requires a mathematical model of the dynamic photocurrent and photovoltage response of the cell. The model of choice for this purpose has been the time-dependent standard diffusion model presented in the Appendix and analyzed in detail in Publication VI.

According to the standard diffusion model, the IMPS and IMVS time constants are related to the diffusion coefficient (D), lifetime (τ), diffusion length (L), and collection efficiency (η_{COL}) of electrons in the photoelectrode film of thickness d according to the following (approximate) relations

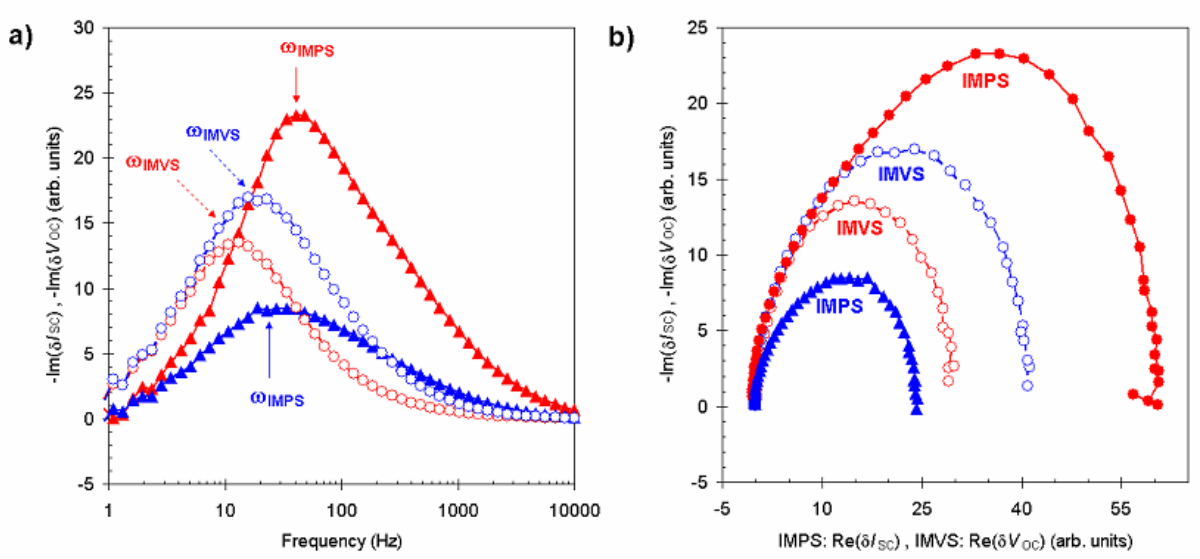

Figure 19. Examples of open-circuit-IMVS and short-circuit-IMPS spectra of pressed and sintered (red) and pressed-only (blue) dyed TiO_2 photoelectrodes. a) Imaginary part vs. frequency b) complex plane plot. The peaks in the imaginary part correspond approximately to the characteristic frequencies of electron transport (ω_{IMPS}) and recombination (ω_{IMVS}). In this case, electron transport appears to be faster (higher ω_{IMPS}) and the recombination slower (lower ω_{IMVS}) in the sintered films.

$$D \approx a \cdot \frac{d^2}{\tau_{IMPS}} \tag{50}$$

$$\tau \approx \tau_{IMVS} \tag{51}$$

$$L = \sqrt{D\tau} \tag{52}$$

$$\eta_{COL} \approx 1 - \frac{\tau_{IMVS}}{\tau_{IMPS}} \tag{53}$$

where $a \approx 0.393$ for very weakly absorbed modulated light. However, these relations are valid only in the limit of high electron collection efficiency and uniform generation profile. In the general case, exact analysis of the IMPS and IMVS spectra with the time-dependent diffusion model is required as discussed in Publication VI.

Another, more fundamental problem related to the dynamic characterization of dye solar cells has been pointed out theoretically by Bisquert and Vikhrenko [61]: the measured τ_{IMPS} and τ_{IMVS} *do not*, in fact, yield information (D and τ) relevant for the steady state cell performance. This is because both the dynamic photocurrent and photovoltage response of the cell is dominated (slowed down) by filling and emptying a large density of electron trap states in the semiconductor band-gap (Figure 20).

When electron trapping and de-trapping is much faster compared to the electron transport and recombination, as well as the light modulation, the electron concentration in the conduction band (n_{CB}) and localized traps states (n_{trap}) remain in common equilibrium with each other during the transient measurement, i.e. they a characterized by a common (modulated) Fermi-level E_F. Assuming this *quasi-static condition* [61], and further that the trap states do not

contribute to electron recombination and transport, the dynamically measured D_μ and τ_μ are related to the electron diffusion coefficient and lifetime of the conduction band electrons D and τ roughly as [61]

$$\tau_\mu \approx \left(\frac{\partial n_{\mathrm{CB}}}{\partial n_{\mathrm{trap}}} \right)^{-1} \tau \tag{54}$$

$$D_\mu \approx \left(\frac{\partial n_{\mathrm{CB}}}{\partial n_{\mathrm{trap}}} \right) D \tag{55}$$

In this special case, the electron diffusion length L_μ calculated from the dynamic D_μ and τ_μ *does*, in fact, correspond to its conduction band value L, since the factors $\partial n_{\mathrm{CB}}/\partial n_{\mathrm{trap}}$ in the above equations cancel each other when forming the product $D\tau$

$$L_\mu = \sqrt{D_\mu \tau_\mu} \approx \sqrt{D\tau} = L \tag{56}$$

Unfortunately, the validity of eq. 56 in realistic DSCs, to accuracy relevant for estimating their steady state η_{COL}, is presently unknown. Hence, the suitability of the prevalent dynamic techniques for estimating the L and η_{COL} based on D_μ and τ_μ is uncertain until they are verified experimentally against steady state data. This is an important and topical question of fundamental DSC research [62,63]. The present work makes a contribution to this question by presenting a method for estimating L based on steady state data (Publication V) and another method (Publication VI) for determining D_μ and τ_μ consistently with it, i.e. with eq. 56 (see Chapters 5.5 and 5.8 for further discussion).

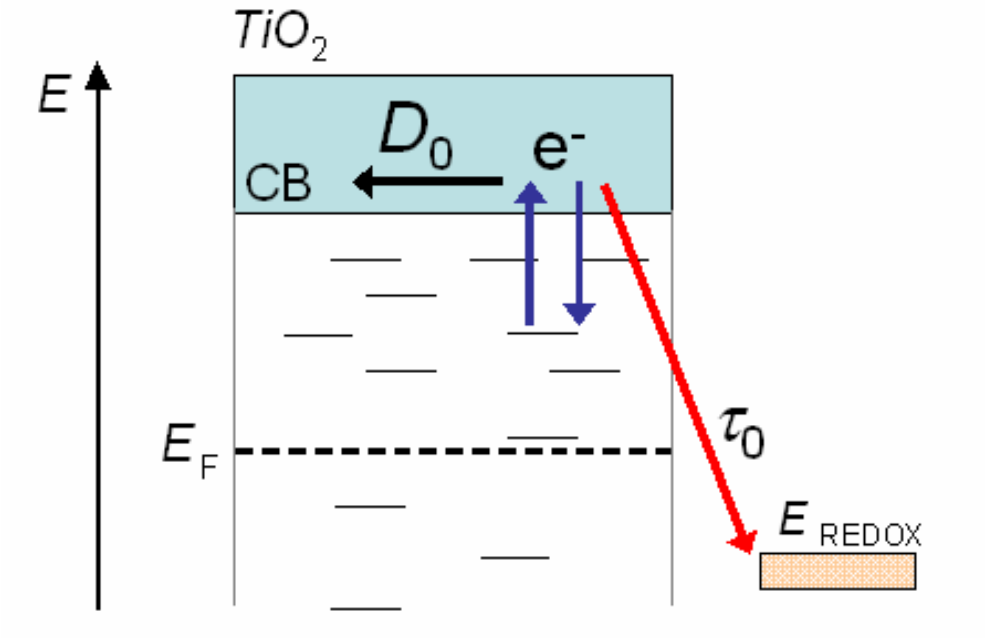

Figure 20. In the quasi-static conditions, dynamic displacement of the electron Fermi-level in the TiO_2, induced by modulation of the light intensity (IMPS, IMVS) or the cell voltage (EIS), is slowed down by the time required for charging and discharging the large capacitance associated with the localized band gap (trap) states in the TiO_2.

4.6. Relation between IMPS, IMVS and EIS

If the same light modulation is used both in the IMPS and IMVS experiments, the measured transfer functions are related to the impedance of the cell according to

$$Z_{\mathrm{CELL}}(\omega) = \frac{F^{*}_{\mathrm{IMVS,CELL}}(\omega)}{F^{*}_{\mathrm{IMPS,CELL}}(\omega)} \tag{57}$$

This can be readily seen by comparing eq. 38 with eqs. 48, and 49, and appears in the theoretical results of Bay and West [58]. Indeed, since the IMPS and IMVS transfer functions are measured at potentiostatic and galvanostatic conditions respectively, they constitute an orthogonal basis of the current-voltage space. When measured with the same light modulation amplitude, they are exactly the orthogonal components of the cell impedance. Figure 18 clarifies this issue. Note that this relation (eq 57) is fundamental, and hence, valid for any solar cell regardless of its properties and function.

The quantitative correspondence of the EIS, IMPS and IMVS transfer functions means that they contain similar dynamic information of the solar cell operation. For example, the voltage relaxation time constant of the photoelectrode, interpreted as electron lifetime, can be determined equally well with EIS or IMVS [54]. Also, the electron diffusion length that is often estimated by combining IMPS and IMVS data [64] can be determined alternatively by EIS [56,60]. Eq. 57 also means that it suffices to measure only two of the three transfer functions EIS, IMPS, and IMVS – the third follows from eq. 57.

In fact, combined IMPS, IMVS, and EIS performed at the same working conditions and analyzed in light of eq. 48 should be a fruitful approach to detailed performance characterization of DSCs. The additional degree of freedom introduced by the light intensity modulation in the IMPS and IMVS should facilitate better resolution of the dynamic characteristics of the cell compared to EIS only. This possibility has remained so far unexplored.

5. Results and Discussion

5.1. Spray deposition and compression of nanoparticle electrodes on ITO-PET plastic substrates (Publication I)

The standard method of preparing nanostructured TiO_2 photoelectrodes on glass starts by depositing a film of TiO_2 nanoparticle paste on the substrate by screen printing. This is followed by drying the film and heat treatment at 450-550 °C for 30-60 min. The paste contains typically organic surfactants and binders that help depositing a uniform film that maintains its integrity and adherence on the substrate during the drying and heating steps. The purpose of the heat treatment is to burn off these organic substances and to sinter the individual TiO_2 nanoparticles together forming a film with good physical and electrical interparticle contacts. The paste may also contain porosity controlling agents that modify the microscopic morphology of the resulting nanostructured film.

Due to the high-temperature step involved, this standard method cannot be used for making flexible dye solar cell on plastic substrates. The temperature limit of the widely used indium-tin-oxide (ITO) coated polyethyleneterephtalate (PET) plastic foils is ca. 150 °C. This rules out the common organic surfactants and binders in the TiO_2 paste, and means that alternative methods for the TiO_2 film deposition and post-treatment are needed. A large number of different techniques have been developed for this purpose, as listed briefly in Publication I.

From the point-of-view of fast roll-to-roll processing, a particularly interesting method for the preparation of nanoparticle films on plastic substrates is the so-called room-temperature compression technique [65,66]. In this method, adhesion and electrical contact formation between the nanoparticles is obtained by simple and quick static [65-72] or dynamic [65,73] mechanical pressing. To take full advantage of this rapid processing, also the deposition of the nanoparticle film should be a fast and continuous process that is capable of producing several tens of micrometers thick uniform electrode films. In this work, spray deposition of powder suspension was found to meet these criteria, as reported in Publication I.

The simplest conceivable way of depositing a film of TiO_2 nanoparticles on a plastic substrate at low temperature is to mix the particles in pure ethanol or water, deposit this suspension on the substrate, and let it dry in air at room temperature. The problem with this is that without surfactants and binders, the stresses and strains in the particle suspension lead to cracking of the film during drying [74]. The problem is more severe for thicker films, can lead to flaking of the fill, and prevents obtaining sufficiently thick films in a single deposition-compression cycle (Figure 21). This is essentially the same phenomenon as the well-known cracking of clay [75]. More generally, compaction and cracking of colloidal suspensions during drying is a complex phenomenon that is not fully understood and a subject of active research due to its importance in many industrial applications.

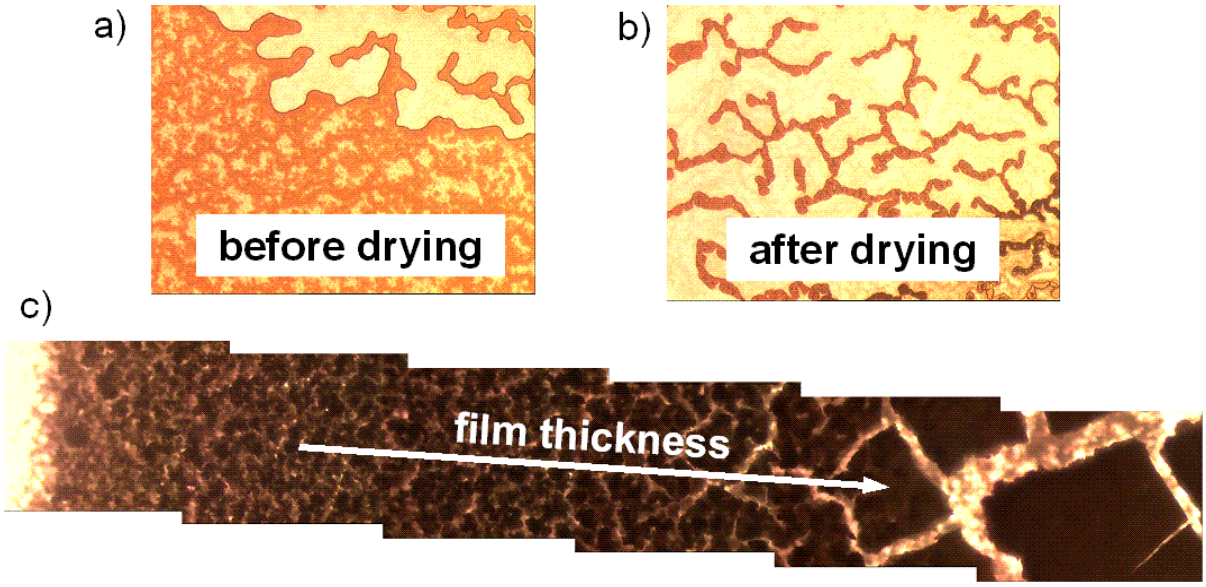

Figure 21. Optical microscope images of crack formation in spray deposited TiO_2 films. Top: Distribution of a small amount of TiO_2-water suspension on a glass slide a) during and b) after drying. The retracting edge of the drying suspension draws TiO_2 powder material within the liquid phase, accumulating and consolidating the material to form thin ridges on the substrate. c) Effect of film thickness on the crack formation in spray-deposited TiO_2 powder film. Too fast deposition has led to severe cracking of the film.

In the present case the cracking problems were solved by spraying the TiO_2 nanoparticle powder on a substrate heated at ca. 100 ºC, followed by room temperature compression of the powder film (Publication I). The success of the spray deposition is based on the fact that the powder material is brought to the substrate within small droplets. When the evaporation of the solvent is sufficiently fast compared to the deposition rate, the powder aggregates in each droplet are able to sustain their integrity during drying of the film. As a result, stresses and strains in the drying film are consumed by the growth of the voids between the powder aggregates rather than formation of macroscopic cracks in the film. Naturally, the evaporation rate of the solvent sets an upper limit to the film deposition rate. If the deposition rate is too high, the film becomes too wet and the powder aggregates collapse leading to cracking of the film.

The compression method was particularly suitable, in fact necessary, as a post-treatment of the highly porous as-deposited TiO_2 powder films. The compression was able to redistribute the TiO_2 nanoparticle material over the substrate to some extent, so that most of the macroscopic voids present in the as-deposited film were closed. As a result of the combined spraying and compression, up to 14 μm thick smooth and uniform nanostructured TiO_2 films could be prepared on plastic substrates reaching up to 2.8 % solar cell efficiency when used as photoelectrodes in the DSC. Although scaling up of the method was not investigated in this work, it can be considered suitable for continuous roll-to-roll deposition of nanoparticle films at low temperatures for flexible DSCs. The method is relatively fast, the materials used are cheap (only TiO_2 and water), and it is suitable for covering large areas.

Recently, Yamaguchi et al. [71] achieved an excellent 7.4 % cell efficiency under 1 sun illumination for a fully plastic DSC using TiO_2 photoelectrodes prepared by static compression on ITO-PEN substrate. The high performance was reported to be a result of systematic optimization of the TiO_2 film preparation including: (1) use of in-house synthesized TiO_2 nanoparticles instead of the commercial P25 powder, (2) addition of larger

light scattering TiO_2 particles in the photoelectrode film to improve light harvesting, (3) use of water instead of ethanol in the TiO_2 suspension, (4) UV-O_3 treatment of the ITO-PEN prior to the TiO_2 film deposition, and (5) optimization of the TiO_2 film thickness. The high cell performance achieved by Yamaguchi et al. [71] may be further explained by the lower sheet resistance of the ITO-PEN (13 Ω/sq.) compared the ITO-PET (50-60 Ω/sq.) and the use of lower viscosity acetonitrile instead of methoxypropionitrile as the electrolyte solvent.

If we compare the 7.4 % efficiency obtained by Yamaguchi et al. on ITO-PEN [71] with the 10.2 % reported by the same research group on glass [18], we may conclude that the DSC technology can be transferred from the rigid glass substrates to flexible plastic substrates with relatively small loss in cell performance. This is a very encouraging result regarding the realization of DSCs as a flexible PV technology.

5.2. Impedance spectroscopy of pressed counter electrodes on ITO-PET plastic substrates (Publication II)

The counter electrode of a glass based DSC is usually a TCO-coated glass with a small amount of Pt catalyst deposited on the TCO surface. In the most frequently used method [76], a drop of liquid Pt precursor solution (e.g. $PtCl_4$ in isopropanol) is distributed on the substrate and let to dry in air. Thermal treatment in air at 385 ºC decomposes the Pt precursor forming Pt nanoparticles adhered on the substrate. The method is simple and the resulting Pt layer has excellent catalytic activity [76,77].

With plastic substrates the thermal Pt catalyst deposition needs to be replaced by a low-temperature process. Lindström et al. [65] showed that good solar cell performance can be achieved with counter electrodes prepared by mechanical pressing of conducting catalyst particles on the ITO-PET at room temperature in the same way as making the pressed TiO_2 photoelectrodes. In Publication II we used the combined spraying and compression method studied in Publication I to deposit the powder counter electrode materials proposed by Lindström et al. [65] on ITO-PET plastic substrates and investigated their electrocatalytic performance by impedance spectroscopy.

Using a common organic liquid electrolyte, the charge transfer resistance (R_{CE}) of the prepared 10-20 μm thick carbon powder counter electrodes was excellent, R_{CE} = 0.5-2 Ωcm^2, being comparable to commonly used sputtered or thermal Pt catalysts [77]. Also 20-40 μm thick porous platinized Sb-doped SnO_2 electrodes showed satisfactory catalytic activity with R_{CE} = 8-13 Ωcm^2. While the both type of electrode films showed fair adherence to the ITO-PET substrate, the thickest films had some tendency to flaking and peeling off. It seems that additional reinforcement and binding of these porous electrode films is most likely needed to facilitate roll-to-roll manufacturing of mechanically durable flexible DSCs. This could perhaps be achieved by mixing suitable polymers to the powder suspension.

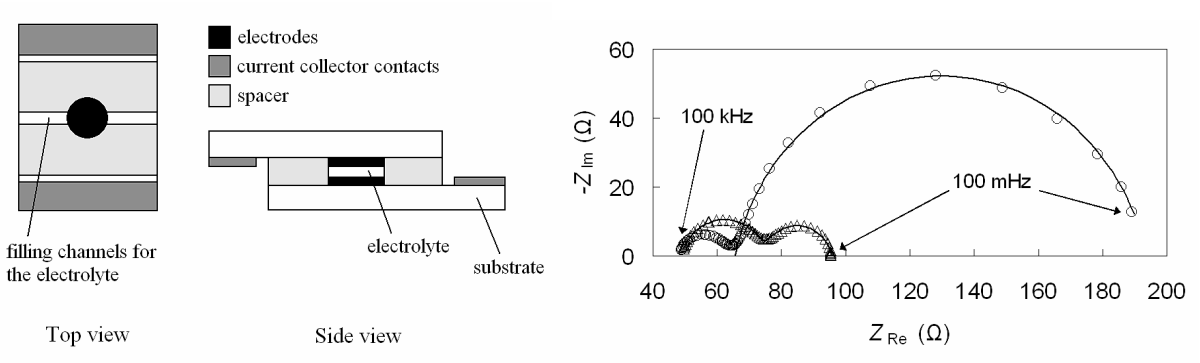

Figure 22. Left: The cell configuration used in Publication II. Right: measured impedance spectra showing an additional (anomalous) impedance arc at the high frequencies. [116]

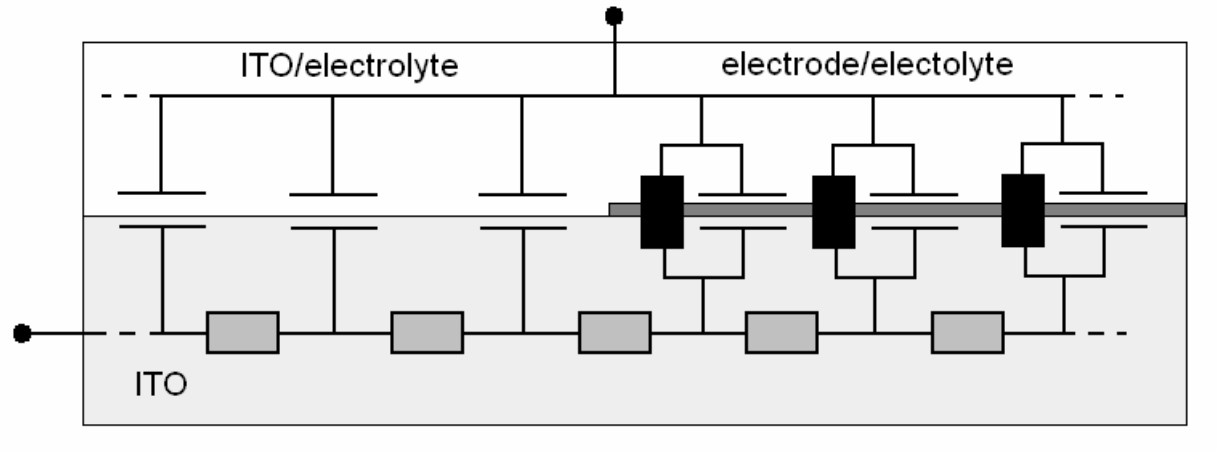

Figure 23. Transmission line representation of the distributed impedance of a thin layer electrochemical cell with active (electrode) and inactive (ITO) areas exposed to the electrolyte. The figure shows the equivalent circuit of the half cell neglecting the mass transport impedance and the resistance of the electrolyte.

As a secondary matter, Publication II reports a lesson learned in impedance spectroscopy of thin layer electrochemical cells. The charge transfer resistance of the counter electrode films was measured using a symmetric CE-CE cell configuration. The impedance spectrum of these cells was found to exhibit an anomalous impedance arc at the high frequencies (Figure 22 right). Correct interpretation of the data was possible only after the reason for this was identified. The effect arises from the impedance of the ITO-electrolyte interface in the electrolyte filling channels cut to the edge sealant polymer (Figure 22 left) and its coupling with the actual electrode impedance via the sheet resistance of the ITO substrate (Figure 23). The problem was solved by separating this parasitic impedance from the actual electrode area by cutting a gap in the ITO layer.

The lesson learned is that in a thin layer electrochemical cell, where current is collected laterally along the substrates, the series resistance due to the conductive substrate has a distributed nature [78] corresponding to a transmission line [79]. The effect is most significant when the sheet resistance of the substrate is high compared to the total impedance of the cell. In that case, the current distribution in the cell becomes two-dimensional and frequency-dependent, and can no longer be modeled with a lumped equivalent circuit. The practical example of Publication II highlights the importance of understanding the influence of geometric and parasitic impedances on the EIS data and minimizing them by careful design of the EIS measurement cell.

5.3. Electrochemical characterization of stainless steel based dye solar cells (Publication III)

The restriction of the solar cell processing to low temperatures with the ITO-PET plastic substrates can be circumvented by using flexible metal substrates instead. The most commonly used material in flexible PV in general is stainless steel [15]. Flexible stainless steel (StS) sheets were introduced to DSC first as the counter electrode substrate [80] and soon later as a conducting support for the photoelectrode [81]. Respectable solar cell efficiencies of 9.15 % [82] with stainless steel counter electrode (StS-CE) and 8.6 % [83] with stainless steel photoelectrode (StS-PE) have been demonstrated recently.

The purpose of the work reported in Publication III was to carry out a detailed electrochemical characterization of the influence of the stainless steel substrate on the DSC performance when used either at the photoelectrode of counter electrode side of the cell, using fully glass based cells as a point of comparison. The purpose of the experiments was to distinguish the role of the different types of electrodes, substrates, and cell configurations in determining the cell performance.

Stainless steel 304 (Outokumpu Ltd.) was found to posses excellent electrochemical properties for its use as a conducting substrate in the DSC. When used to replace FTO-coated glass at the photoelectrode side, the conversion efficiency (4.4 %) of the solar cells at 1 sun illumination was lower than in the glass based cells (5.2 %) due only to the optical losses inherent to the StS-PE cell configuration in questions. As the light comes from the counter electrode side, it is partially absorbed by the Pt catalyst and bulk electrolyte layers. These optical losses can be avoided by using the stainless steel as the counter electrode substrate, i.e. StS-CE configuration. In that case however, the catalytic activity of the Pt deposited on the stainless steel was lower than on the FTO glass (larger R_{CE}), which resulted in fill factor losses (Figure 24).

Electrochemical characterization by EIS, open circuit voltage decay and polarization measurements revealed that when used as the photoelectrode substrate, the stainless steel had, nevertheless, an effect on the function of the TiO_2 photoelectrode: it lowered the recombination resistance of the TiO_2 photoelectrode film and shortened the electron life time. However, these effects were significant only at relatively low negative polarization of the photoelectrode, and hence, did not impair the photovoltaic performance of the cells at high light intensity. Unfortunately, the stability of the stainless steel based cells was poor [84]. Based on our observations, to be reported in detail elsewhere, it seems that, although very good initial cell performance can be reached with uncoated stainless steel substrates, they need to be coated with a protective layer until satisfactory long-term stability can be reached.

As an additional contribution, Publication III demonstrates how current dependent EIS can be used to factor the steady state IV curve of the cell to partial contributions from different series connected internal cell resistances without using additional reference electrodes. This method, described in Chapter 4.4, is particularly useful for studying performance and stability of permanently sealed DSCs. Note that using reference electrodes in the thin solar cell structure, e.g. an add-layer of porous Ti metal [85] or a Pt wire [86], could pose the risk that the cell stability and operation are influenced by the foreign materials of the reference electrode and its effect on the structure of the cell. With EIS the electrical characteristics of the individual cell components in a typical DSC can be determined without modification of its structure and materials.

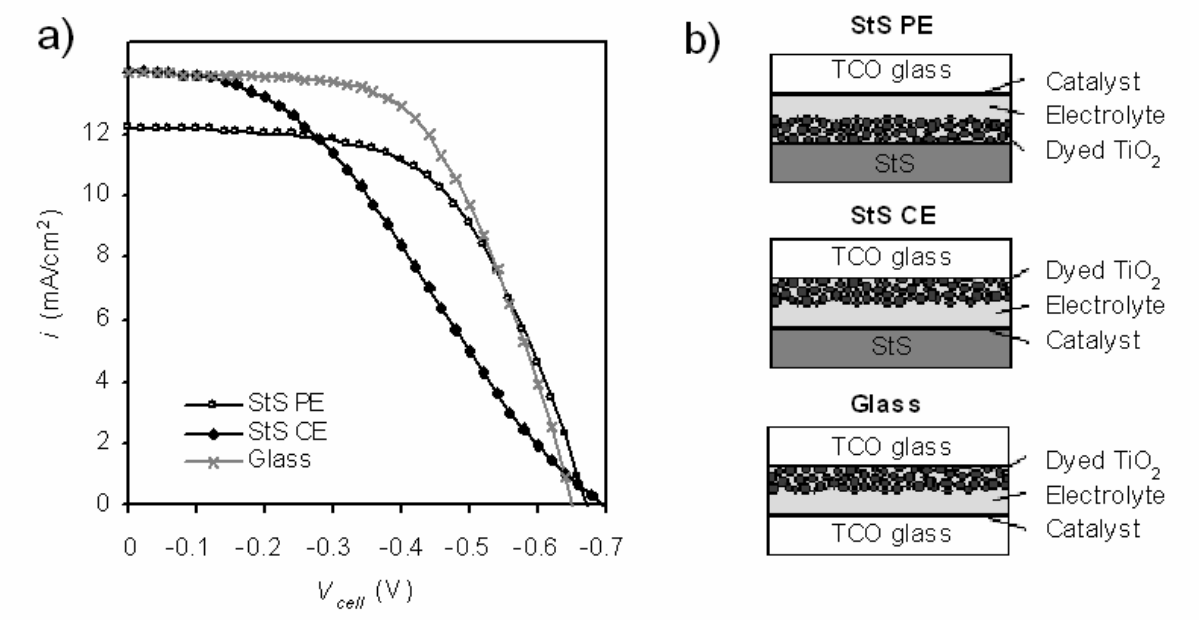

Figure 24. Comparison of stainless steel and glass based dye solar cells. a) IV characteristics at 1000 W/m^2 AM1.5G equivalent illumination. b) Schematic representation of the cell structures studied in Publication III. [117]

5.4. Substrate mediated recombination and contact resistance in pressed TiO_2 photoelectrodes on ITO-PET plastic (Publication IV)

The purpose of the work reported in Publication IV was to investigate the role of the ITO-PET plastic substrate on the photovoltaic and electrochemical performance of the DSC. Similar experiments as in Publication III were carried out using again FTO-coated glass substrates as a point of comparison.

Flexible plastic DSCs may find use first in low power applications that operate at low light intensities. To maintain good performance at low light intensity, the solar cell must have excellent rectifying diode characteristics, i.e. very low leakage or "dark" current density. An issue of particular importance in DSCs with this respect is the back reaction of electrons with tri-iodide ions in the electrolyte at the substrate-electrolyte interface. This additional electron recombination pathway works like an internal voltage dependent shunt resistance in the cell and can cause significant loss of cell performance, in particular V_{OC}, at low light intensities. This occurs with the standard FTO-glass substrates [87], and turned out to be the case also with the ITO-PET substrates used in this work (Figure 25b, Publication IV). In fact, the ITO-PET was found to have electrochemical characteristics very similar to the FTO-glass.

In order to suppress the substrate leakage current, compact TiO_2 recombination blocking layers were deposited on the ITO-PET by low-temperature atomic layer deposition (ALD). The blocking layers had two kinds of effects. On one hand they were very effective in suppressing the triiodide reduction reaction at the ITO-electrolyte interface, leading to improved V_{OC} at low light intensities (Figure 25b). On the other hand, as the compact TiO_2 layer was situated between the ITO and the TiO_2 photoelectrode film, it introduced a contact resistance (R_{CO}) between them. This resistance component could be identified by impedance

spectroscopy (Publication IV), and caused decrease of the fill factor and cell efficiency (Figure 25a).

The contact resistance was found to be reduced by heat treatment at 450 ºC that induced crystallization of the amorphous low-temperature deposited ALD TiO_2 layer, thereby improving its conductivity. Indeed, 35 nm thick ALD blocking layers worked well with high-temperature sintered TiO_2 photoelectrodes on FTO-glass, but completely blocked current collection from low-temperature compressed TiO_2 films on ITO-PET.

The results indicate that in order to reach positive effect on the cell performance at high light intensities, where the effect of the internal cell resistances are emphasized due to high current densities, this type of low-temperature ALD TiO_2 blocking layers need to be extremely thin, below 4 nm. Actually, the thinner the blocking layer the better, as long as satisfactory suppression of the leakage current is maintained – thinner ALD layers are faster and cheaper to produce.

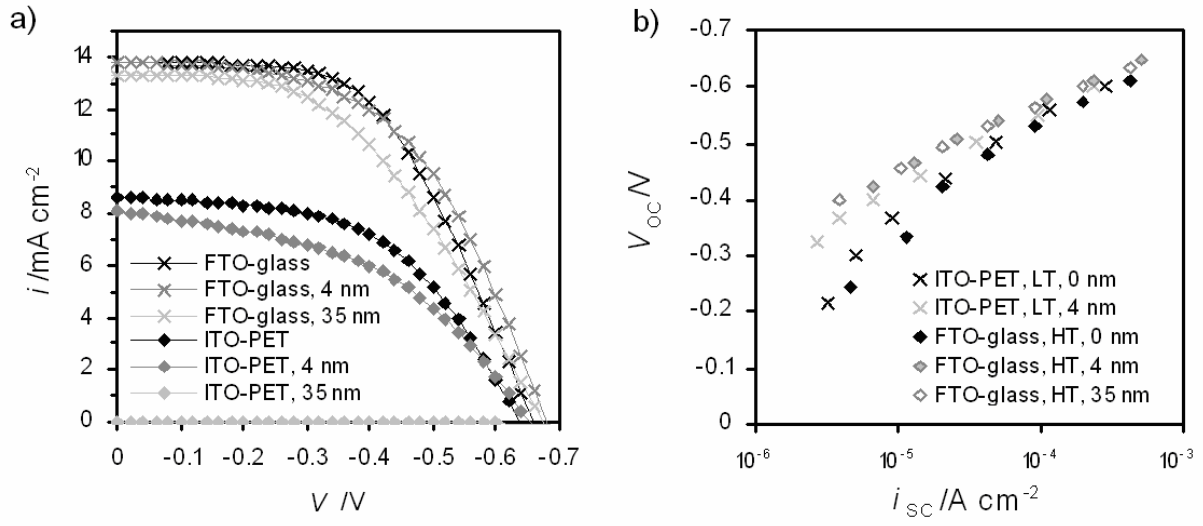

Figure 25. Comparison of dye solar cells with pressed TiO_2 photoelectrodes on ITO-PET or FTO-glass substrates and the effect of ALD TiO_2 blocking layers. a) IV characteristics at 1000 W/m^2 AM1.5G equivalent illumination. b) Effect of ligh intensity (proportional to i_{SC}) on the open circuit voltage. [119]

5.5. Quantitative estimation of the light harvesting, electron injection and charge collection efficiencies by optical and IPCE measurements (Publication V)

Nanostructured TiO_2 photoelectrode films prepared below 150 ºC give typically lower short circuit current densities (i_{SC}) compared to similar films that have been subject to heat treatment above 450 ºC [68,70,72,88-90]. This was also the case with the pressed TiO_2 photoelectrodes studied in this thesis (Publications I, IV, and V). One of the reasons for this is that at high temperature, the TiO_2 nanoparticles sinter slightly together forming good electrical contact between them. Without sintering the interparticle contacts tend to be insufficient and act as bottle-necks to electron transport. This decreases the diffusion length and collection efficiency of the electrons, and hence, the photocurrent output of the solar cell. Indeed, low-temperature fabrication of nanostructured photoelectrode films with good

conductivity and long electron diffusion length is the main problem for realizing high performance DSCs on flexible plastic substrates.

Nevertheless, replacing the conventional high-temperature sintering method with an alternative low-temperature one can change also many other properties of the photoelectrode besides electron transport. Organic residues and other impurities left on the TiO_2 surface due to absence of heating may change the amount of adsorbed dye molecules and their electron injection properties, affect electron recombination, or shift the TiO_2 conduction band edge position. Sintering may also influence the light scattering properties of the film by modifying its structure or the shape of the TiO_2 particles.

It follows that, if one aims to a quantitative understanding of the performance limiting factors of low-temperature prepared DSCs, many different effects need to be taken into account. The difficulty with this is that not all of these effects necessarily decrease the cell performance, but may instead improve it, and the observed differences in the solar cell IV curve and conversion efficiency may be a result of negative and positive changes that partially compensate each other.

Hence, to make systematic progress in the development of DSCs we need simple yet accurate experimental techniques that enable us to decouple and quantify the different factors that determine the cell performance. Development of such methods for identifying the photocurrent limitations in DCSs is the main contribution of Publications V and VI.

As described in Chapter 3.1, the i_{SC} of the DSC at given illumination depends on its spectral quantum efficiency (IPCE) that consists of the partial efficiencies of light harvesting (η_{LH}), electron injection (η_{INJ}), and electron collection (η_{COL})

$$\eta_{IPCE}(\lambda) = \eta_{LH}(\lambda, d)\eta_{INJ}(\lambda)\eta_{COL}(L, d, \alpha(\lambda)) \tag{58}$$

Each of these factors is generally a wavelength dependent property of the dye-sensitized semiconductor photoelectrode. In order to understand the reasons for a limited i_{SC}, each of them needs to be determined at conditions relevant to the normal solar cell operation.

The η_{LH} can be estimated by careful optical characterization of the cell components and application of an optical model (Chapter 3.1.1), and combined with measured IPCE to determine the absorbed-photon-to-collected electron efficiency (APCE)

$$\eta_{APCE}(\lambda) = \frac{\eta_{IPCE}(\lambda)}{\eta_{LH}(\lambda, d)} = \eta_{INJ}(\lambda)\eta_{COL}(L, d, \alpha(\lambda)) \tag{59}$$

The η_{INJ} has normally been measured using relatively complicated kinetic techniques such as ultrafast transient absorption spectroscopy [91,92], time-resolved single-photon counting [62,93], time-resolved photoacoustic calorimetry [94], etc. [92]. However, these techniques require special expertise and equipment that are not available in most of the laboratories engaged with the research and development of DSCs. Perhaps partly for this reason, it has been a common assumption in many studies that $\eta_{INJ} \approx 100$ %, e.g. [95,96], which is indeed the case in high performance DSCs, e.g. [97-99].

The first attempts to estimate η_{COL} were based on interpretation of the features of measured IPCE spectra by the standard diffusion model [96,100,101]. Studying unsensitized TiO_2

nanoparticle electrodes in the UV region, Södergren et al. [96] showed that if the spectral absorption coefficient $\alpha(\lambda)$ and the thickness (d) of the TiO_2 film are known, the electron diffusion length (L) can be estimated by fitting the diffusion model to the IPCE data. Lindström et al. [100] extended this method to dye-sensitized nanostructured TiO_2 photoelectrodes and found qualitative agreement of the diffusion model with respect to the variation of d and the direction of illumination. Nevertheless, they did not pursue quantitative estimation of L. Boschloo and Goossens [101] applied the IPCE analysis to porphyrin-sensitized DSCs. In particular, they used the difference between IPCE at PE and CE illumination to conclude that $L < d$ in their solar cells, and used the ratio of IPCE at two different wavelengths to derive an estimate for L.

In these early works, the IPCE analysis relied on the assumption that η_{INJ} was either 100 % [96,100] or independent of the light wavelength [101]. In the work reported in Publication V, we developed the IPCE based approach further and showed that these assumptions can be relaxed: the characteristics of the diffusion model enable quantitative decoupling of η_{APCE} into its η_{INJ} and η_{COL} parts even in the general case when both of them are less than 100 % and wavelength-dependent.

Two methods were developed for this purpose (Publication V). One of the methods named the *IPCE-ratio* is particularly useful since it allows estimation of L and η_{INJ} at each wavelength based on no more than two IPCE measurements of a single DSC taken at the same conditions: one with illumination from the photoelectrode (PE) side and one with the opposite, counter electrode (CE) side illumination. The only additional information required is the thickness (d) and light absorption coefficient (α) of the photoelectrode film, and the optical losses associated with the both illumination directions. All of these can be determined by independent experiments. The method is explained by the following equations.

The ratio of the IPCE at CE *vs.* PE illumination can be expressed as

$$\frac{\eta_{IPCE,CE}(\lambda)}{\eta_{IPCE,PE}(\lambda)} = \left[\frac{\eta_{LH,CE}(\lambda,d)}{\eta_{LH,PE}(\lambda,d)}\right] \cdot \left[\frac{\eta_{INJ,CE}(\lambda)}{\eta_{INJ,PE}(\lambda)}\right] \cdot \left[\frac{\eta_{COL,CE}(L,d,\alpha(\lambda))}{\eta_{COL,PE}(L,d,\alpha(\lambda))}\right] \tag{60}$$

Since η_{INJ} and the absorptance of the photoelectrode film are independent of the direction of light they cancel out in eq. 60. Applying the simple optical model described in Chapter 3.1.1, eq. 60 can be rearranged to

$$\frac{\eta_{COL,CE}(L,d,\alpha(\lambda))}{\eta_{COL,PE}(L,d,\alpha(\lambda))} = \frac{T_{TCO}(\lambda)}{T_{CE}(\lambda)T_{EL}(\lambda)} \cdot \frac{\eta_{IPCE,CE}(\lambda)}{\eta_{IPCE,PE}(\lambda)} \tag{61}$$

The standard diffusion model gives the η_{COL}-ratio on the left hand side as a function of d, α, and the diffusion length L. Hence, when d, α, the IPCE-ratio, and the optical transmittances on the right hand side are measured independently, L can be estimated by simple fitting of eq. 61 to these data.

Once L is known, it can be used to calculate η_{COL} by the diffusion model. The η_{INJ} can thereafter be estimated based on the measured η_{IPCE}, optically determined η_{LH} and the diffusion-model-calculated η_{COL} as

$$\eta_{\mathrm{INJ}}(\lambda) = \frac{\eta_{\mathrm{IPCE,PE}}(\lambda)}{\eta_{\mathrm{LH,PE}}(\lambda, d)\eta_{\mathrm{COL,PE}}(L, d, \alpha(\lambda))} \tag{62}$$

using data corresponding either to the PE illumination (as in the above expression) or CE illumination. Both will give the same result by definition.

Note that exact calibration of the photon flux used in the IPCE measurement is not needed for the estimation of L by the IPCE-ratio: All light intensity calibration factors cancel out when calculating the IPCE-ratio. This simplifies considerably the IPCE experiments and improves the accuracy of the L estimates. On the other hand, estimation of η_{INJ} *does* require exact light intensity calibration since it is based on the absolute value of the IPCE (eq 62).

The main advantage of the IPCE-ratio method is that it is inherently *consistent* with the steady state photocurrent output of the cell. Nevertheless, its capability to estimate η_{INJ} and L *correctly* depends on the validity of the standard diffusion model in reality. This needs to be verified by comparison to other, independent, methods for determining η_{INJ} and L, and by checking the consistency of the their estimated values with other aspects of the solar cell function.

Encouraging results with this respect was recently reported by Barnes at al. [62] who applied the IPCE-ratio method to an extensive set of standard DSCs with varied electrolyte composition and $TiCl_4$ treatment of the photoelectrode film. The authors found that the η_{INJ} values determined by the IPCE-ratio were in quantitative agreement with those derived from time-correlated single-photon counting, and further, they correlated expectedly with the relative TiO_2 conduction band-edge position and V_{OC} of the cell. These results are the first independent experimental verification of the IPCE-ratio method and confirm its utility for studying the photocurrent limitations in DSCs.

5.6. Photocurrent limiting factors of pressed TiO_2 dye solar cells (Publication V)

In Publication V, the new IPCE based methods were used to study the photocurrent limiting factors in pressed DSCs. Two types of cells were investigated: with or without high-temperature sintering of the nanostructured TiO_2 photoelectrode film prepared by the room-temperature compression on FTO-glass substrates. The high temperature sintering had an effect of more than doubling the i_{SC} from 5.0 mA/cm^2 to 9.7 mA/cm^2 and the cell efficiency from 2.6 % to 5.5 %.

Optical characterization showed that η_{LH} was very good in these cells, reaching over 80 % at the maximum at 535 nm and being as high as 60 % still at 700 nm with the thickest films (Figure 26). However, their photocurrent generation was significantly limited by a low and wavelength dependent η_{INJ} (ca. 49 % at maximum). The likely reason for this is poor energetic match between the excited states of the dye and the TiO_2 conduction band states due to the specific electrolyte composition used in these cells. Without sintering the TiO_2 film, the i_{SC} was further limited by a low η_{COL}, as expected.

What was not expected however, was that L, and even η_{COL}, increased with the photoelectrode film thickness (Figure 26). The likely reason for this is improvement of the film quality as a function of thickness, and this is also supported by impedance results

discussed in Chapter 5.9 below. Indeed, thicker pressed TiO_2 films had smaller porosity (Publication V), which is known to improve electron transport in the disordered nanoparticle network [102-104].

While optimization of the i_{SC} of pressed TiO_2 DSCs was not investigated in this thesis, the results of Publication V give clear guidelines to it. Increasing η_{INJ} close to 100 % should be possible by changing the electrolyte composition to a one that favors electron injection by lowering the TiO_2 conduction band position relative to the LUMO levels of the dye, and if necessary, purifying the dye and optimizing dyeing conditions to prevent dye aggregation. Improvements to η_{COL} could be sought along the lines demonstrated by Yamaguchi et al. [71] (see Chapter 5.1).

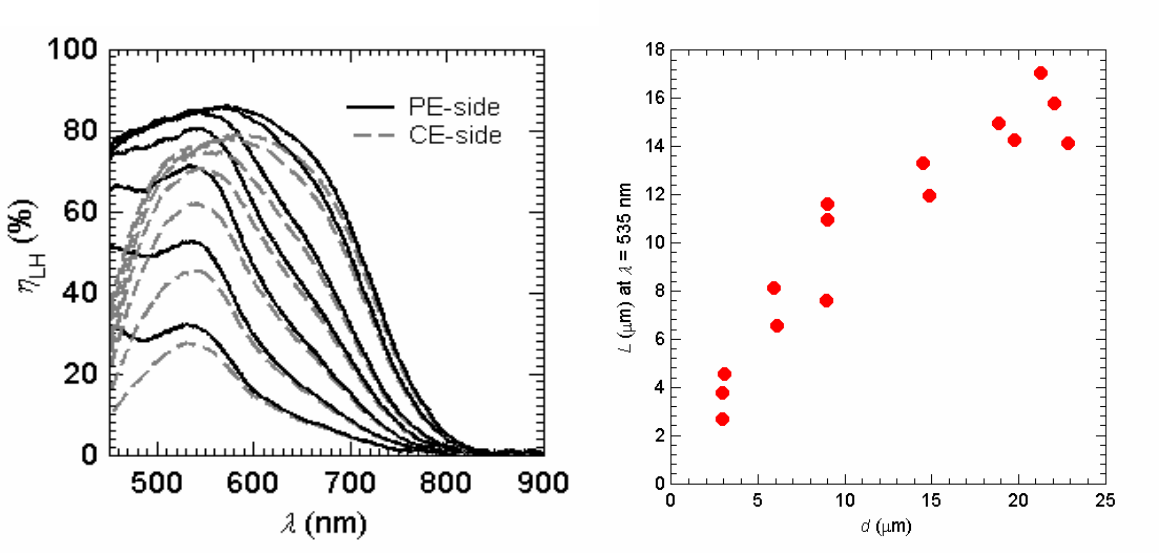

Figure 26. Left: Light harvesting efficiency of dye solar cells with pressed 3-23 μm thick TiO_2 photoelectrodes. Right: Steady state electron diffusion length determined with the IPCE-ratio method. Data from Publication V. [118]

5.7. Effect of non-uniform light absorption and inefficient electron collection on the IMPS and IMVS response (Publication VI)

Quite soon after Södergren et al. [96] had demonstrated the idea of using spectral IPCE measurements for studying electron transport in nanostructured photoelectrodes, this steady state approach was replaced by newly developed dynamic photocurrent and photovoltage techniques, such as the IMPS [79] and IMVS [105,106]. The advantage of these techniques over IPCE was that they gave estimates separately for the electron diffusion coefficient D and lifetime τ (see Chapter 4.5). The use of these dynamic methods over the years generated a great deal of what is currently known on the electron transport and recombination dynamics of the DSC. At the same time they were established as the standard methodology for the experimental evaluation of η_{COL} (Chapter 3.1.3), and hence, were also used and studied in this thesis.

As a part of the author's work at KTH in 2005, comprehensive experiments with IMPS and IMVS in combination with other "toolbox" [68] techniques were carried out using the same 36 pressed TiO_2 dye solar cells that were studied by optical and IPCE techniques in

Publication V. In half of the cells the pressed TiO_2 films had been additionally sintered at 450 ºC for 1 h while the other half had pressed-only films. The photoelectrode film thickness ranged between 3 μm and 23 μm in six categories, each having three identical samples.

Short-circuit-IMPS and open-circuit-IMVS measurements were carried out at six different light intensities, from 0.47 to 42 mW/cm^2, using a red LED (λ_{peak} = 640 nm) as a light source that provided both the DC background intensity and its small amplitude modulation, both incident on the cell from the photoelectrode side. Charge extraction technique [107,108] was used to measure the electron concentration in the photoelectrode at the short circuit and open circuit conditions corresponding to each IMPS and IMVS measurement.

To rationalize the amount of data the experiments were divided to two sets: 1) thickness dependent measurements (all cells) at fixed light intensity (10.5 mW/cm^2), and 2) light intensity dependent measurements at fixed film thickness (14.5 μm, four-layer TiO_2 films). The fixed intensity corresponded roughly to 0.1 sun in terms of i_{SC}, and the 4-layer films were chosen since they gave the best cell performance (see Publication V).

The experiments had originally two objectives. First, the purpose was to clarify the effect of high-temperature sintering on the electron transport and recombination in the pressed TiO_2 photoelectrodes. Second, the idea was to investigate the effect of film thickness on the electron transport, recombination, and accumulation in the nanostructured photoelectrode films, since this issue had not been covered well in the literature. Unfortunately however, the extensive set of data gathered turned out to be very hard to interpret and understand.

Figure 27 demonstrates the problem. It shows the IMPS time constant as a function of the extracted electron concentration, both measured at the same condition (light intensity and short circuit). The thin straight lines connect data of sintered (S) and pressed-only (P) TiO_2 films of equal thickness measured with same bias light intensity. Note how in the thinnest films, electron transport appears to be, as expected, slower in the pressed-only films (higher τ_{IMPS}) than in the sintered films, both having equal electron concentration (q_{SC}). In contrast to this, in the four-layer TiO_2 films the τ_{IMPS} *vs.* q_{SC} data of the both type of films (P4, S4) measured by varying the bias light intensity (Φ_{DC}), overlap each other exactly. Imagine that if we had only this light intensity dependent data, it would quite convincingly suggest that the high-temperature sintering *does not* improve electron transport in the pressed TiO_2 films. This can hardly be the case in reality which makes the data questionable. Indeed, the thickness dependent τ_{IMPS} vs. q_{SC} data in Figure 27 point to a systematic error in our method: the conclusions made on the electron transport based on τ_{IMPS} at fixed q_{SC} depend on the TiO_2 film thickness used in the sample. These problems prompted us to carry out theoretical investigations to clarify the inconsistencies in these data, and resulted in Publication VI.

Interpreting the data Figure 27 is difficult mainly for two reasons. Firstly, the low η_{COL} in the pressed-only films (Publication V) means that a certain fraction of the electrons present in the film at short circuit are lost by recombination in the charge extraction experiment [107,108], this fraction increasing with increasing d. The extracted q_{SC} is thus an underestimation of the total charge in the film. Secondly, the low η_{COL} means that those electrons that contribute to the measured photocurrent response in the IMPS are generated into the film no farther than the electron diffusion length L from the collecting contact – the rest are lost by recombination. This decreases the measured τ_{IMPS}, i.e. the arrival time of the collected electrons, compared to the situation when $L >> d$, and makes the electron transport appear faster than it really is (see eq. 50 and Publication VI). As a result, the low η_{COL} biases the τ_{IMPS} vs. q_{SC} trace of the

pressed-only TiO_2 films downwards and to the left in Figure 27. The exact match with the sintered films at $d = 14.5$ μm is thus purely coincidental.

The interpretation of the τ_{IMPS} data is further complicated by non-uniform light absorption in the photoelectrode film, especially since modulated light incident from the photoelectrode side was used in these experiments (see Publication VI for discussion of this issue). Taking further into account that the quality of the pressed TiO_2 films was not constant but their porosity decreased with the film thickness (Publication V), it become clear that the data presented in Figure 27 (and many more) had to be rejected as invalid for their original purpose.

It is hoped that the results of Publication VI help designing, performing and analyzing dynamic electron transport experiments more sensibly in the future. In fact, it proposes a new method for this purpose: the IMPS-ratio.

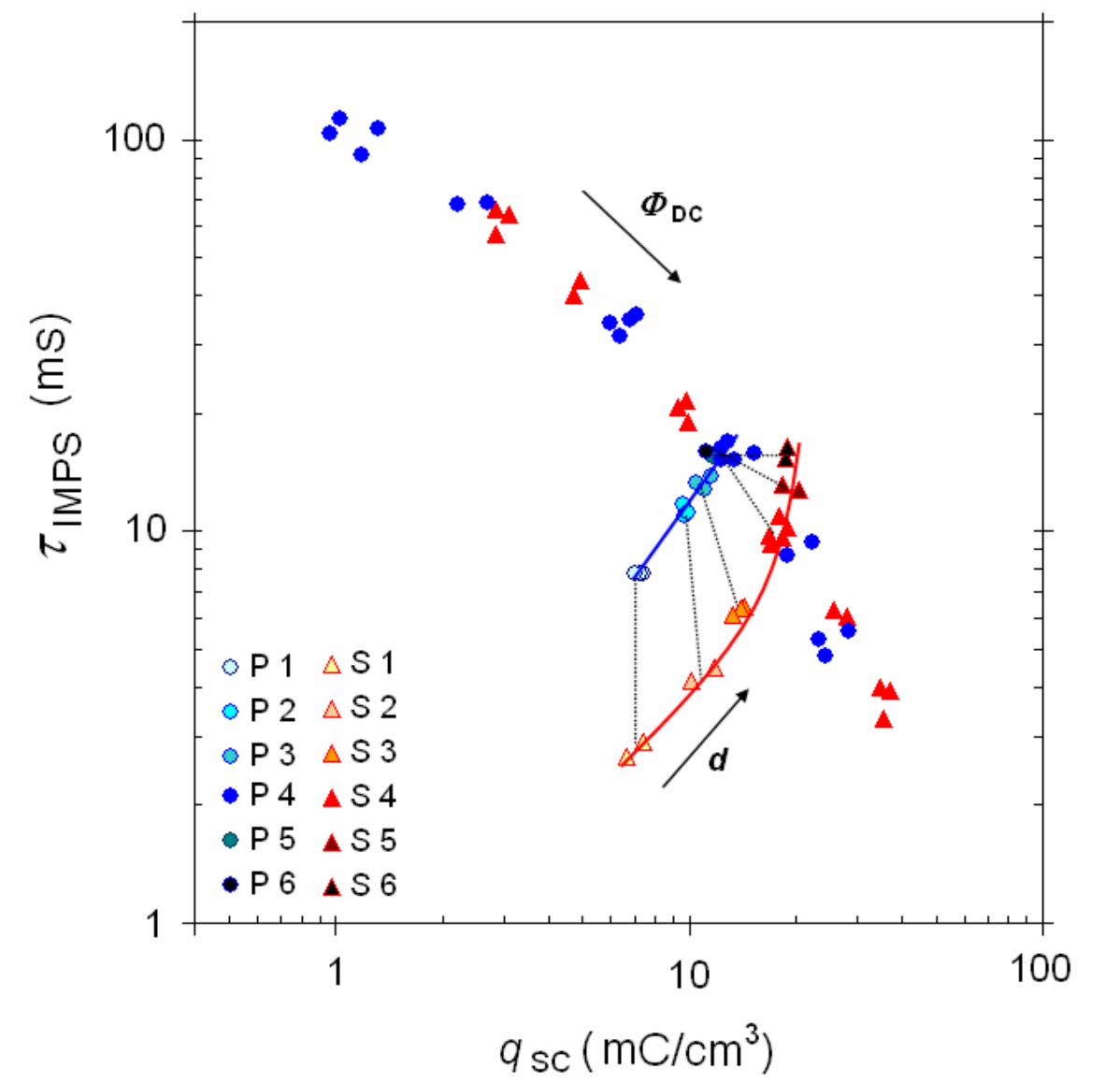

Figure 27. Effect of photoelectrode film thickness (d) and bias light intensity (Φ_{DC}) on the measured IMPS time constant (τ_{IMPS}) and extracted electron concentration (q_{SC}) at the short circuit.

5.8. IMPS-ratio (Publication VI)

As a solution to the problems in the IMPS data analysis discussed in the previous Chapter, Publication VI introduces a new dynamic performance characteristic called the IMPS-ratio:

$$\frac{F_{\mathrm{IMPS,CE}}(\omega, D, \tau, d, \alpha(\lambda))}{F_{\mathrm{IMPS,PE}}(\omega, D, \tau, d, \alpha(\lambda))} = \frac{T_{\mathrm{TCO}}(\lambda)}{T_{\mathrm{CE}}(\lambda) T_{\mathrm{EL}}(\lambda)} \cdot \frac{F^{*}_{\mathrm{IMPS,CE}}(\omega, \lambda)}{F^{*}_{\mathrm{IMPS,PE}}(\omega, \lambda)} \tag{63}$$

It is essentially the dynamic counterpart of the IPCE-ratio discussed in Chapter 5.5 and Publication V. The left hand side of eq. 63 is the ratio of the dynamic (frequency-dependent) electron collection efficiencies, given by the analytical solution of the time-dependent diffusion model, and on the right hand side we have the measured IMPS-ratio (spectrum) multiplied by the ratio of the optical transmittances.

In the limit of low frequencies, the IMPS-ratio equals to the IPCE-ratio that yields an estimate of the steady state L, when d, α, and the optical transmittances are known. The additional frequency dependent information in the IMPS data allows factorization of L further to D and τ by fitting eq. 63 to an experimental IMPS-ratio spectrum.

In other words, the IMPS-ratio facilitates simultaneous estimation of D, τ, and L at the short circuit condition by exact fitting of the diffusion model to the measured IMPS data. A major advantage of this method is that the resulting D and τ estimates are inherently consistent with the steady state L, η_{COL}, η_{IPCE}, and i_{SC} of the cell. However, since they are derived based on dynamic data, they are nevertheless the "dynamic" electron diffusion coefficient and lifetime, D_μ and τ_μ, and not their "conduction band values" that describe the steady state electron transport and recombination (see Chapter 4.5). It must therefore be emphasized that the IMPS-ratio method does not solve the problem [61] induced by electron trapping on the interpretation of the dynamic data. It merely offers an analysis method that, by definition, yields D_μ and τ_μ that are consistent with the standard diffusion model fitted in terms of L to reproduce the measured steady state i_{SC} of the cell.

It should also be noted that the IMPS-ratio-derived D_μ and τ_μ have to be regarded as effective or averaged quantities of their spatially varying local values in the photoelectrode film. The dynamically measured electron transport and recombination characteristics depend strongly on the electron concentration that due to electron diffusion and collection has a steep profile across the film at the short circuit condition [55,85,109]. The relevance and usefulness of these "effective" and "dynamic" D_μ and τ_μ for analyzing, comparing, and understanding the photocurrent limiting factors in DSCs is an open question for the time being. More work is evidently needed to clarify, which of the presently available experimental methods, namely IMPS combined with IMVS [64], the IPCE-ratio (Publication V), or EIS [56,60,110], is most reliable for estimating L and η_{COL}. While this is beyond the scope of the present study, it is interesting to carry out a qualitative comparison of these techniques inasmuch as data for this was available from the pressed TiO_2 DSCs.

5.9. Comparison of electron diffusion length determined by different techniques

Figure 28 shows the electron diffusion length L in the pressed TiO_2 dye solar cells determined by different techniques. This comparison needs to be taken only qualitative since the measurements were carried out at different light intensity, cell voltage, and age of the cells. Nevertheless, it can be seen that the different techniques yield qualitatively the same result: L increases with d in the pressed TiO_2 photoelectrodes, both with and without high-temperature sintering of the TiO_2 film.

This result is interesting inasmuch as the different techniques used data from widely different operating conditions: the IPCE-ratio was based on the steady state i_{SC}, the IMPS-IMVS analysis combined dynamic short circuit and open circuit data, and the EIS was carried out in the dark at a negative polarization corresponding roughly to the V_{OC} at the IMVS measurements. An intriguing subject of future research is to investigate whether this consistency can be found also quantitatively when the different techniques are applied at the same conditions and interpreted with a common dynamic solar cell device model. Interestingly with this respect, recent results by Barnes et al. [62] point to a systematic difference between L determined with the IPCE-ratio method and the L values derived from dynamic photocurrent and photovoltage measurements. It should be noted however, that the analysis of these authors did not take into account the effects of low η_{COL} and non-uniform light absorption profile on the transient photocurrent response (Publication VI).

Note finally that the EIS data (Figure 28c) measured at relatively high Fermi-level position, where the electron concentration in the TiO_2 film is relatively uniform, gives a strong indication that the increase of L with d in these cells is, in fact, a result of the pressing technique and not a fundamental feature of electron transport in DSCs at short circuit conditions, answering thus the question raised in the conclusions of Publication V.

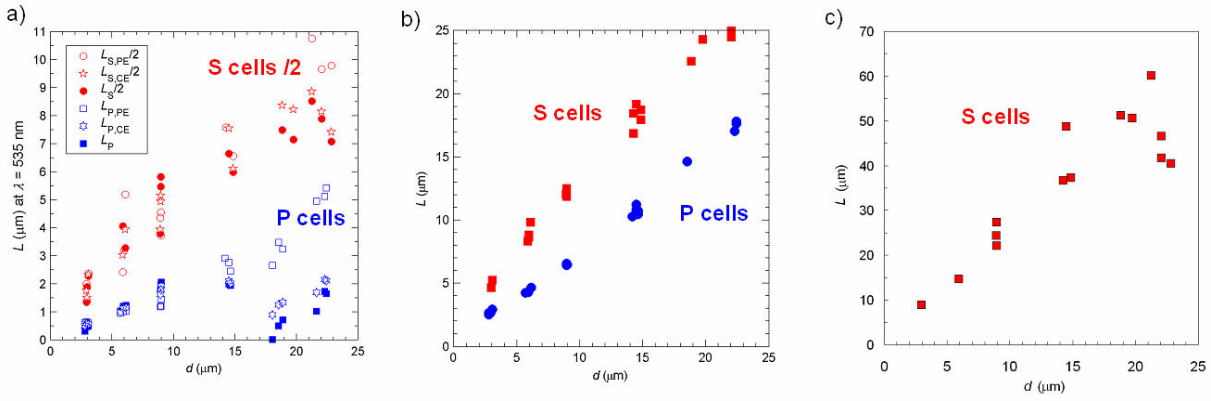

Figure 28. Comparison of the electron diffusion length in pressed dye solar cells determined with different techniques. a) The IPCE ratio method (eq 61 and Publication V), b) conventional interpretation of the short-circuit-IMPS and open-circuit-IMVS, using eqs. 50-52 (10.5 mW/cm^2 red bias light, PE-side illumination), c) EIS in the dark at V_{CELL} = -0.7 V, analyzed with the transmission line model [56,59,60]. [118]

6. Summary and Conclusions

Solar energy is the most abundant renewable energy resource. One of the ways to utilize it is to generate electricity directly from the sunlight by photovoltaic (PV) cells. The main limitation for large scale implementation of photovoltaics is the high manufacturing costs of the present silicon based PV panels. To bring down the costs of PV, cheaper solar cell materials and manufacturing methods are needed.

Massive production of thin and flexible large area solar panels by roll-to-roll techniques is likely required if PV is to make a significant contribution to satisfying the world's rapidly increasing energy demand. In addition to this ultimate goal, flexible solar cells are expected to find new markets as power supplies for portable applications and the emerging printable electronics.

Electrochemical dye solar cell (DSC) is a promising candidate for low-cost flexible photovoltaics due to its cheap and abundant primary materials, simple solution based manufacturing, and proven stability on glass substrates. Furthermore, the fundamental operating principle of the DSC offers unique freedom to material design, development and optimization towards higher performance, lower costs, and improved durability of the solar cells.

The purpose of this thesis was to investigate the realization of DSCs on flexible plastic and metal substrates, generate better understanding of the factors that limit their photovoltaic performance, and develop better methods for their measurement.

The main challenge in the manufacturing of flexible DSCs on plastic substrates is that the photoelectrode and counter electrode films have to be deposited at low temperatures, which tends to compromise the solar cell performance. One of the problems behind this is the difficulty to deposit crack-free colloidal films with sufficient thickness without surfactants and binders in the colloidal suspension. In Publications I and II, this problem was solved by combining spray deposition with the pressing technique. As a result, 2.8 % solar cell efficiency was achieved with TiO_2 photoelectrodes and less than 1 Ωcm^2 charge transfer resistance with porous carbon counter electrode on ITO-PET plastic substrates.

Stainless steel is the most commonly used metal substrate in solar cells, including the DSC. In Publication III, the influence of stainless steel substrate on the DSC performance was studied by photovoltaic and electrochemical techniques. In particular, current dependent impedance measurements were used to discern the effect of different cell components on the solar cell IV curve. Stainless steel 304 was found to be an excellent photoelectrode substrate material in term of its electrochemical properties, yielding 4.4 % cell efficiency.

In Publication IV similar investigations were carried out for ITO-PET plastic substrates with pressed TiO_2 photoelectrodes. These substrates were found to suffer from the same performance loss mechanism as the common FTO-coated glass substrates: back reaction of electrons via the substrate-electrolyte interface decreases the V_{OC} at low light intensities. Deposition of a 4 nm thick compact TiO_2 recombination blocking layer by atomic layer deposition (ALD) suppressed this effect, but introduced a contact resistance between the ITO and TiO_2, which decreased the fill factor (*FF*) and cell efficiency. These results indicate that an optimal thickness of the ALD TiO_2 blocking layer of this kind is below 4 nm.

Low-temperature prepared nanostructured TiO_2 photoelectrodes typically deliver lower short circuit current density (i_{SC}) compared to equivalent films that have been subject to heat treatment. At high temperature, the TiO_2 nanoparticles sinter slightly together which improves the electrical contact between them. In the absence of the sintering, the interparticle contacts are usually insufficient and act as bottle-necks to electron transport, which decreases the electron diffusion length and collection efficiency, and hence, the photocurrent output of the cell. Indeed, low i_{SC} due to poor electron collection was found to be the main performance limiting factor in the DSCs made with pressed TiO_2 photoelectrodes (Publications I, IV, V, and VI).

Systematic development of DSCs through better materials, cell designs and fabrication methods is possible only when assisted by simple but accurate experimental techniques that can be used to identify and quantify the different factors that limit the cell performance. Development and improvement of such techniques was an important part of this thesis.

Publication III demonstrated how electrochemical impedance spectroscopy carried out as a function of current density can be used to factor the steady state IV curve of the cell to the partial contributions from different series connected internal cell resistances, without using additional reference electrodes. This is particularly useful for studying performance and stability of permanently sealed complete DSCs.

In Publication V, a new method called the IPCE-ratio was introduced that allows quantitative estimation of all the three photocurrent limiting factors of DSC, namely the quantum efficiencies of light harvesting, electron injection and electron collection. The method combines optical characterization and modeling of the solar cell with IPCE measurements taken with front and back side illumination of the cell. Importantly, the IPCE and optical spectroscopy required are standard techniques available in most PV research and development laboratories.

Due to its central importance to the flexible plastic DSCs, major emphasis in this thesis was given to the experimental and theoretical study of the electron collection efficiency. A key parameter with this respect is the electron diffusion length L that for a high performance solar cell needs to be much longer than the photoelectrode film thickness. The dominant way of estimating L is based on the effective electron diffusion coefficient D_μ and lifetime τ_μ measured by transient photocurrent and photovoltage techniques. Yet, their relevance to the steady state cell performance has been criticized, which calls into questions the dynamic estimation of L as well. This thesis contributes to solving this dilemma by introducing a method that gives L estimates that are inherently consistent with the steady state i_{SC} of the solar cell: the IPCE-ratio. Furthermore, its dynamic equivalent named the IMPS-ratio, proposed in Publication VI, allows simultaneous estimation of D_μ and τ_μ at the short circuit conditions, again consistently with the steady state cell performance.

One of the overall conclusions of this thesis is that interpretation of the dynamic response of DSC is non-trivial, and erroneous conclusions can be easily reached unless the data are analyzed correctly by a valid model. A particularly good example of this is the effect of non-uniform light absorption and inefficient electron collection on the dynamic photocurrent and photovoltage response of DSC clarified in Publication VI.

Indeed, an important goal of further research is to develop a complete time-dependent DSC device model that with a common set of parameters correctly reproduces all the experimentally measured dynamic responses (IMPS, IMVS, and EIS) and the steady state

performance of the cell (IV, IPCE) at all conditions relevant to the normal solar cell operation. The challenge is to keep the model simple enough so that it can be used routinely in the practical development of DSCs through better materials, manufacturing and cell design. Equivalent circuit modeling used successfully with EIS has clear benefits with this respect and should be used as the modeling framework.

Considering the different dynamic techniques used in this thesis, EIS has the advantage that it gives information (differential resistances) directly related to the steady state IV curve of the solar cell, whereas IMPS and IMVS give time-constants that are meaningful only to the transient behavior of the cell. Nevertheless, the EIS, IMPS, and IMVS transfer functions are fundamentally related to each other and to the solar cell IV curve. These relations should be establish theoretically and utilized in the characterization and modeling of DSCs in the future.

To conclude, the practical results of this study demonstrate that transfer of the dye solar cell technology from rigid glass substrates to flexible plastic and metal substrates is possible, but leads to some losses in the solar cell performance. As a result of this thesis, these performance losses are better understood, and more accurate experimental techniques and data analysis methods are available for their measurement from complete solar cells at realistic operating conditions. The results help in the development of more efficient and stable flexible dye solar cells in the future.

I. Appendix: Time-dependent standard diffusion model and its solution

The standard diffusion model, introduced by Södergren et al. [96] and used in Publications V and VI, is the basic model of the photocurrent and photovoltage response of the dye solar cell. The model gives a simplified description of the generation, transport, and collection of electrons in the nanostructured photoelectrode film and forms the basis for more advanced and complete models of the DSC function. The model was initially applied to qualitative analysis of the spectral characteristics of steady state IPCE measurements to elucidate the nature of the electron transport [96,100,101,111] and to obtain estimates for the electron diffusion length [96,101].

Electron transport in the nanostructured TiO_2 photoelectrodes occurs mainly via diffusion – contributions from electric field induced drift can be neglected to a good approximation. This is firstly due to the small size and low doping density of the TiO_2 nanoparticles, which allows only negligible electric fields within each particle [112], and secondly due to the highly conductive electrolyte in the pores of the photoelectrode film, which effectively screens any macroscopic electric fields across the film [113]. For this reason, significant electrostatic field (potential gradient) exists only within the first nanoparticles at the photoelectrode substrate contact [114,115].

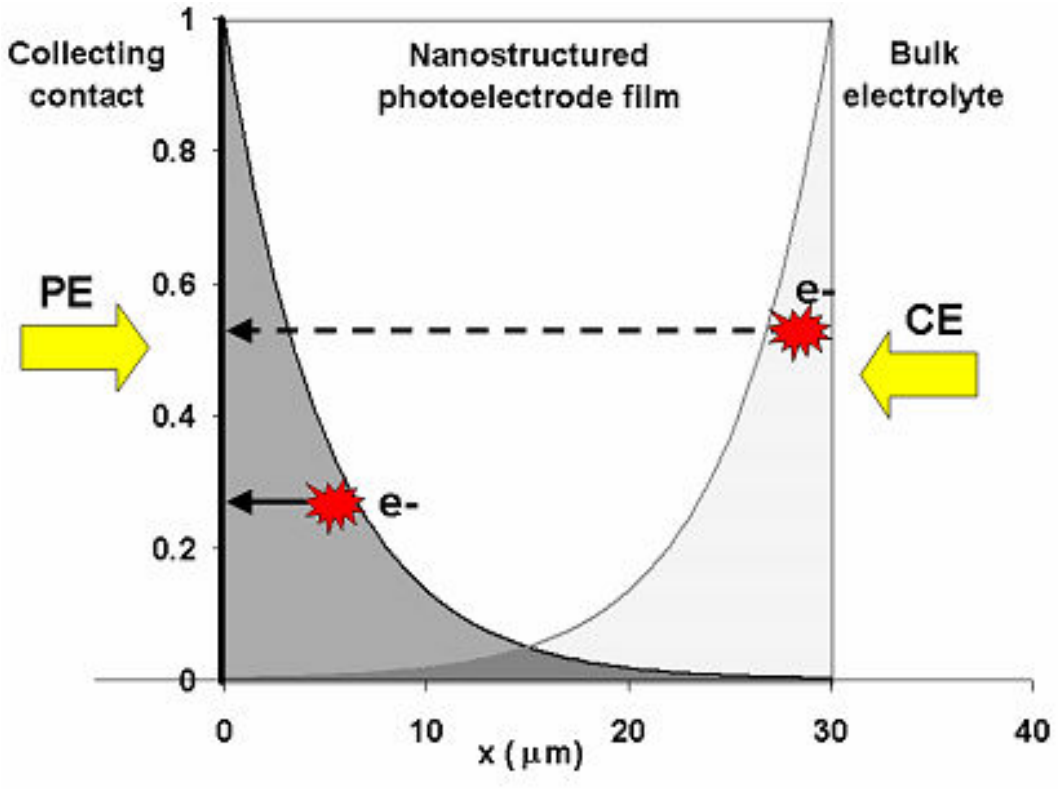

Figure 29. Geometry of the standard diffusion model with d = 30 μm . Light absorption in the film leads to non-uniform generation of electrons within the photoelectrode film. This, and the direction of illumination, determine the average distance of electron generation from the collecting contact.

The diffusion model is based on solving the time dependent continuity equation of the electrons in the nanostructured photoelectrode film, treating the film as a homogenous effective medium

$$\frac{\partial n}{\partial t} = D\frac{\partial^2 n}{\partial x^2} - \frac{n - n_0}{\tau} + g \tag{A1}$$

where D and τ are respectively the electron diffusion coefficient and lifetime, $n = n(x,t)$ the local electron density, n_0 the equilibrium electron density in the dark, and $g = g(x,t)$ the local electron generation rate. The generation rate is directly proportional to the local light absorption rate and the quantum efficiency of electron injection η_{INJ}. The absorption rate is further assumed to scale linearly with the incident photon flux Φ ($\mathrm{m^{-2}s^{-1}}$). Hence, in the general case we write

$$g(x,t) = \eta_{\mathrm{INJ}}\Phi(t) f_{\mathrm{LH}}(x) \tag{A2}$$

where the function $f_{\mathrm{LH}}(x)$, having units $\mathrm{m^{-1}}$, is the spatial light harvesting efficiency that defines the electron generation profile in the photoelectrode film.

Using appropriate boundary conditions eqs. A1 with eq. A2 can be solved to calculate the steady state photocurrent output of the cell [96]. More generally, the time-dependent solution of the diffusion model provides the basis for modeling and interpretation of the dynamic photocurrent and photovoltage response of the cell.

Of particular importance are the small amplitude periodic techniques called intensity modulated photocurrent (IMPS) and photovoltage (IMVS) spectroscopy, introduced briefly in Chapter 4.5. In these techniques, the dynamic photocurrent or photovoltage response of the solar cell to a small amplitude sinusoidal modulation of the incident light intensity is measured as a function of the modulation frequency ω at a certain steady state conditions. The incident photon flux constitutes a monochromatic modulated (AC) part superimposed on a constant background (DC) part

$$\Phi(\omega,t) = \Phi_{\mathrm{DC}} + \Phi_{\mathrm{AC}}(\omega,t) = \Phi_{\mathrm{DC}}\left(1 + \delta e^{i\omega t}\right) \tag{A3}$$

where the modulation depth δ is set less than 0.1 to maintain linearity of the response.

If D and τ are assumed independent on n, eq. A1 is a linear ordinary differential equation, the solution of which is found as the sum of solutions for the steady state DC and the modulated AC parts:

$$n(x,\omega,t) = n_{\mathrm{DC}}(x) + n_{\mathrm{AC}}(x,\omega,t) \tag{A4}$$

Due to the linearity of eq. A1 it suffices to solve it for the AC part only. The DC solution is then readily obtained by setting $\omega = 0$ in the AC solution. To further simplify the analysis, we consider the total electron density being the sum of the (constant) dark equilibrium density n_0 and the excess (light induced) electron density n_{e}

$$n(x,\omega,t) = n_0 + n_{\mathrm{e}}(x,\omega,t) = n_0 + n_{\mathrm{e,DC}}(x) + n_{\mathrm{e,AC}}(x,\omega,t) \tag{A5}$$

Inserting eq. A5 into eq. A1 yields the time-dependent continuity equation for the *excess* electron density

$$\frac{\partial n_e}{\partial t} = D\frac{\partial^2 n_e}{\partial x^2} - \frac{n_e}{\tau} + g \qquad \text{(A6)}$$

the solution of which has the DC and AC parts

$$n_e(x,\omega,t) = n_{e,DC}(x) + n_{e,AC}(x,\omega,t) \qquad \text{(A7)}$$

The boundary conditions relevant to the problem are [79,105]

$$D\frac{\partial n_e}{\partial x}\bigg|_{x=0} = k_{EXT} n_e(0,t) \qquad \text{for all } t \qquad \text{(A8a)}$$

$$\frac{\partial n_e}{\partial x}\bigg|_{x=d} = 0 \qquad \text{for all } t \qquad \text{(A8b)}$$

where d is the photoelectrode film thickness, and k_{EXT} is the kinetic rate constant for electron extraction at the photoelectrode substrate contact. Setting $k_{EXT} = 0$ corresponds to open circuit condition and yields solutions for the open-circuit-IMVS response. The short-circuit-IMPS response is found in the limit $k_{EXT} \rightarrow \infty$, in which case the substrate contact acts as a perfect sink for the excess electrons.

According to eqs. A2 and A3 the modulated part of the electron generation rate can be written as

$$g_{AC}(x,t) = G(x)e^{i\omega t} \qquad \text{(A9)}$$

where

$$G(x) = \eta_{INJ}\delta\Phi_{DC} f_{LH}(x) \qquad \text{(A10)}$$

Hence, the solution of eq. A6 for the AC part can be obtained by separation of variables, i.e. the solution is of the form

$$n_{e,AC}(x,\omega,t) = N(x,\omega)e^{i\omega t} \qquad \text{(A11)}$$

Inserting eqs. A10 and A11 into eq. A6 yields the equation for the complex electron density $N = N(x,\omega)$

$$\left(\frac{1}{\tau} + i\omega\right)N - D\frac{\partial^2 N}{\partial x^2} = G \qquad \text{(A12)}$$

and eqs. A8a-b give the corresponding boundary conditions

$$D\frac{\partial N}{\partial x}\bigg|_{x=0} = k_{EXT} N(0,\omega) \qquad \text{(A13a)}$$

$$\left.\frac{\partial N}{\partial x}\right|_{x=d} = 0 \tag{A13b}$$

To summarize, the small amplitude AC photocurrent and photovoltage response of dye solar cell is described by the differential equation eq. A12, subject to the boundary conditions A13a-A13b, and the generation term given by eq. A10. Its solution $N(x,\omega)$, gives the time-dependent excess electron concentration $n_e(x,\omega,t)$ according to eq. A11. Based on it, the total steady state electron density $n(x)$ can found in the limit of zero frequency ($\omega \rightarrow 0$) and full modulation depth ($\delta = 1$) by neglecting the explicit DC term $n_{e,DC}(x)$ in eq. A5.

As shown in Publication VI, the solution of eqs. A12-A13b can be expressed for any (arbitrary) electron generation profile in the general form (ω is omitted in the expressions below for brevity)

$$N(x) = \int_0^d f_{LH}(\xi) N_\delta(x,\xi) d\xi \tag{A14}$$

where $N_\delta(x,\xi)$ given by

$$N_\delta(x,\xi) = \frac{\delta \Phi_{DC} \eta_{INJ}}{\gamma D}\left[\cosh(\gamma(d-\xi))\frac{\gamma D\cosh(\gamma x) + k_{EXT}\sinh(\gamma x)}{\gamma D\sinh(\gamma d) + k_{EXT}\cosh(\gamma d)} - \sinh(\gamma(x-\xi))\,u(x-\xi)\right] \tag{A15}$$

is the solution of the same problem for localized electron generation at $x = \xi$, described by the spatial light harvesting efficiency (in eq. A10)

$$f_\delta(x,\xi) = \delta(x,\xi) \tag{A16}$$

where $\delta(x,\xi)$ is the Dirac's delta function, and further,

$$\gamma = \sqrt{\frac{1}{D}\left(\frac{1}{\tau} + i\omega\right)} \tag{A17}$$

and $u(x-\xi)$ is the unit step function. The mathematical derivation of this result was given as supporting information for Publication VI.

It follows that coupling of any (arbitrary) optical model of the dye solar cell to the standard diffusion model is as simple as calculating the integral of eq. A14. The coupling occurs *via* the spatial light harvesting efficiency function $f_{LH}(x)$. In some cases, such as for uniform or exponential generation profile, the integration in eq. A14 can be calculated analytically. In the more general case, if the analytical expression of $f_{LH}(x)$ is complicated or it is available only in the form of tabulated data, the integration can be done numerically.

The above result (eq A14) is specific to the kinetic boundary condition eq. A13a. It is therefore of interest to complete the theoretical analysis of Publication VI by considering whether a similar result exists for other boundary conditions as well.

Firstly, with a minor modification of the derivation given in the supporting information of Publication VI, it can be shown that the general solution of eq. A12 for the localized generation (eqs A10 with A16) is

$$N_\delta(x,\xi) = B_1 \cosh(\gamma x) + \frac{B_2}{\gamma D}\sinh(\gamma x) - \frac{G_0}{\gamma D}\sinh(\gamma(x-\xi))\,\mathrm{u}(x-\xi) \qquad \text{(A18)}$$

where B_1 and B_2 are the two unknown constants to be determined by the two boundary conditions of some kind. Secondly, the result expressed by eq. A14 is indeed valid for any boundary conditions restricting the final result $N(x)$ that corresponds to the arbitrary generation function $G(x)$: no boundary conditions were needed in the derivation of eq. A14. This means that the general solution of the standard diffusion model in the case of arbitrary electron generation profile $f_{\mathrm{LH}}(x)$ is

$$N(x) = \eta_{\mathrm{LH}}\left[B_1 \cosh(\gamma x) + \frac{B_2}{\gamma D}\sinh(\gamma x)\right] - \frac{G_0}{\gamma D}\int_0^x f_{\mathrm{LH}}(\xi)\sinh(\gamma(x-\xi))d\xi \qquad \text{(A19)}$$

where η_{LH} is the light harvesting efficiency corresponding to the arbitrary generation in question. Note that the unit step function in eq. A18 cuts the integration range to x in eq. A19. To find the complete analytical solution one merely needs to use the two boundary conditions relevant to the case at hand to find expressions for the constants B_1 and B_2, and then insert these expressions to eq. A19 together with the function $f_{\mathrm{LH}}(x)$ in question, and perform the remaining integrations, numerically if necessary.

References

(1) Zhu, K.; Neale, N. R.; Miedaner, A.; Frank, A.; J. *Nano Letters* 2007*, 7*, 69-74.

(2) Lewis, N. S.; Nocera, D. G.; *Proc. Natl. Acad. Sci. U. S. A.* 2007*, 104*, 20142.

(3) Service, R. F.; *Science,* 2005*, 309*, 548-551.

(4) Schiermeier, Q.; Tollefson, J.; Scully, T.; Witze, A.; Morton, O.; *Nature* 2008*, 454*, 816-823.

(5) Basic Research Needs for Solar Energy Utilization - Report on the Basic Energy Sciences Workshop on Solar Energy Utilization; Office of Science, U.S. Department of Energy, 2005, http://www.sc.doe.gov/bes/reports/files/SEU_rpt.pdf, (accessed 03/02, 2009)

(6) Solarbuzz 2007 Worlds PV Industry Report Highlights; *http://www.solarbuzz.com/Marketbuzz2008-intro.htm* (accessed February/26, 2009).

(7) Solarbuzz Solar Electricity Prices. *http://www.solarbuzz.com/SolarPrices.htm* (accessed 03/02, 2009).

(8) Goerten, J.; Ganea, D. C.; Electricity prices for first semester 2008, Issue number 45/2008, Eurostat Environment and energy. *http://epp.eurostat.ec.europa.eu/cache/ITY_OFFPUB/KS-QA-08-045/EN/KS-QA-08-045-EN.PDF*.

(9) Solar module retail price environment, Solar consultancy reports. *http://www.solarbuzz.com/Moduleprices.htm* (accessed 93/03, 2009).

(10) Green, M. A.; *Progress in Photovoltaics* 2001*, 9*, 123-135.

(11) Guenes, S.; Neugebauer, H.; Sariciftci, N. S.*; Chemical Reviews* 2007*, 107*, 1324-1338.

(12) Hara, K.; Arakawa, H.; *Handbook of Photovoltaic Science and Engineering* 2003, 663-700.

(13) Peter, L. M.; *Phys. Chem. Chem. Phys.* 2007*, 9*, 2630-2642.

(14) Grätzel, M.; Durrant, J. R.; *Series on Photoconversion of Solar Energy* 2008*, 3*, 503-538.

(15) Pagliaro, M.; Ciriminna, R.; Palmisano, G.; *ChemSusChem* 2008*, 1*, 880-891.

(16) Ito, S.; Murakami, T. N.; Comte, P.; Liska, P.; Grätzel, C.; Nazeeruddin, M. K.; Grätzel, M.; *Thin Solid Films* 2008*, 516*, 4613-4619.

(17) Ito, S.; Nazeeruddin, K.; Liska, P.; Comte, P.; Charvet, R.; Pechy, P.; Jirousek, M.; Kay, A.; Zakeeruddin, S. M.; Grätzel, M.; *Progress in Photovoltaics* 2006*, 14*, 589-601.

(18) Wang, Z.; Kawauchi, H.; Kashima, T.; Arakawa, H.; *Coordination Chemistry Reviews* 2004/7*, 248*, 1381-1389.

(19) Kroon, J. M.; Bakker, N. J.; Smit, H. J. P.; Liska, P.; Thampi, K. R.; Wang, P.; Zakeeruddin, S. M.; Grätzel, M.; Hinsch, A.; Hore, S.; Würfel, U.; Sastrawan, R.; Durrant, J. R.; Palomares, E.; Pettersson, H.; Gruszecki, T.; Walter, J.; Skupien, K.; Tulloch, G. E.; *Progress in Photovoltaics* 2007*, 15*, 1-18.

(20) Shi, D.; Pootrakulchote, N.; Li, R.; Guo, J.; Wang, Y.; Zakeeruddin, S. M.; Grätzel, M.; Wang, P.; *J.Phys.Chem.C* 2008*, 112*, 17046-17050.

(21) Bisquert, J.; Cahen, D.; Hodes, G.; Rühle, S.; Zaban, A.; *J Phys Chem B* 2004*, 108*, 8106-8118.

(22) Würfel, P.; *Physics of Solar Cells - From Principles to New Concepts;* Wiley-VCH: Weinheim, 2005.

(23) Fisher, A. C.; Peter, L. M.; Ponomarev, E. A.; Walker, A. B.; Wijayantha, K. G. U.; *J. Phys. Chem. B* 2000*, 104*, 949-958.

(24) Halme, J.; Boschloo, G.; Hagfeldt, A.; Lund, P.; *J. Phys. Chem. C* 2008*, 112*, 5623-5637.

(25) Trupke, T.; Würfel, P.; Uhlendorf, I.; *J. Phys. Chem. B* 2000*, 104*, 11484-11488.

(26) Maheu, B.; Gouesbet, G.; *Appl. Opt.* 1986*, 25*, 1122-1128.

(27) Rothenberger, G.; Comte, P.; Grätzel, M.; *Solar Energy Materials and Solar Cells* 1999/7/15*, 58*, 321-336.

(28) Lin, Y.; Ma, Y. T.; Yang, L.; Xiao, X. R.; Zhou, X. W.; Li, X. P.; *Journal of Electroanalytical Chemistry* 2006/3/1*, 588*, 51-58.

(29) Tachibana, Y.; Akiyama, H. Y.; Kuwabata, S.; *Solar Energy Materials & Solar Cells* 2007*, 91*, 201-206.

(30) Zhang, Z.; Zakeeruddin, S. M.; O'Regan, B. C.; Humphry-Baker, R.; Grätzel, M.; *J Phys Chem B* 2005*, 109*, 21818-21824.

(31) Rühle, S.; Greenshtein, M.; Chen, S.; Merson, A.; Pizem, H.; Sukenik, C. S.; Cahen, D.; Zaban, A.; *J Phys Chem B* 2005*, 109*, 18907-18913.

(32) Neale, N. R.; Kopidakis, N.; van de Lagemaat, J.; Grätzel, M.; Frank, A. J.; *J Phys Chem B* 2005*, 109*, 23183-23189.

(33) Kelly, C. A.; Farzad, F.; Thompson, D. W.; Stipkala, J. M.; Meyer, G. J.; *Langmuir* 1999*, 15*, 7047-7054.

(34) Qu, P.; Meyer, G. J.; *Langmuir* 2001*, 17*, 6720-6728.

(35) Hara, K.; Horiguchi, T.; Kinoshita, T.; Sayama, K.; Arakawa, H.; *Solar Energy Mater. Solar Cells* 2001*, 70*, 151-161.

(36) Fukui, A.; Komiya, R.; Yamanaka, R.; Islam, A.; Han, L.; *Solar Energy Materials & Solar Cells* 2006*, 90*, 649-658.

(37) Kusama, H.; Kurashige, M.; Arakawa, H.; *Journal of Photochemistry and Photobiology, A: Chemistry* 2005*, 169*, 169-176.

(38) Zaban, A.; Ferrere, S.; Gregg, B. A.; *J Phys Chem B* 1998*, 102*, 452-460.

(39) Watson, D. F.; Meyer, G. J.; *Coord. Chem. Rev.* 2004*, 248*, 1391-1406.

(40) Moser, J.; Grätzel, M.; *Chimia* 1998*, 52*, 160-162.

(41) Haque, S. A.; Palomares, E.; Cho, B. M.; Green, A. N. M.; Hirata, N.; Klug, D. R.; Durrant, J. R.; *J. Am. Chem. Soc.* 2005*, 127*, 3456-3462.

(42) Kallioinen, J.; Benkö, G.; Sundström, V.; Korppi-Tommola, J. E. I.; Yartsev, A. P.; *J Phys Chem B* 2002*, 106*, 4396-4404.

(43) Benkö, G.; Kallioinen, J.; Korppi-Tommola, J. E. I.; Yartsev, A. P.; Sundström, V.; *J. Am. Chem. Soc.* 2002*, 124*, 489-493.

(44) Dor, S.; Grinis, L.; Rühle, S.; Zaban, A.; *J.Phys.Chem.C* 2009*, 113*, 2022-2027.

(45) Cameron, P. J.; Peter, L. M.; *J Phys Chem B* 2003*, 107*, 14394-14400.

(46) Ito, S.; Liska, P.; Comte, P.; Charvet, R.; Pechy, P.; Bach, U.; Schmidt-Mende, L.; Zakeeruddin, S. M.; Kay, A.; Nazeeruddin, M. K.; Grätzel, M.; *Chemical Communications* 2005, 4351-4353.

(47) Hore, S.; Kern, R.; *Appl. Phys. Lett.* 2005*, 87*, 263504/1-263504/3.

(48) Xia, J.; Masaki, N.; Jiang, K.; Yanagida, S.; *J Phys Chem C* 2007*, 111*, 8092-8097.

(49) Koide, N.; Han, L.; *Rev. Sci. Instrum.* 2004*, 75*, 2828-2831.

(50) Seaman, C. H.; *Solar Energy* 1982*, 29*, 291-298.

(51) Keis, K.; Roos, A.; *Optical Materials* 2002/8*, 20*, 35-42.

(52) Tachibana, Y.; Hara, K.; Sayama, K.; Arakawa, H.; *Chemistry of Materials* 2002*, 14*, 2527-2535.

(53) Argazzi, R.; Bignozzi, C. A.; Yang, M.; Hasselmann, G. M.; Meyer, G. J.; *Nano Lett.; Nano Letters* 2002*, 2*, 625-628.

(54) Kern, R.; Sastrawan, R.; Ferber, J.; Stangl, R.; Luther, J.; *Electrochim. Acta* 2002*, 47*, 4213-4225.

(55) Han, L.; Koide, N.; Chiba, Y.; Islam, A.; Mitate, T.; *Comptes Rendus Chimie* 2006*,* 9, 645-651

(56) Fabregat-Santiago, F.; Bisquert, J.; Garcia-Belmonte, G.; Boschloo, G.; Hagfeldt, A.; *Solar Energy Mater. Solar Cells* 2005*, 87*, 117-131.

(57) Wang, Q.; Moser, J.; Grätzel, M.; *J Phys Chem B* 2005*, 109*, 14945-14953.

(58) Bay, L.; West, K.; *Solar Energy Mater. Solar Cells* 2005*, 87*, 613-628.

(59) Fabregat-Santiago, F.; Bisquert, J.; Palomares, E.; Otero, L.; Kuang, D.; Zakeeruddin, S. M.; Grätzel, M.; *J. Phys. Chem. C* 2007, *111*, 6550-6560

(60) Bisquert, J.; Garcia-Belmonte, G.; Fabregat-Santiago, F.; Ferriols, N. S.; Bogdanoff, P.; Pereira, E. C.; *J. Phys. Chem. B* 2000*, 104*, 2287-2298.

(61) Bisquert, J.; Vikhrenko, V. S.; *J. Phys. Chem. B* 2004*, 108*, 2313-2322.

(62) Barnes, P. R. F.; Anderson, A. Y.; Koops, S. E.; Durrant, J. R.; O'Regan, B. C.; *J Phys Chem C* 2009*, 113*, 1126-1136.

(63) Dunn, H. K.; Peter, L. M.; *J Phys Chem C* 2009, *113*, 4726-4731

(64) Peter, L. M.; Wijayantha, K. G. U.; *Electrochem. Comm.* 1999*, 1*, 576-580.

(65) Lindström, H.; Holmberg, A.; Magnusson, E.; Lindquist, S.; Malmqvist, L.; Hagfeldt, A.; *Nano Letters* 2001*, 1*, 97-100.

(66) Lindström, H.; Magnusson, E.; Holmberg, A.; Södergren, S.; Lindquist, S.; Hagfeldt, A.; *Solar Energy Mater. Solar Cells* 2002*, 73*, 91-101.

(67) Boschloo, G.; Lindström, H.; Magnusson, E.; Holmberg, A.; Hagfeldt, A.; *Journal of Photochemistry and Photobiology, A: Chemistry* 2002*, 148*, 11-15.

(68) Hagfeldt, A.; Boschloo, G.; Lindström, H.; Figgemeier, E.; Holmberg, A.; Aranyos, V.; Magnusson, E.; Malmqvist, L.; *Coord. Chem. Rev.* 2004*, 248*, 1501-1509.

(69) Haque, S. A.; Palomares, E.; Upadhyaya, H. M.; Otley, L.; Potter, R. J.; Holmes, A. B.; Durrant, J. R.; *Chem. Commun.* 2003*, 24*, 3008-3009.

(70) Dürr, M.; Schmid, A.; Obermaier, M.; Rosselli, S.; Yasuda, A.; Nelles, G.; *Nature Materials* 2005*, 4*, 607-611.

(71) Yamaguchi, T.; Tobe, N.; Matsumoto, D.; Arakawa, H.; *Chemical Communications* 2007, 4767-4769.

(72) Grinis, L.; Dor, S.; Ofir, A.; Zaban, A.; *J. Photochem. Photobiol. A.* 2008*, 198*, 52-59.

(73) Santa-Nokki, H.; Kallioinen, J.; Kololuoma, T.; Tuboltsev, V.; Korppi-Tommola, J.; *J. Photochem. Photobiol. A.* 2006*, 182*, 187-191.

(74) Holmes, D. M.; Tegeler, F.; Clegg, W. J.; *J.Eur.Ceram.Soc.* 2008*, 28*, 1381-1387.

(75) Pasricha, K.; Wad, U.; Pasricha, R.; Ogale, S.; *Physica A: Statistical Mechanics and Its Applications* 2009*, 388*, 1352-1358.

(76) Papageorgiou, N.; Maier, W. F.; Grätzel, M.; *J. Electrochem. Soc.* 1997*, 144*, 876-884.

(77) Hauch, A.; Georg, A.; *Electrochim. Acta* 2001*, 46*, 3457-3466.

(78) Peter, L. M.; Ponomarev, E. A.; Franco, G.; Shaw, N. J.; *Electrochim. Acta* 1999*, 45*, 549-560.

(79) Dloczik, L.; Ileperuma, O.; Lauermann, I.; Peter, L. M.; Ponomarev, E. A.; Redmond, G.; Shaw, N. J.; Uhlendorf, I.; *J. Phys. Chem. B* 1997*, 101*, 10281-10289.

(80) Ma, T.; Fang, X.; Akiyama, M.; Inoue, K.; Noma, H.; Abe, E.; *J Electroanal Chem* 2004*, 574*, 77-83.

(81) Kang, M. G.; Park, N.; Ryu, K. S.; Chang, S. H.; Kim, K.; *Chem. Lett.* 2005*, 34*, 804-805.

(82) Murakami, T. N.; Grätzel, M.; *Inorg. Chim. Acta* 2008*, 361*, 572-580.

(83) Park, J. H.; Jun, Y.; Yun, H.; Lee, S.; Kang, M. G.; *J. Electrochem. Soc.* 2008*, 155*, F145-F149.

(84) Miettunen, K.; Toivola, M.; Halme, J.; Armentia, J.; Vahermaa, P.; Lund, P.; *Optimization of dye-sensitized solar cells on stainless steel;* Proceedings of the 22nd European Photovoltaic Solar Energy Conference and Exhibition; 512-515.

(85) Lobato, K.; Peter, L. M.; Würfel, U.; *J Phys Chem B* 2006*, 110*, 16201-16204.

(86) Hoshikawa, T.; Kikuchi, R.; Eguchi, K. *J Electroanal Chem* 2006*, 588*, 59-67.

(87) Cameron, P. J.; Peter, L. M.; Hore, S.; *J Phys Chem B* 2005*, 109*, 930-936.

(88) Pichot, F.; Pitts, J. R.; Gregg, B. A.; *Langmuir* 2000*, 16*, 5626-5630.

(89) Miyasaka, T.; Kijitori, Y.; Murakami, T. N.; Kimura, M.; Uegusa, S.; *Chem. Lett.* 2002, 1250-1251.

(90) Agrios, A. G.; Hagfeldt, A.; *J.Phys.Chem.C* 2008*, 112*, 10021-10026.

(91) Durrant, J. R.; Haque, S. A.; Palomares, E.; *Coord. Chem. Rev.* 2004*, 248*, 1247-1257.

(92) Anderson, N. A.; Lian, T.; *Annu. Rev. Phys. Chem.* 2005*, 56*, 491-519.

(93) Koops, S. E.; Durrant, J. R.; *Inorg. Chim. Acta* 2008*, 361*, 663-670.

(94) Serpa, C.; Schabauer, J.; Piedade, A. P.; Monteiro, C. J. P.; Pereira, M. M.; Douglas, P.; Burrows, H. D.; Arnaut, L. G.; *J. Am. Chem. Soc.* 2008*, 130*, 8876-8877.

(95) O'Regan, B.; Moser, J.; Anderson, M.; Grätzel, M.; *J. Phys. Chem.* 1990*, 94*, 8720-8726.

(96) Södergren, S.; Hagfeldt, A.; Olsson, J.; Lindquist, S.; *J. Phys. Chem.* 1994*, 98*, 5552-5556.

(97) O'Regan, B.; Grätzel, M.; *Nature* 1991*, 353*, 737-740.

(98) Nazeeruddin, M. K.; Kay, A.; Rodicio, I.; Humphry-Baker, R.; Müller, E.; Liska, P.; Vlachopoulos, N.; Grätzel, M.; *J. Am. Chem. Soc.* 1993*, 115*, 6382-6390.

(99) Kubo, W.; Sakamoto, A.; Kitamura, T.; Wada, Y.; Yanagida, S.; *Journal of Photochemistry and Photobiology A: Chemistry* 2004/6/1*, 164*, 33-39.

(100) Lindström, H.; Rensmo, H.; Södergren, S.; Solbrand, A.; Lindquist, S.; *J. Phys. Chem.* 1996*, 100*, 3084-3088.

(101) Boschloo, G. K.; Goossens, A.; *J. Phys. Chem.* 1996*, 100*, 19489-19494.

(102) Benkstein, K. D.; Kopidakis, N.; van de Lagemaat, J.; Frank, A. J. *Mater. Res. Soc. Symp. Proc.* 2004*, 789*, 325-330.

(103) Dittrich, T.; Ofir, A.; Tirosh, S.; Grinis, L.; Zaban, A.; *Appl. Phys. Lett.* 2006*, 88*, 182110/1-182110/3.

(104) Ofir, A.; Dor, S.; Grinis, L.; Zaban, A.; Dittrich, T.; Bisquert, J.; *J. Chem. Phys.* 2008*, 128*, 064703/1-064703/9.

(105) Franco, G.; Gehring, J.; Peter, L. M.; Ponomarev, E. A.; Uhlendorf, I.; *J. Phys. Chem. B* 1999*, 103*, 692-698.

(106) Schlichthörl, G.; Huang, S. Y.; Sprague, J.; Frank, A. J.; *J. Phys. Chem. B* 1997*, 101*, 8141-8155.

(107) Duffy, N. W.; Peter, L. M.; Rajapakse, R. M. G.; Wijayantha, K. G. U.; *Electrochem. Comm.* 2000*, 2*, 658-662.

(108) Bailes, M.; Cameron, P. J.; Lobato, K.; Peter, L. M.; *J. Phys. Chem. B* 2005*, 109*, 15429-15435.

(109) Würfel, U.; Wagner, J.; Hinsch, A.; *J Phys Chem B* 2005*, 109*, 20444-20448.

(110) Wang, Q.; Ito, S.; Grätzel, M.; Fabregat-Santiago, F.; Mora-Sero, I.; Bisquert, J.; Bessho, T.; Imai, H.; *J Phys Chem B* 2006*, 110*, 25210-25221.

(111) Rensmo, H.; Lindström, H.; Södergren, S.; Willstedt, A.; Solbrand, A.; Hagfeldt, A.; Lindquist, S.; *J. Electrochem. Soc.* 1996*, 143*, 3173-3178.

(112) Hagfeldt, A.; Grätzel, M.; *Chemical Reviews* 1995*, 95*, 49-68.

(113) Zaban, A.; Meier, A.; Gregg, B. A.; *J Phys Chem B* 1997*, 101*, 7985-7990.

(114) Bisquert, J.; Garcia-Belmonte, G.; Fabregat-Santiago, F.; *Journal of Solid State Electrochemistry* 1999*, 3*, 337-347.

(115) Ferber, J.; Luther, J.; *J Phys Chem B* 2001*, 105*, 4895-4903.

(116) Reprinted from Solar Energy Materials and Solar Cells, 90, Halme, J.; Toivola, M.; Tolvanen, A.; Lund, P.; Charge transfer resistance of spray deposited and compressed counter electrodes for dye-sensitized nanoparticle solar cells on plastic substrates; 872-886, Copyright (2006), with permission from Elsevier.

(117) Reprinted with permission from *J. Phys. Chem. C*, 2008, 112(10), 4011-4017. Copyright 2008 American Chemical Society.

(118) Figure 8b, Figure 30 left and Figure 31a reprinted with permission from *J. Phys. Chem. C*, 2008, 112(14), 5623-5637. Copyright 2008 American Chemical Society.

(119) Figures 25a and 25b are reproduced by permission of ECS – The Electrochemical Society.

ISBN 978-951-22-9900-3
ISBN 978-951-22-9901-0 (PDF)
ISSN 1795-2239
ISSN 1795-4584 (PDF)